EVALUATION OF DAMAGE IN CELLULOSE FIBER REINFORCED CONCRETE USING ACOUSTIC EMISSION

By

YU CHEN

A DISSERTATION PRESENTED TO THE GRADUATE SCHOOL
OF THE UNIVERSITY OF FLORIDA IN PARTIAL FULFILLMENT
OF THE REQUIREMENTS FOR THE DEGREE OF
DOCTOR OF PHILOSOPHY

UNIVERSITY OF FLORIDA

2010

To My Family

ACKNOWLEDGMENTS

I would like to thank my advisor, Dr. David Bloomquist, for his support throughout my graduate studies. I would also like to thank my committee members, Dr. Dennis R. Hiltunen, Dr. Mang Tia, and Dr. Youping Chen for their valuable time and suggestions.

I appreciate Mr. Adrian Pollock from Mistras Group, Inc. for his valuable advice on Acoustic Emission.

I would also like to thank everyone at the UF structures lab who always lent a helping hand when needed, particularly: Mr. Chuck Broward, Mr. George Lopp, Mr. Yu Chen, Mr. Xingsong Sun, Mr. Weitao Li. Thank you all for your assistance.

Finally, I would like to acknowledge Mr. Daniel J. Pitocchi and the employees of the Florida Department of Transportation for their assistance in providing test facilities.

TABLE OF CONTENTS

LIST OF TABLES

LIST OF FIGURES

LIST OF ABBREVIATIONS

AE Acoustic	Emission
CFRC	Cellulose Fiber Reinforced Concrete
FRC	Fiber Reinforced Composite
SRC	Steel Reinforced Concrete

Abstract of Dissertation Presented to the Graduate School
of the University of Florida in Partial Fulfillment of the
Requirements for the Degree of Doctor of Philosophy

EVALUATION OF DAMAGE IN CELLULOSE FIBER REINFORCED CONCRETE USING ACOUSTIC EMISSION

By

Yu Chen

December 2010

Chair: David Bloomquist
Major: Civil Engineering

The objectives of the research program were to evaluate the damage effect of moisture and fatigue loading regarding the performance of Cellulose Fiber Reinforced Concrete (CFRC) and to develop a reliable inspection methodology using acoustic emission (AE) to identify the failure mechanism.

ASTM third-point bending tests were conducted on CFRC beams; both monotonic and fatigue loading. The AE data were collected and compared using visual observations from a Scanning Electronic Microscope to identify the failure mechanisms at various damage levels. The failure mechanisms were determined to be matrix cracking, fiber/matrix debonding and fiber breakage. These fracture mechanisms were found to associate with low, middle and high amplitudes, respectively.

The knowledge of fracture mechanisms was then applied to identify the effect of various moisture conditions towards CFRC's properties and the material's fatigue property. ASTM three-edge-bearing tests were performed on pipe sections with AE.

Data analysis involved correlating mechanical properties and AE results. Various methods were used to interpret the AE signals. Analysis of conventional AE parameters

including hits, counts, energy and signal strength show that AE can provide real-time inspection of internal damage, both minor and visible. Methods of AE amplitude distribution, AE cumulative amplitude distribution and b-value are powerful tools to discern the fracture mechanism. Duration versus amplitude, on the other hand, proved to be useful in interpreting the quality of AE data and distinguishing friction data from valid data.

In summary, the fracture mechanism, moisture effects and fatigue properties of CFRC were studied. The AE analysis methodology developed in this research program are believed to be reliable for future inspection of structures made with CFRC materials.

CHAPTER 1
INTRODUCTION

Background

Cellulose Fiber Reinforced Concrete (CFRC) pipe is a popular product widely used in utility and storm water conduits, sewer lines, etc. Compared with steel reinforced concrete pipe, it has advantages such as higher strength to weight ratio, higher toughness and impact resistance, longer single runs, lighter weight, and better corrosion resistance.

However, when installed in harsh environments such as high rainfall areas, or frequent wetting and drying environments, CFRC pipes demonstrated more brittle and fragile characteristics. CFRC pipes were found to crack in a brittle manner, at a load level far below their ultimate strength. The unexpected pre-mature failures have caused not only economic loss, but also safety and environmental concerns. The question of how CFRC pipe changes its behavior during in-service life is important. In addition, how to detect pre-mature failure before it results in damage to the pipe network and creating a threat to the public safety is critical. Therefore, it is important to develop a method for real-time inspection of pipe to detect damage initiation and to prevent further damage development.

In recent years, Acoustic Emission (AE) has been successfully applied in composite materials related research and industry. Acoustic Emission is defined by ASTM Standard as “the class of phenomena whereby transient elastic waves are generated by the rapid release of energy from a localized source or sources within a material”. Due to its ability of detecting damage initiation and tracking its

propagation, AE is potentially a powerful tool to characterize the CFRC pipe damage and also to help understand the effects of different environmental conditions associated with CFRC installation.

Problem Statement

The purpose of this research is to develop a method to detect damage initiation and to monitor the damage propagation in CFRC pipes using Acoustic Emission.

Objectives

To develop an effective inspection method, it is necessary to understand how CFRC pipe reacts to different environmental conditions, and how they alter its failure mechanism. Finally, how AE can be used to identify the different failure mechanisms in an effective and accurate way. With these questions in mind, the objectives for this research are:

- To understand the failure mechanism under different moisture and loading conditions with the aid of SEM and AE.
- To evaluate and calibrate the AE method in detecting damage initiation and monitoring damage propagation in CFRC materials.
- To develop recommendations on the testing procedure as well as data analysis for an inspection method

Scope

All the experiments for this project were performed in the laboratory. Common problems occurred during insitu testing such as attenuation and environmental noise are discussed but were not the main focus of this project.

Dissertation Structure

This dissertation presents the details of a research program on CFRC materials. The overall work is organized into the following sections:

Chapter 2 contains the fundamental background and a literature review of Acoustic Emission, Scanning Electron Microscope, and CFRC materials.

Chapter 3 details the experimental program, i.e., static third point bending and fatigue third point bending tests on CFRC beams and three-edge-bearing tests on CFRC pipe sections. The testing procedures, instrumentation and specimens are introduced in this chapter.

Chapter 4 studies the fracture mechanism of CFRC. The SEM was used at different load levels to observe the corresponding fracture mechanism. Recorded AE data are analyzed and compared to establish a relationship between AE signals and the fracture mechanism. A fracture mechanism model is hypothesized. Knowledge on fracture mechanisms and AE results will be applied in Chapter 5 and 6.

Chapter 5 focuses on static third point bending test on CFRC samples. Five groups of samples were exposed to five water treatments. The comparison of their fracture mechanism, mechanical and AE properties are presented. AE analysis performed in this and the following chapter includes conventional AE data analysis, historic index, duration and amplitude analysis, amplitude distribution and b-values. The AE results are expected to be a valuable inspection tool for in-service CFRC structures.

Chapter 6 discusses the ability of AE to detect the initiation and propagation of damage in CFRC beams under fatigue third-point bending tests. Special attention to identify the AE resulting from internal friction is provided.

Chapter 7 applies the AE technique to three-edge-bearing tests on pipe sections.

Chapter 8 documents the conclusions of the research and suggests future research areas. Finally recommendations for using AE to inspect in-service pipes are presented.

CHAPTER 2
AE FUNDAMENTALS AND LITERATURE REVIEW

This chapter presents background information on the Acoustic Emission (AE) method, Scanning Electron Microscope (SEM), and Cellulose Fiber Reinforced Concrete (CFRC). Also included is a review of the literature regarding the fracture mechanism and fatigue properties of Fiber Reinforced Composites (FRC).

Cellulose Fiber Reinforced Concrete

Material Constitution

The CFRC specimens were taken from fiber reinforced concrete pipes commercially manufactured by Hardie pipe, Inc. The CFRC matrix material used in the experiments was ASTM Type I Portland Cement produced by Suwannee American Cement, LLC (SAC). The chemical composition and the cement mass percentage are listed in Table 2-1.

Kraft pulp softwood fibers were used as reinforcement at a 4% fiber volume fraction in the cement paste. The average diameter of applied fibers was roughly 0.3 mm, with a length of 3 mm. Some important data on this fiber are provided in Table 2-2 (Moslemi 1999).

Manufacturing

The Hatschek process (Mohr et al. 2005) is the most common technique to produce fiber-cement products for a variety of building and construction markets. In the Hatschek process, as shown in Figure 2-1, aqueous slurry of fiber and cement, about 7-10% solids by weight, is supplied to a holding tank with a number of rotating screen cylinders (Moslemi 1999). A band travels over the top

surfaces of the cylinders and picks up a thin layer of fiber-cement formulation from each cylinder. The sheet product subsequently wraps around an “accumulation” roll and continues to build additional thickness until the desired thickness is obtained. The fiber-cement sheet is further subjected to pressure to consolidate the product.

Acoustic Emission

Introduction to Acoustic Emission

Acoustic Emission is defined by ASTM standards as; “the class of phenomena whereby transient elastic waves are generated by the rapid release of energy from a localized source or sources within a material”. In contrast with most complementary Non-Destructive Testing (NDT) methods, AE detects the local movement and growth of flaws created by localized stresses which are part of a global stress field. Other NDT methods detect the presence of flaws and geometric discontinuities.

Acoustic activity can be observed in various materials including metal, wood, plastic, polymer, and composites. The possible sources of AE are damage-related structural changes, e.g., crack initiation and propagation within brittle materials, dislocation movement accompanying plastic deformation in metals, stress corrosion cracking in a stress and chemical environment, etc. In Fiber Reinforced Composites (FRC), the AE signals come from matrix breaking, fiber breaking, fiber-matrix debonding, fiber pullout and combinations of the above.

Due to the characteristics of AE technique and sources, the principal limitations of the AE method are:

1. It cannot detect unstressed flaws which do not emit signals.

2. It is dependent on stress history.
3. Wave attenuation can occur in certain materials.
4. Noise exists during detection.

Acoustic Emission Apparatus

The typical testing apparatus used for acoustic emission (shown in Figure 2-2) consists of transducers, receiver/amplifier, signal processors, transient digitizers, display, and coupling agent.

Transducer is commonly referred to as a sensor. The most important single factor in successfully performing an AE application is the reliability of an AE sensor. Sensors must be properly mounted, assuring accurate configuration to attain the desired signal. An array of different sensors is shown in Figure 2-3.

An important factor in acoustic monitoring is sensor location. For monitoring cases in which the location of a crack or deficiency is known, a single sensor is sufficient for monitoring. However, for detection of deficiencies in a two dimensional plane or three dimensional solid, the geometric configuration of the sensors is vital to the location of the deficiencies. ASTM Standard Guide for Mounting Piezoelectric Acoustic Emission Sensors (ASTM E-650-97) specifies guidelines for mounting piezoelectric acoustic emission sensors. The performance of sensors relies heavily upon the methods and procedures used in mounting. Detection of acoustic emission signals requires both appropriate sensor–mounting fixtures and consistent sensor–mounting procedures.

Receiver/amplifier is used to amplify the weak signals and prevent loss in sensor activity. The receiver has four basic components: the preamplifier, logarithmic amplifier, rectifier, and low pass amplifier. The preamplifiers' function is to ensure that any signal from the transducers arrives at the time measuring

circuit. Since electrical output from the transducer is relatively small, signal amplification is necessary to overcome the resistance from the transducer cable, which can be relatively long. The function of the logarithmic amplifier is to process weak echo signals. Once the echo signals are amplified, the low pass filter processes the signals. After the signal has been processed by the receiver/amplifier, a useable signal can be transmitted to the display. Microprocessor-based systems have become widely used in recent years. Such units perform single channel analysis, along with source location for up to eight AE channels.

Signal processors are designed to allow data collection only on certain portions of a load cycle. Envelope processors attempt to filter out the high frequencies, leaving only the signal envelope to be counted. Logarithmic converters allow the output of the signal analyzer electronics to be plotted in logarithmic form. A unit allows combination of several preamplifier outputs so that several sensors can be monitored by one channel of electronics [Reese, 1993].

Transient digitizers (also called transient recorders) are used to study individual AE burst signals. A signal is digitized in real time and then stored into memory. A transient digitizer uses an oscilloscope or spectrum analyzer to display AE signals at visible speeds. Digital rates vary on transient digitizers. One advantage of transient digitizers is an additional mode of triggering, the pretriggering mode, where the input signal is continuously digitized and the data fed into the memory (Reese 1993). This configuration allows a digitized picture

of the signal to be displayed as received. More advanced digitizers allow recording of multiple signals simultaneously.

Display uses an interval timer and a direct reading of display time on an x-y coordinate system. The x-axis displays the time trigger and the y-axis represents the mechanical energy received. The display units can also illustrate defect / anomaly locations and sizes depending on the type of scan request by the user. Older acoustic emission systems used monitors to display received acoustic emission signals, however, more current acoustic emission systems use computer software in combination with monitors to display results.

A **coupling agent** is usually required to ensure the efficient transfer of mechanical energy between the tested material and the transducer. The purpose of placing the coupling material between transducer and test specimen is to eliminate air between the contact surfaces. Typical coupling agents are viscous liquids such as grease, petroleum jelly, and water-soluble jelly.

In acoustic emission testing it is common to bond sensors to the test specimen. This setup is used for long term testing or monitoring of structures and specimens. When applying bonds, it is possible to damage the sensor or the surface of the structure during sensor removal.

Acoustic Wave Propagation Theory

In Acoustic Wave Propagation Theory, when a structure is subjected to an external stimulus, a sudden redistribution of stress triggers the release of energy in the form of transient elastic waves, which propagate to the surface and are recorded by sensors (Figure 2-4). Therefore, the detected signal from a sensor is, in principle, a combination of four factors: a primitive wave released at the AE

source, the propagation medium in which the wave travels, a sensor which transfers the elastic wave into an electric signal and the processor which collects the sensor output signal.

Combined with the primitive wave, the output signal has been through a considerable change. Elastic wave source and elastic wave motion theories are investigated to determine the complicated relationship between the AE source pulse and the recorded movement at the sensor site. However, most researchers and inspectors are not concerned with the intricate knowledge of each source event. Instead, they are primarily interested in the broader, statistical aspects of AE.

Noise Discrimination

The key issue for Acoustic Emission analysis is the ability to discriminate false emission from genuine AE signals. False emissions arise from many sources, such as electromagnetic interference, mechanical friction between an instrumented structure and the surrounding soil, sliding friction, unwanted thermal expansion, and scattering of AE signals from structure boundaries. To eliminate the false AE signals, research has been performed in order to develop various discriminating methods.

- Swansong II filter

A post-processing filter termed “Swansong II” filter has been developed and was recommended by the Association of American Railroads (AAR IM-101). The essential theory is that false AE signals resulting from sliding friction and mechanical friction are always characterized by long durations and low

amplitudes. AE data are removed within the minus and plus 0.5 second of the telltale hits. The Swansong II definition is as following:

If $(A_i - A_{th}) < 5$ and $D_i > 2$,

or $(A_i - A_{th}) < 10$ and $D_i > 3.5$,

or $(A_i - A_{th}) < 15$ and $D_i > 4.5$,

then eliminate all the data during the period $T_i - 0.5$ to $T_i + 0.5$ (seconds), where

A_i = Amplitude at a given hit i (dB),

A_{th} = Data acquisition threshold (dB),

D_i = Hit duration (ms),

T_i = Arrival time for hit I (sec).

The Swansong II filter must be applied on a channel-by-channel basis using specific thresholds for each channel.

- Amplitude versus duration plot

The plot of amplitude versus duration is very useful in distinguishing the spurious AE signals. It has been found that the genuine signals generally create a triangle cluster on the plot, while false hits resulting from mechanical friction and electromagnetic interference appear outside of the triangle (Fowler 1986).

For this project both of the above methods were applied.

Typical Acoustic Emission Parameters

When an AE signal is correctly obtained, parameters like amplitude, counts, measured area under the rectified signal envelope (MARSE), duration, and rise

time can be collected. Each of the AE signal features shown in the image are described below and shown in Figure 2-8.

Threshold: "A voltage level on an electronic comparator such that signals with amplitudes larger than this level will be recognized. The voltage threshold may be user adjustable, fixed or automatic floating" (ASTM E 1316).

Count: "The number of times the acoustic emission signal exceeds a preset threshold during any selected portion of a test" (ASTM E 1316). Depending on the magnitude of the AE event and the characteristics of the material, one hit may produce one or many counts. While this is a relatively simple parameter to collect, it usually needs to be combined with amplitude and/or duration measurements to provide quality information about the shape of a signal.

Amplitude (Peak Amplitude): "The peak voltage of the largest excursion attained by the signal waveform from an emission event" (ASTM E 1316). The amplitude is the absolute value of the greatest measured voltage in a waveform and is measured in decibels (dB). This is an important parameter in acoustic emission inspection because it determines the detectability of the signal. Signals with amplitudes below the operator-defined, minimum threshold will not be recorded. Voltage is converted into decibels through the following equation:

$$A = 20\log\left(\frac{V}{V_{ref}}\right)$$

where A = Amplitude in decibel

V = Voltage of peak excursion

V_{ref} = Reference voltage, typically $1\mu V$.

Duration: "The time between AE signal start and AE signal end" (ASTM E 1316). It is the time difference between the first and last threshold crossings. Duration can be used to identify different types of sources and to filter out noise. Like counts (N), this parameter relies upon the magnitude of the signal and the acoustics of the material.

Rise time: "The time between AE signal start and the peak amplitude of that AE signal" (ASME E 1316). It is the time interval between the first threshold crossing and the signal peak. This parameter is related to the propagation of the wave between the source of the acoustic emission event and the sensor. Therefore, rise time is used for qualification of signals and as a criterion for noise filter.

Signal Strength: The area under the envelope of the linear voltage signal. It is defined through the following equation (Fowler et al. 1989):

$$S_0 = \frac{1}{2}\int_{t_1}^{t_2} f_+(t)dt - \frac{1}{2}\int_{t_1}^{t_2} f_-(t)dt$$

where f_+ = positive signal envelope function

f_- = negative signal envelope function

t_1 = time at first threshold crossing

t_2 = time at last threshold crossing

MARSE: The area under the envelope of the rectified linear voltage signal (ASME V, article 12). It is defined as:

$$S_r = \frac{1}{2}\int_{t_1}^{t_2} f_r(t)dt$$

where f_r = rectified signal envelope function

This can be thought of as the relative signal amplitude and is useful because the energy of the emission can be determined. MARSE is also sensitive to the duration and amplitude of the signal, but does not use counts or user defined thresholds and operating frequencies. MARSE is an approximation of signal strength.

Energy: "The energy contained in a detected acoustic emission burst signal, with units usually reported in joules and values which can be expressed in logarithmic form (dB, decibels)" (ASTM E 1316). Energy is defined as:

$$E_t = \frac{1}{2}\int_{t_1}^{t_2} f_+{}^2(t)dt - \frac{1}{2}\int_{t_1}^{t_2} f_-{}^2(t)dt$$

Hit: "The detection and measurement of an AE signal on a channel" (ASTM E 1316).

Event: "A local material change giving rise to acoustic emission" (ASTM E 1316).

Kaiser Effect: "The absence of detectable acoustic emission at a fixed sensitivity level, until previously applied stress levels are exceeded" (ASTM E 1316).

Felicity Effect: "The presence of detectable acoustic emission at a fixed predetermined sensitivity level at stress levels below those previously applied" (ASTM E 1316). The Felicity Effect is a breakdown of the Kaiser Effect. It occurs when the structure generates emission during reloading, before the previous

maximum stress is reached. The Felicity Ratio is an indication of the amount of damage, and is defined as the ratio of the load at which emissions occur to the previous maximum load:

$$Felicity \quad Ratio = \frac{load \quad at \quad which \quad emissions \quad occur}{previous \quad \max imum \quad load}$$

Historic index: Historic Index is a parameter to determine the changes of signal strength rate throughout a test. It measures changes in slope of the cumulative signal strength per hit. The Committee on Acoustic Emission from Reinforced Composites (CARP) procedure defines historic index as:

$$H(t) = \frac{N}{N-K}\left(\frac{\sum_{i=K+1}^{N} S_{oi}}{\sum_{i=1}^{N} S_{oi}}\right)$$

H(t) = historic index at time t;

N = number of hits up to and including time t;

S_{oi} = signal strength of the ith event;

K = empirically derived constant based on material type. For fiber reinforced composite materials, K is defined as in Table 2-3.

Historic Index is normally low at the beginning of a test and increases with increasing damage. A jump in the historic index can be seen once the structure starts having significant damage.

Severity: The average signal strength of J hits having the maximum numerical value of signal strength (MONPAC 1992). Severity is defined as:

$$S_r = \frac{1}{J} \cdot \left(\sum_{i=1}^{J} S_{om}\right)$$

S_r = Severity, the average signal strength for a given number of events (J) compared to the largest value.

S_{om} = signal strength of the mth hit, with the ordering of m based on magnitude of signal strength.

J = empirically derived constant based on material type. For fiber reinforced composite, J value is defined as in Table 2-4.

Scanning Electron Microscope

The Scanning Electron Microscope (SEM) is a type of electron microscope that scans the sample surface with an electron beam and forms images. The images result from interactions of the electron beams with atoms at the sample surface. Compared with traditional optical microscopes, the SEM has a large depth of field which yields a characteristic three-dimensional appearance for better understanding the surface structure of the sample. SEM produces very high resolution images which reveal details less than 1 to 5 nm in size. It also has more control in the degree of magnification with a range from 10 to more than 500,000 times. With these advantages, the SEM is one of the most widely used instruments in material research.

SEM Testing

The current project used the University of Florida Material Lab's SEM (model number JSM-6400 provided by JEOL LTD). It is shown in Figure 2-6 A, while Figure 2-6 B provides details of the column structure. The beam of electrons emanates from an electron gun at the top of the microscope by heating a metallic filament. The anode forms powerful attractive forces and causes

electrons to accelerate toward the anode and down the vacuum column. The electromagnetic lenses and fields impose a force along the axis of the electrons and focus the beam towards the sample. When the electron beam interacts with the sample surface, the electrons exchange energy with the sample atoms, resulting in the reflection of high-energy electrons by elastic scattering, emission of secondary electrons by inelastic scattering and the emission of electromagnetic radiation. These electrons are collected by detectors, converted to a voltage, and amplified. The amplified voltage is digitalized as variations in brightness and thus a distribution map of the intensity of the signal being emitted from the scanned area of the specimen. In modern machines, the image is displayed on a computer monitor and saved to a hard drive.

Sample Preparation

Special sample preparation has to be performed prior to SEM observation. For most conventional SEM machines, any water and/or solvents must be removed from the sample or else they would vaporize and impair the vacuum environment in the column. A non-metallic sample needs to be made conductive by covering it with a thin layer of conductive material in order to prevent the accumulation of electrostatic charge at the surface, to maximize the signal, and improve spatial resolution. All samples must be sized to fit in and mounted firmly in the sample chamber.

SEM Applications

The SEM permits the observation of materials in macro and submicron ranges. The instrument is capable of generating three-dimensional images for analysis of topographic features. In the fiber reinforced composites, the SEM had

been used with Acoustic Emission to analyze damage mechanisms (Barlow et al. 1990)

Fracture Mechanism of Fiber Reinforced Composites in the Literature

Failure of composite materials often involves more than one damage mode, such as matrix cracking, fiber breaking, fracture of the fiber-matrix interface, delamination and fiber pull-out (Barlow et al. 1990).

Splitting of a thin ply unidirectional reinforced material along its fiber direction is the most simple damage mode in a composite. The composite will fail via a single damage mode, i.e. matrix cracking. Slight deviation of the crack path or of the fiber alignment will cause the crack front to intercept the fiber-matrix interface. If the interface is weak, fracture of the fiber-matrix interface will occur as a second damage mode in the failure process. The crack front will then continue to propagate within the fiber-matrix interface.

The crack front may also kink out from the fiber-matrix interface into the adjacent fiber, causing the fibers to break. In this case the failure process will be governed by a combination of three damage modes, i.e., matrix cracking, fiber-matrix fracture, and fiber breaking. If the fiber-matrix interface is strong enough, the crack front which intercepted the interface will continue to propagate into the fibers, breaking them. Thus, failure of the composite will be controlled by a combination of matrix cracking and fiber breaking.

Sato and Kurauchi (1997) studied the failure process of three different composites: short-glass fiber reinforced thermoplastic polyamide (FRTP), sheet molding compound (SMC), and carbon-fiber reinforced epoxy resin composite (CFRP). The damage process for FRTP initiated with interfacial failure,

developed with matrix crack and fiber pull-out at final failure. The microfailure process of SMC started with inner strand crack propagating along the fiber/matrix interface. Intra-strand cracking results from accumulation of microcracks in the boundary between the strands. The first indication of failure for CFRP, on the other hand, was observed to be fiber breakage. With the increasing load, matrix crack occurred from the tip along the fiber. Just before failure, breakage of fiber bundle accompanied by delamination failure occurred. The research showed that the failure process of different types of composites depends on the materials property and can occur in various sequences. The results are shown in Figures 2-7, 8 and 9.

Fracture Mechanism of Fiber Reinforced Composites and AE Parameters

It is a common aim among researchers and engineers to establish a correlation between damage modes and characteristics of their acoustic emission signals. Peak amplitude is the most frequent acoustic emission parameter. From several studies on FRP, the larger amplitude acoustic events are generally associated with fiber breakage, whereas matrix cracking is more likely to produce medium-to-low amplitude signals. Quantitative results differ among individual studies due to variation in particular load tests, acquisition equipment and type or size of the test materials. Barre and Beneggagh (1994) provided a range of AE amplitude values measured for glass-fiber- reinforced polypropylene composites: 40-55 dB for matrix cracks, 60-65 dB for interfacial fracture, 65-85 dB for fiber pullout and 85-95 dB for fiber fracture. For carbon / epoxy composites, Komai et al. (1991) suggested less than 60 dB for interfacial debonding, less than 70 dB for matrix failure and less than 75 dB for fiber

fracture. Ji and Ong (1994) reported less than 30 dB for delamination, 30-40 dB for matrix cracks, and 40-80 dB for fiber fracture. Similar trends were observed by Rizzo and Lanza (2001).

The frequency content of AE signals can similarly be associated with a particular type of damage. Specifically, fiber and matrix failures in carbon-reinforced composites are generally associated with higher and lower acoustic frequencies. De Groot et al. (1995) proposed four ranges corresponding to acoustic frequency released by different types of damage: 90-180 kHz for matrix cracking, 180-310 kHz for fiber pullout or debonding, and more than 300 kHz for fiber failure. Surgeon and Wevers (1999) measured the acoustic frequency of matrix cracks below 530 kHz and fiber failure in the 1,000-2,000 kHz range. Bohse (2000) proposed ranges of 100-350 kHz and 350-700 kHz for matrix and fiber failure. For fiber-reinforced concrete, Kumar and Gupta (1996) reported low frequencies corresponded to failure in mortar, while frequency around 800 kHz accompanies fiber bond failure.

Analysis of AE Amplitude Distribution

AE amplitude distribution is a histogram of the number of hits at different amplitudes. Barre and Benzeggagh (1994) studied the amplitude distribution for short-glass-fiber-reinforced thermoplastics. Figure 2-10 shows an example of an amplitude distribution plot, which is number of hits versus amplitude. α, β, γ and δ represent different stress levels. The amplitude distribution for various materials showed different behaviors, and tended to confirm the materials'

hypothesized properties. For example, for the material with poor adhesion quality, its AE amplitude distribution exhibited more AE events linked to fiber pull-out.

Berthelot and Rhazi (1986) conducted an experiment with steel fiber-epoxy composites. They categorized three types of amplitude distribution, namely, discontinuous, continuous and intermediate distribution (Figure 2-11). It was believed that the discontinuous distribution was associated with the development of the basic failure modes in composites; while continuous distribution was characteristic of development of complex failure modes.

Amplitude distribution has been widely studied by many researchers' work. Several researchers have studied it and good correlations were observed between fracture mechanisms and several ranges of AE amplitude (Pollock 1978, Valentin, 1985).

Cumulative Amplitude Distribution and b-value Theory

Pollock published a paper on the application of cumulative amplitude distribution and theory of b-value (Pollock 1978). The cumulative amplitude distribution is a log plot of histogram of the number of hits at named amplitude and higher. The slope of the plot is termed the b-value. An example is given in Figure 2-12.

Theory of b-value

As mentioned before, the amplitude in dB is derived through the following equation:

$$A = 20\log\left(\frac{V}{V_{ref}}\right)$$

where A = Amplitude in decibel

V = Measured voltage

V_{ref} = Reference voltage, typically $1\mu V$.

Each measured voltage corresponds to a dB amplitude. For the purposes of simplicity, we discuss voltage first. Given F(V) is a cumulative amplitude distribution plot of the number of hits for which the amplitudes are equal to or higher than the value V. $\Phi(V)$ is a normalized function representing the probability that amplitude exceeds V. Then the relationship between F(V) and $\Phi(V)$ is:

$$F(V) = N_0 \Phi(V),$$

where N_0 = total number of hits. Note that for the smallest value of V, V_0, $\Phi(V_0) = 1$.

In 1981, Pollock suggested the function:

$$\Phi(V) = \left(\frac{V}{V_0} \right)^{-b},$$

where b = parameter characteristic of the distribution function.

Therefore,

$$F(V) = N_0 \left(\frac{V}{V_0} \right)^{-b}.$$

Taking the log on both sides, the equation becomes

$$\log F(V) = -b \log \left(\frac{V}{V_0} \right) + \log N_0 .$$

Now considering the relation between amplitude and voltage, we have,

$$\log F(A) = -B(A - A_0) + \log N_0 ,$$

which can be simplified to

$$\log F(A) = -BA + C,$$

in which C is a constant, and $B = \frac{b}{20}$.

The above equation means that if we plot the histogram of the number of hits above a specified amplitude, e.g., F(A) or F(V) in log scale versus amplitude, the resulting plot is a straight line with slope equal to –B or -b.

Pollock claimed that this B value is unique for each failure mechanism and the log scale will remove the effect of wave attenuation, if the signals are attenuated equally for each amplitude (Pollock 1981). Thus, the changing of B value can be explained as the transition from on mechanism to another. The average of b-values ranges from 0.7 to 1.5, but with possible low value as 0.4 or high value as 4.0. The lower values always imply discontinuous crack growth in high-strength brittle metals, where the high values result from plastic zone growth prior to crack extension.

Summary

In this part, we discussed the background information on CFRC, its material composite and manufacturing process. We reviewed the fracture process for fiber reinforced composites, which are believed to include matrix fracture, fiber-matrix breakage, fiber pull-out and fiber breakage. Literature on the relationship between AE amplitude and the fracture mechanism was reviewed. Good correlations were found by various researchers for different types of materials. Two experimental tools, SEM and AE technology were discussed in detail, and a

literature review was made on the application of AE analysis. The following is a summary of the literature review:

1. AE is one of the most effective and reliable testing methods for evaluating composite materials. It is widely utilized in research work as well as in-situ field testing.

2. A large amount of research has been done to establish the relationship between amplitude and fracture mechanism. For different types of materials, the correlation was found to be different.

3. Typical AE parameters such as amplitude, hit, count, energy have been studied. Other useful parameters such as Historic Index, Severity, amplitude distribution, b-value theory are also introduced here in detail.

4. It is believed by the author that the analysis methods involving whole data sets and their evolution are more promising. Such methods include amplitude distribution, cumulative amplitude distribution and Historic Index. The determination of b-value is expected to be very useful in field testing since it reduces the influence of attenuation.

Table 2-1. Chemical composition of ASTM Type I Portland cement by SAC

Chemical Composition	Percent by mass
SiO_2	20.4
Al_2O_3	5.2
Fe_2O_3	3.3
CaO	64.0
MgO	0.8
C_3S	51
C_3A	8
SO_3	3.3
CO_2	1.1
Limestone	3.5
Limestone $CaCO_3$ content	74
Insoluble Residue	0.17
Equiv. Alkalies ($Na_2O+0.658K_2O$)	0.31
Sum of $C_3S + 4.75\ C_3A$	90
Loss on Ignition	2.2

Table 2-2. Important data on Kraft wood fiber

Material	Density ($lbs/\ ft^3$)	Tensile Strength (psi)	Elastic Modulus (ksi)
Softwood Fiber	22	7250	800

Table 2-3. Definition of K for Historic Index (CARP, 1999)

Number of Hits (N)	K Value
<20	Not applicable
20 to 100	0
101 to 500	0.8N
>500	N-100

Table 2-4. Definition of J for Severity (CARP, 1999)

Number of Hits (N)	J Value
<20	Not applicable
>20	20

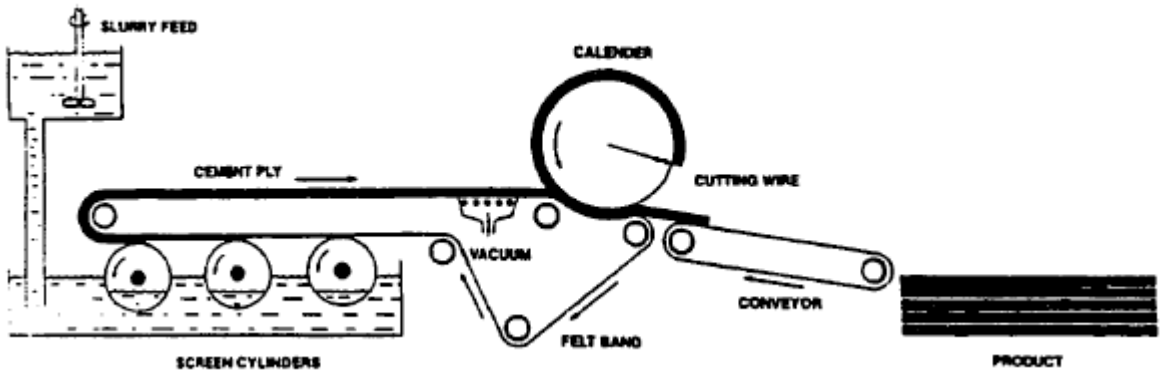

Figure 2-1. Schematic drawing showing the basic Hatschek machine.

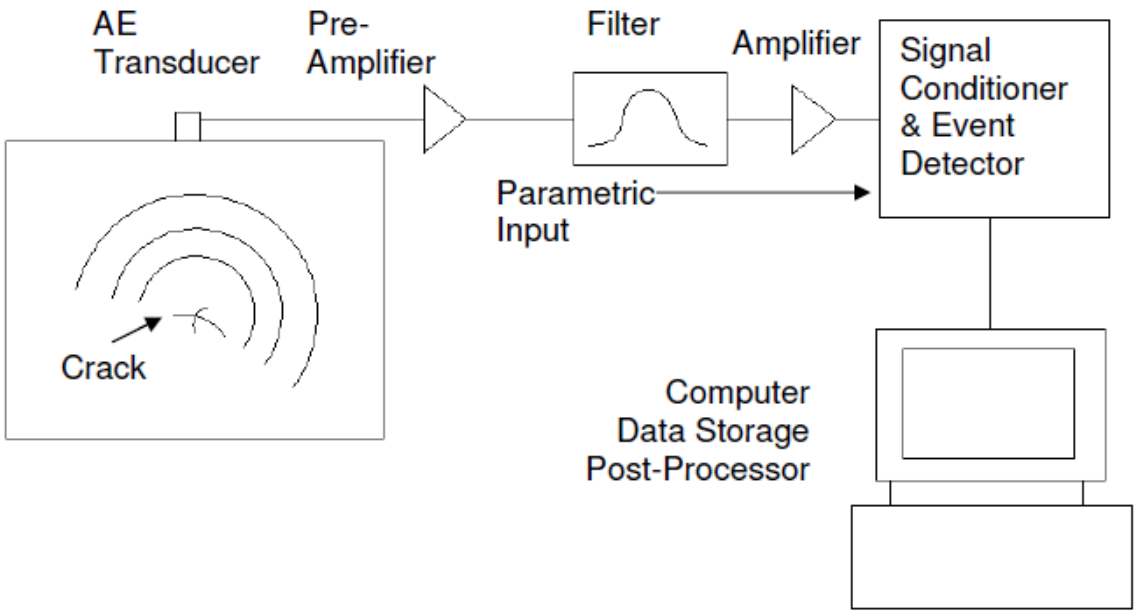

Figure 2-2. A typical AE system

Figure 2-3. Various Acoustic Emission sensors (Miller 1985)

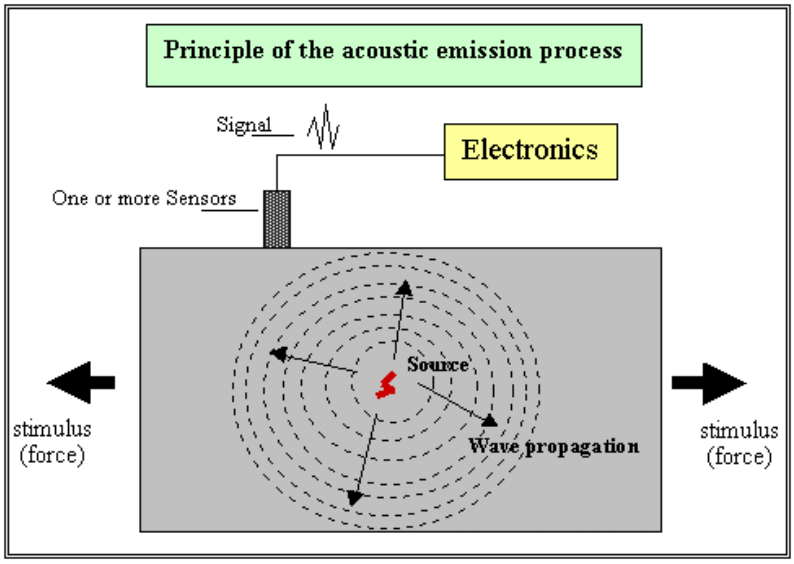

Figure 2-4. Acoustic wave propagation. (Vallen 2002)

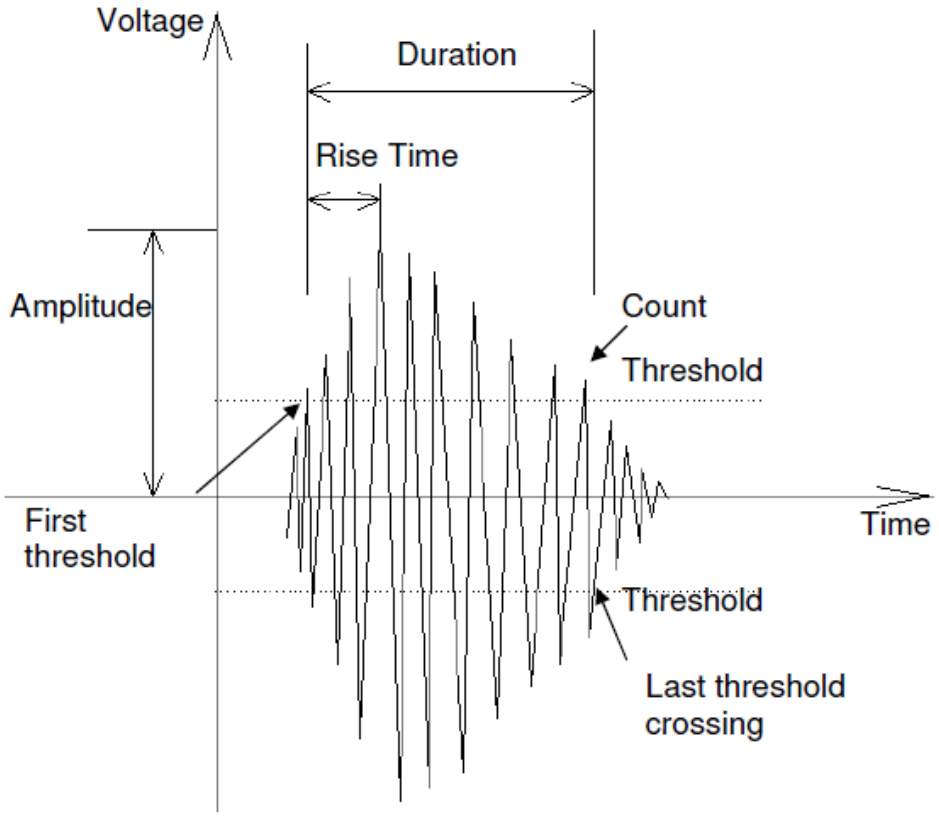

Figure 2-5. Acoustic Emission signal parameters

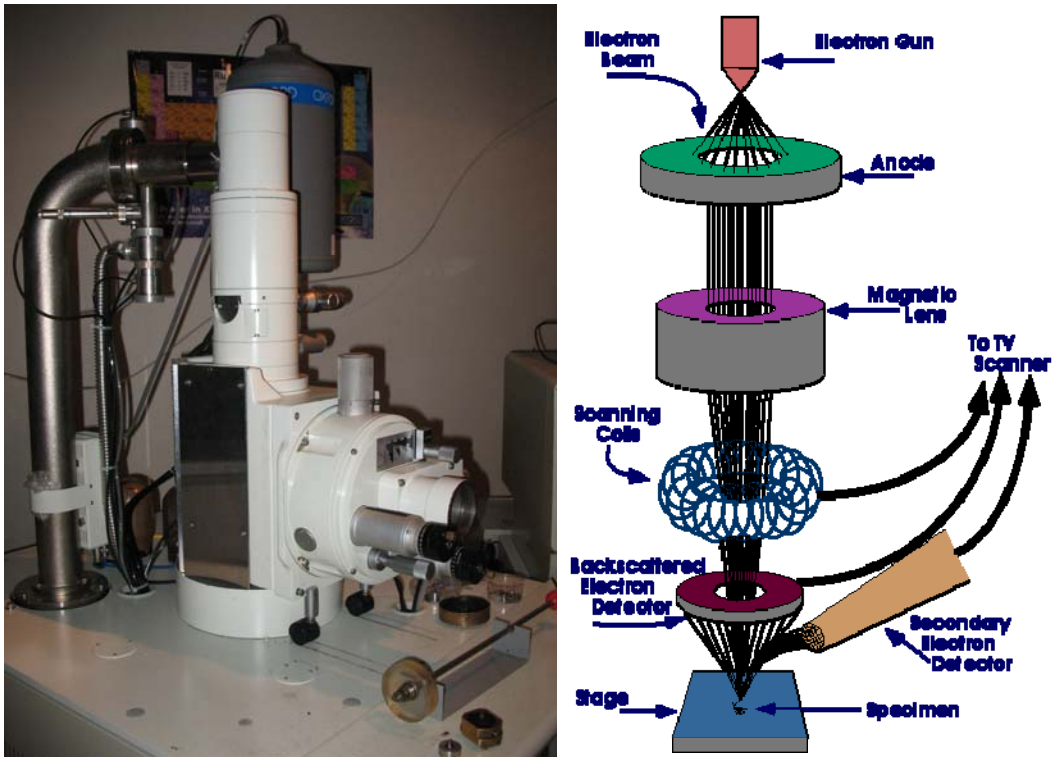

A B

Figure 2-6. SEM machine setup A. JEOL SEM machine at the University of Florida; B. SEM column structure (Iowa State University SEM Homepage)

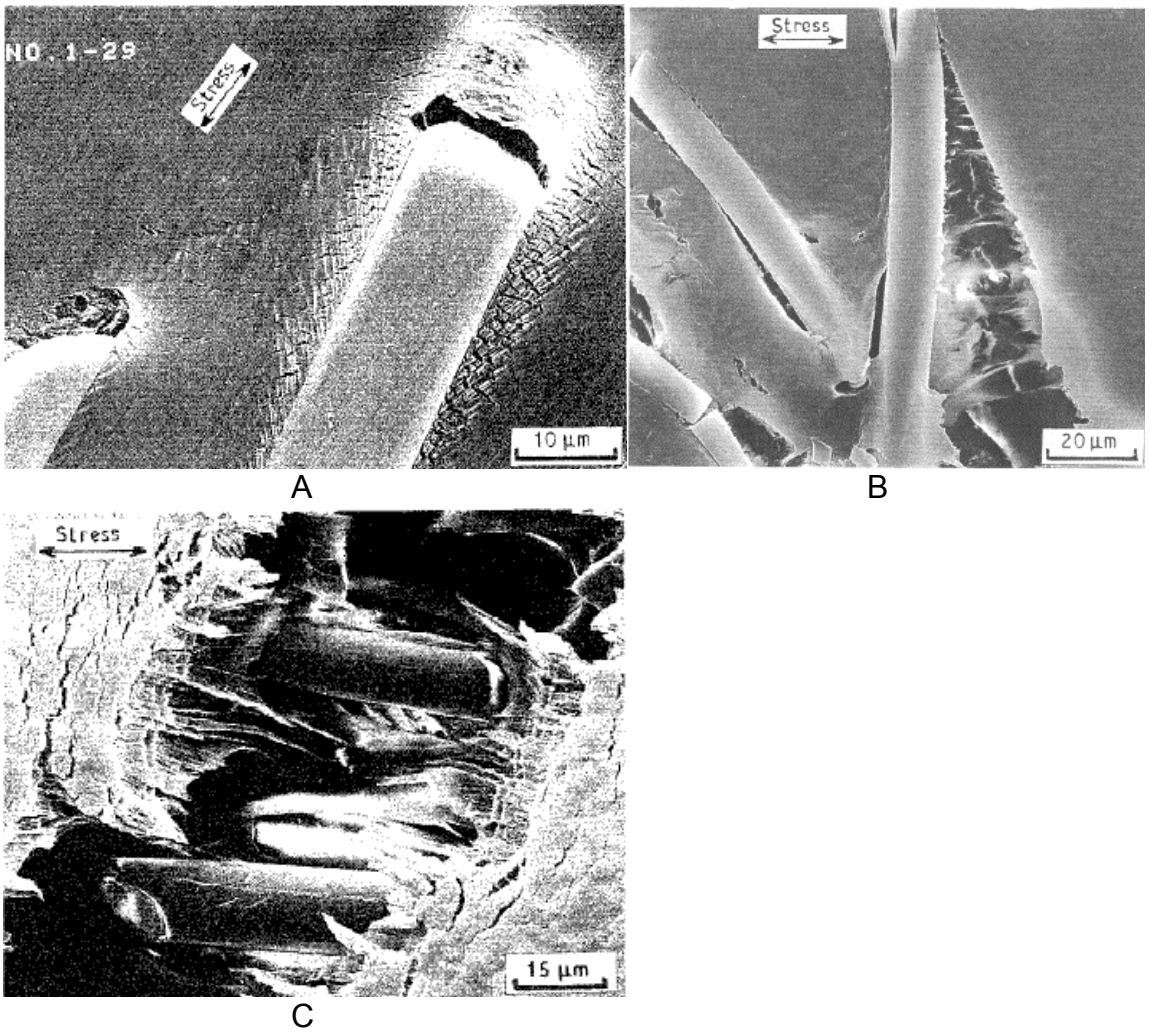

A B C

Figure 2-7. Microfailure process of FRTP (Sato and Kurauchi 1997). A. Interfacial failure; B. Matrix crack; C. Fiber pull-out.

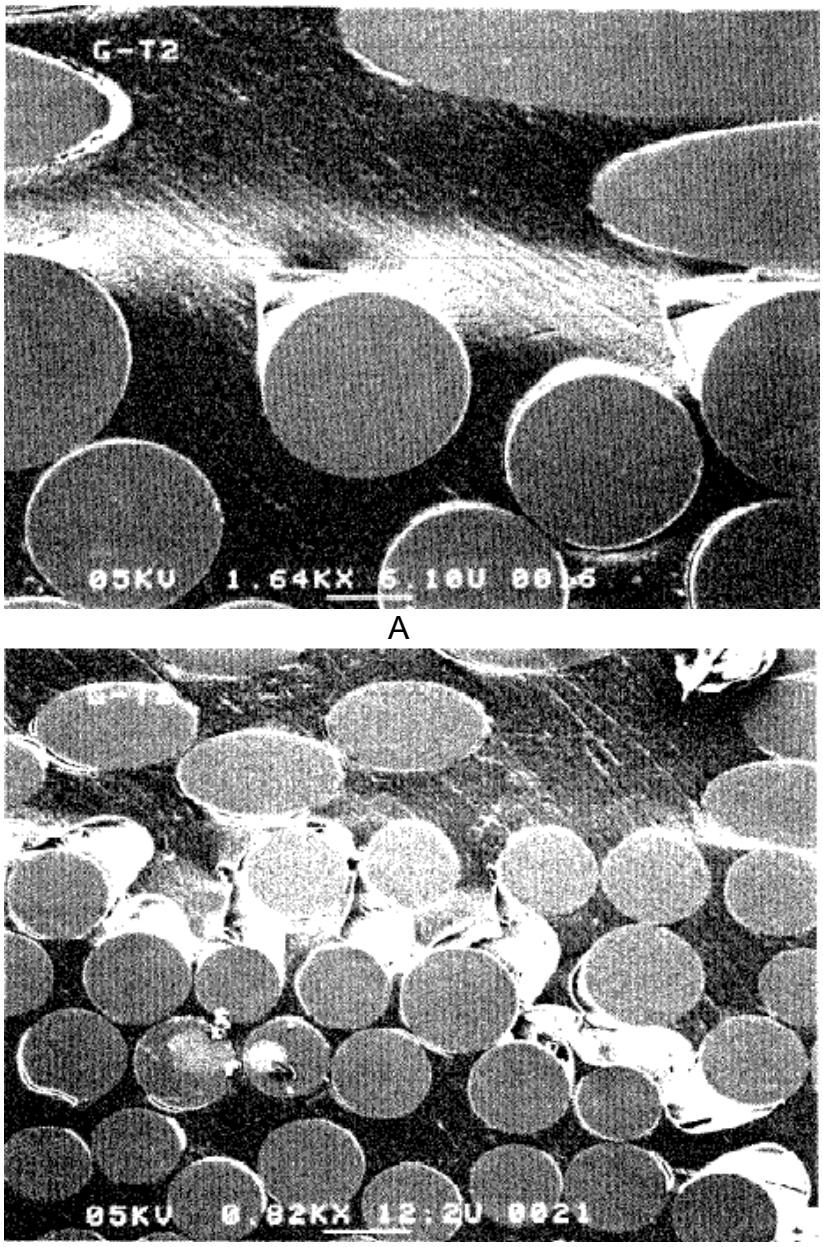

Figure 2-8. Microfailure process of SMC (Sato and Kurauchi 1997). A. Inner Strand crack; B. Intrastrand crack.

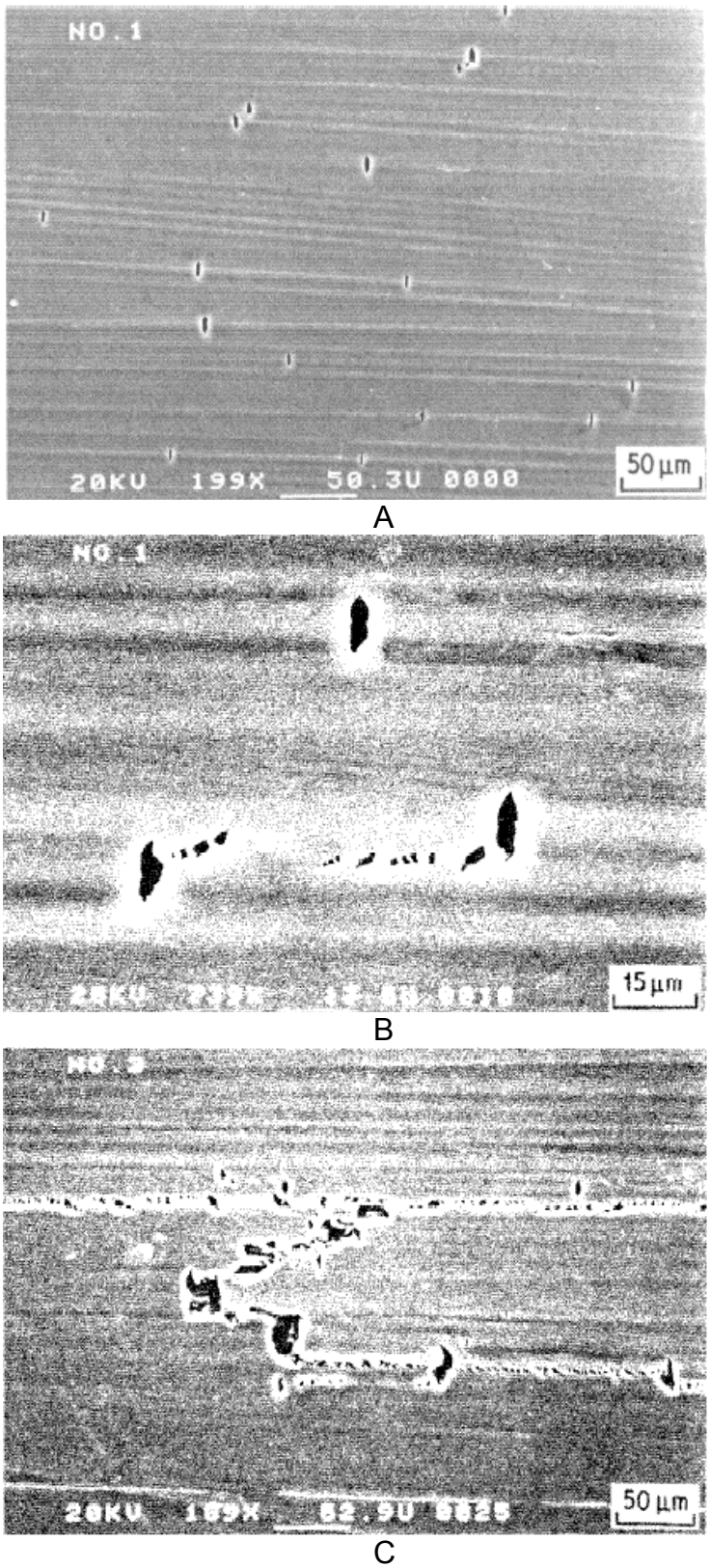

Figure 2-9. Microfailure process of CFRP (Sato and Kurauchi 1997). A. Fiber breakage; B. Matrix crack; C. Delamination failure.

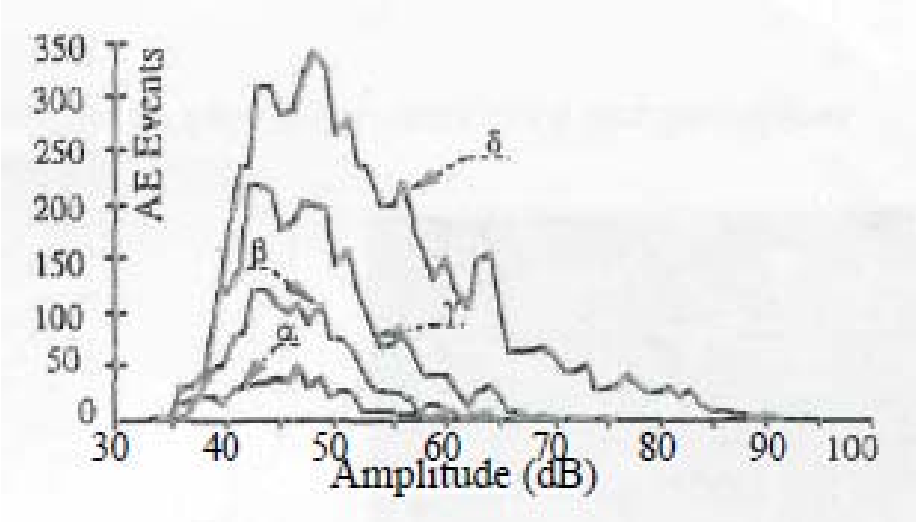

Figure 2-10. AE amplitude distribution (Barre and Benzeggagh 1994)

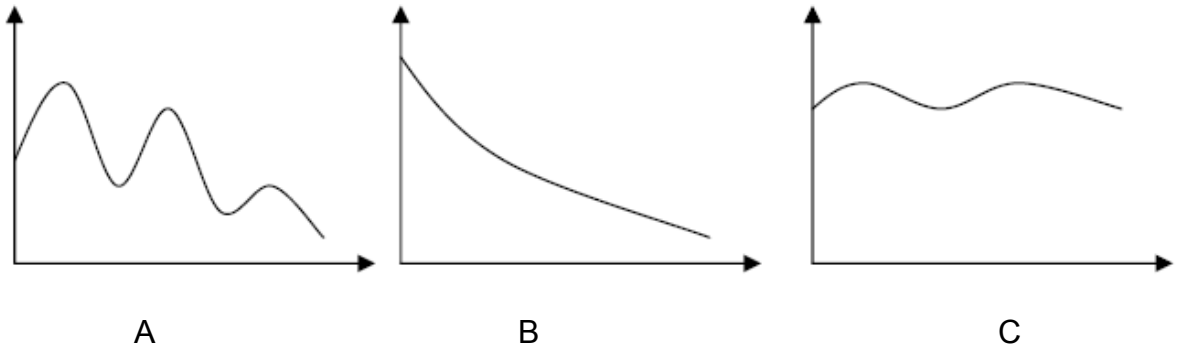

Figure 2-11. Three types of amplitude distribution A. Discontinuous; B. Continuous; C. Intermediate.

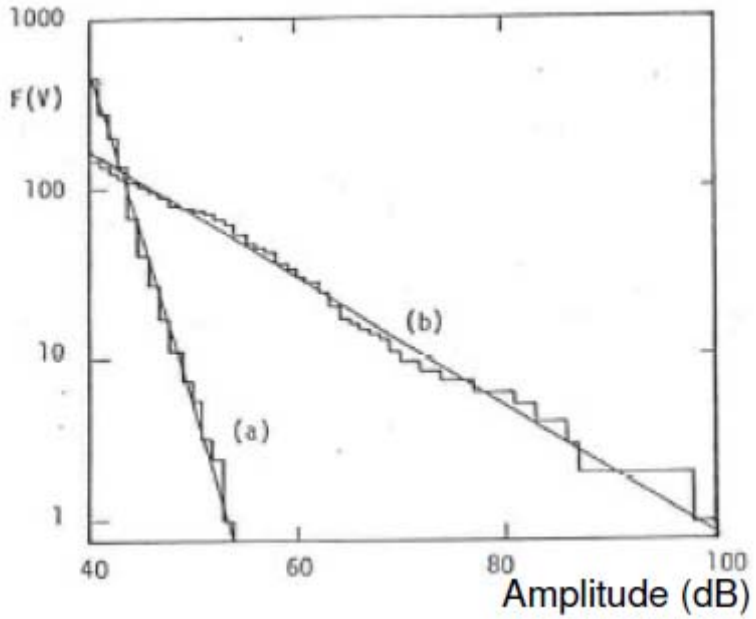

Figure 2-12. Cumulative Amplitude Distribution Plot a) plastic zone growth in A516 steel b) stress corrosion cracking in 4340 steel (Pollock 1978).

CHAPTER 3
FRACTURE MECHANISM

Introduction

The objective of this study is to use the SEM to identify the fracture mechanisms of CFRC specimens by observing different load stages. This study includes third-point bending tests of three identical CFRC specimens. Evolution of the failure mechanisms was determined by comparing the SEM observation. AE was also used during the tests in order to correlate the AE data with fracture mechanisms. The AE and fracture mechanism information are used as a foundation in understanding CFRC based material and structures in the following experiments.

Experimental Program

Four CFRC coupon specimens were cut from the same pipe section. Their dimensions followed ASTM C 78, which were 8 inch long, 2 inch wide and 2 inch thick. Before testing, the samples were cleaned carefully using acetone to remove dust.

Static third-point bending tests were performed by monotonically loading them to different maximum loads. After specific load levels were reached, the specimens were unloaded and cut into small pieces. The pieces were carefully examined with a scanning electronic microscope to observe different fracture levels on their surface. Table 3-1 shows the designation of specimens and their maximum loads. Specimen SEM3 was loaded to failure. The maximum stresses imposed on the other two specimens were determined to be 70% and 95% of ultimate stress. SEM1 was unloaded at 70% to observe the early fracture

mechanism where acoustic emissions remained between 45 and 65 dB. SEM2 was unloaded at 95% of the ultimate load in order to observe the evolution of fracture mechanisms during the final failure phase.

Physical Results

Strain gages were placed along the center line at the bottom of the samples. The measured maximum strains and stresses calculated from beam theory are given in Table 3-2. The testing procedures for the three tests were video taped. No visual damage was observed for SEM1 and SEM2. Since the only specimen loaded to failure was SEM3, its visual damage was observed only in the last half second as shown in Figure 3-1. The crack initiated from the bottom up to the top, and the macro-crack was roughly along the center line of the specimen.

SEM Results

Although for SEM1 and SEM2 no damage was observed visually, microscopic damage did appear in the SEM images showing the damage evolution. For each of the specimens, three small sections were photographed in the SEM.

Specimen SEM1 (70% of the ultimate load)

For SEM 1, two of the sections were cut in sizes 1 inch by 1 inch, and 1 inch by 0.3 inch. Figure 3-2 shows an image taken of the smaller piece. It showed shallow and smooth cracks over the surface. The cracks are believed to result from the cutting process during SEM preparation. Therefore compared to the other images the image does not provide proof of damages associated with testing. In order to avoid the influence of cutting, specimens for SEM2 and SEM3 were both cut 1 inch by 1 inch. In the other two small specimens from SEM1,

only a few cracks were observed as shown in Figure 3-3. The cracks were sharp and propagated deep into the internal structure, and it was believed to be associated with matrix cracking.

Specimen SEM2 (95% of the ultimate load)

When the load reached 95%, both matrix-cracking and fiber/matrix debonding occurred as shown in Figure 3-4. One can see the sharp tip propagating between the matrix and fiber in Figure 3-4A and B. At the same time, Figure 3-4C and D shows a fiber being pulled out of the matrix. The long, string-like object in the image is a fiber with its end embedded in the matrix, and the part pulled out has been detached from the matrix. The debonding between matrix and fiber was still developing.

Specimen SEM3 (100% of the ultimate load)

Specimen SEM3 was loaded to failure. The specimen broke into two parts. Samples were taken from the cross section to observe the damage. From Figure 3-5A, one can see fibers totally pulled out of matrix, with some of the fibers broken in the middle. Figure 3-5b shows a broken section at the end of a fiber.

AE Results

Table 3-2 presents the total number of AE hits for each specimen. It is clear that with the development of loading and therefore damage, the number of AE hits increased as well.

The amplitude versus normalized load for all specimens is shown in Figure 3-6. It was noticed that for SEM1, as in Figure 3-6A, the majority of AE amplitude remains within 45 dB to 65 dB range and the AE signals were scattered hits. For SEM2, there was a dramatic increase in number of AE hits and high amplitude

hits, i.e., amplitude between 65 dB and 75 dB. Specimen SEM3 emitted high amplitude hits, that is, amplitude higher than 75 dB with the maximum value of 99 dB.

Discussion

From these tests, three fracture mechanisms were identified from the SEM: matrix cracking, fiber/matrix debonding, and fiber breakage. Matrix cracking was observed for all three load levels. Fiber breakage was observed only after final failure, when the cross section was available to be inspected.

The matrix cracking is found to be associated with low amplitude hits ranging from 45 dB to 65 dB, and the signals were scattered emissions. Thus it was concluded that the AE which occurred at the beginning of the test actually correlated with matrix cracking, with little debonding of fibers and matrix. For CFRC material, the low amplitude AE dominates until the occurrence of higher amplitude AE at roughly 85% of maximum stress.

It is believed that the middle amplitude AE, i.e., AE amplitude between 65 dB and 75 dB, is an indication of fiber-matrix debonding. Above that, with increasing load, the stress is redistributed between fiber and matrix. Debonding occurs between the fiber and matrix due to the difference in their deformation characteristics.

Previous research results performed by others show that high amplitude hits were associated with fiber breakage. In this research, it was noted that after the AE amplitude reached 75 dB, failure would occur with very little increase of load. At this damage level, the number of hits increased exponentially, while AE beyond 75 dB also occurred. SEM observed fiber breakage solely at this damage

level. Therefore it is concluded that for CFRC, high amplitude AE can be considered as an indication of fiber breakage and ultimate failure.

Table 3-4 summarizes the observed fracture mechanisms for each load level and their AE amplitude ranges. Generally speaking, with the evolution of damage the AE amplitude increases from low to high levels.

An illustration of the fracture process model is shown in Figure 3-7. The damage starts with scattered matrix cracking. With increasing load, the microcracks propagate through the matrix and start to develop between the fiber and matrix. At the end of the damage phase, the material is broken into two parts. At the cross section, some of the fibers are pulled out from the matrix and others broken.

Table 3-1. Description of specimens and maximum loads.

Specimen	Maximum Load (percentage of ultimate load)
SEM1	70
SEM 2	95
SEM 3	100

Table 3-2. Results of maximum stress and strain for each specimen.

Specimen	Maximum stress (psi)	Maximum strain $(\times 10^{-3})$
SEM1	1,060	2.76
SEM 2	1,438	4.05
SEM 3	1,520	5.07

Table 3-3. Summary of total number of AE hits for each specimen.

Specimen	Total number of AE hits
SEM1	231
SEM2	2,175
SEM3	16,250

Table 3-4. Correspondence between fracture mechanism and AE amplitude

Dominate Mode of Damage	AE Amplitude
Cement Matrix Microcracking	45-65 dB (low amplitude)
Fiber/matrix debonding	65-75 dB (middle amplitude)
Fiber Breakage	>75 dB (high amplitude)

A (ΔT=0.00 sec)

B (ΔT=0.07 sec)

C (ΔT=0.14 sec)

D (ΔT=0.21 sec)

E (ΔT=0.28 sec)

F (ΔT=0.35 sec)

G (ΔT=0.42 sec)

Figure 3-1. Crack propagation for a CFRC beam.

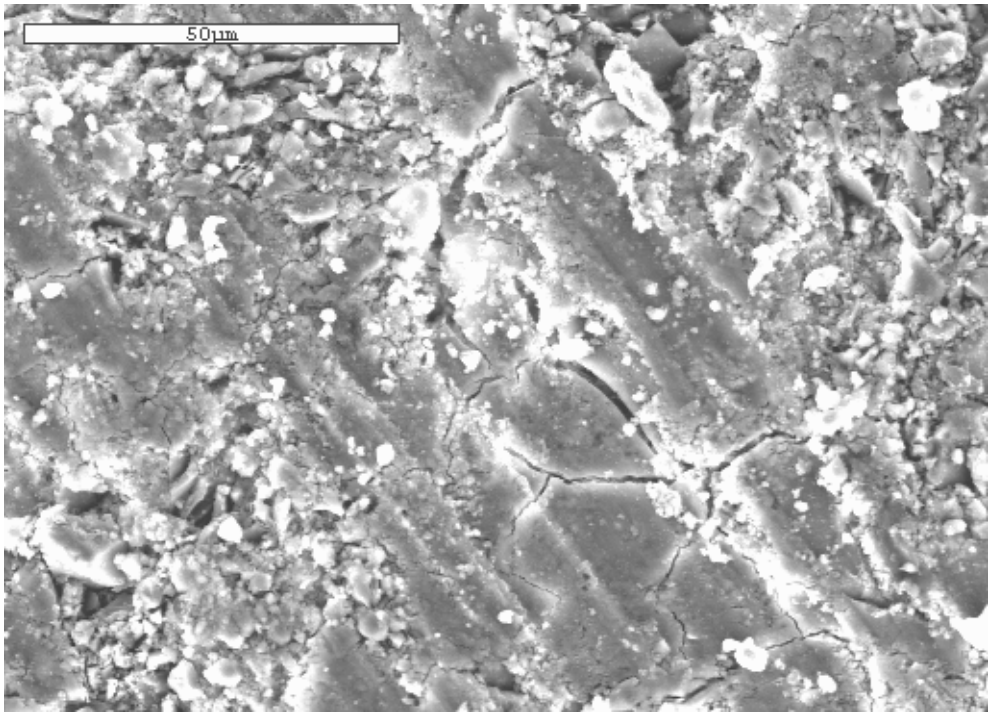

Figure 3-2. SEM image of specimen SEM1.

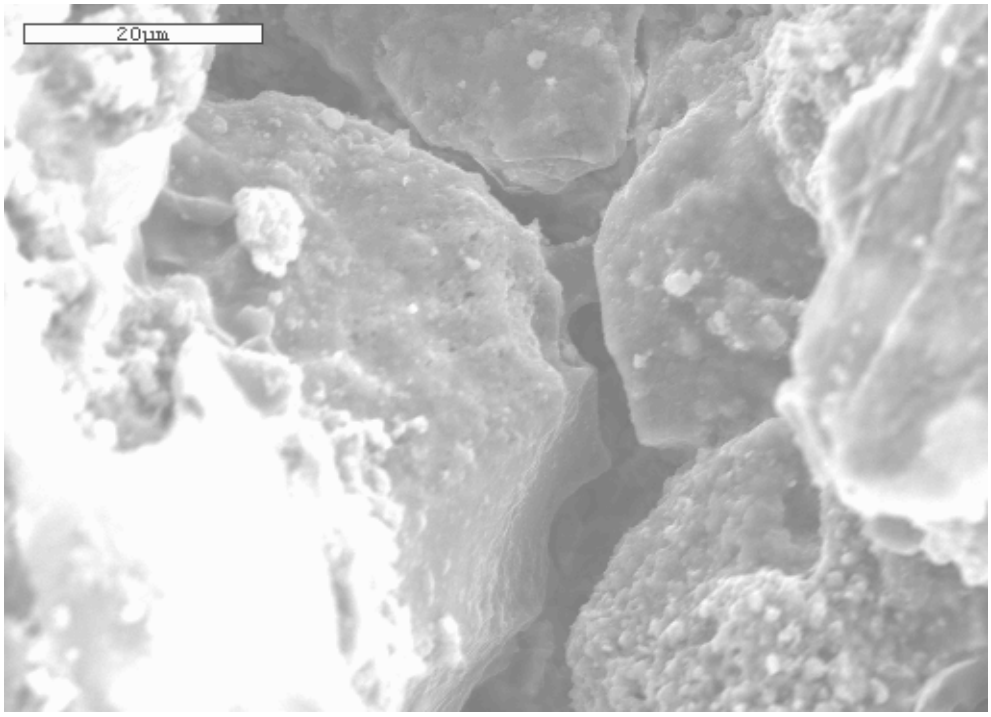

Figure 3-3. Matrix cracking of specimen SEM1

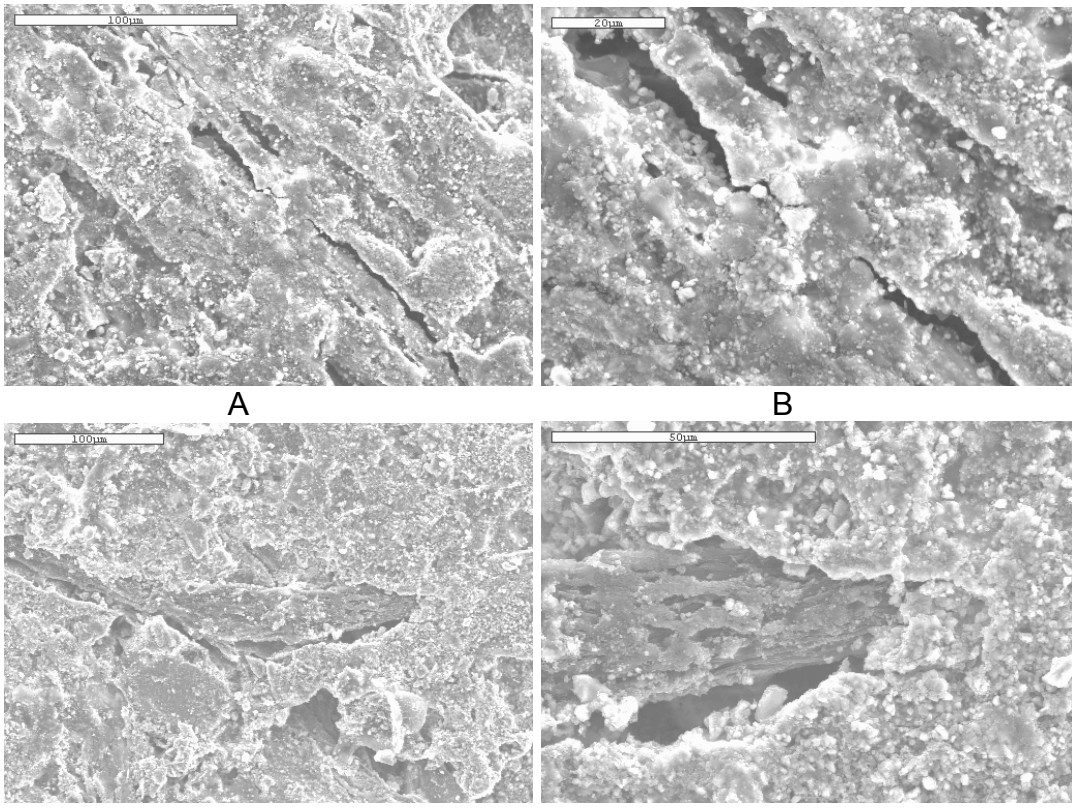

Figure 3-4. Fiber/matrix debonding of specimen SEM2. A. Matrix/fiber breakage; B. Close-up photo of fiber/matrix debonding; C. A fiber is being pulled out of matrix D. Close-up photo of crack tip.

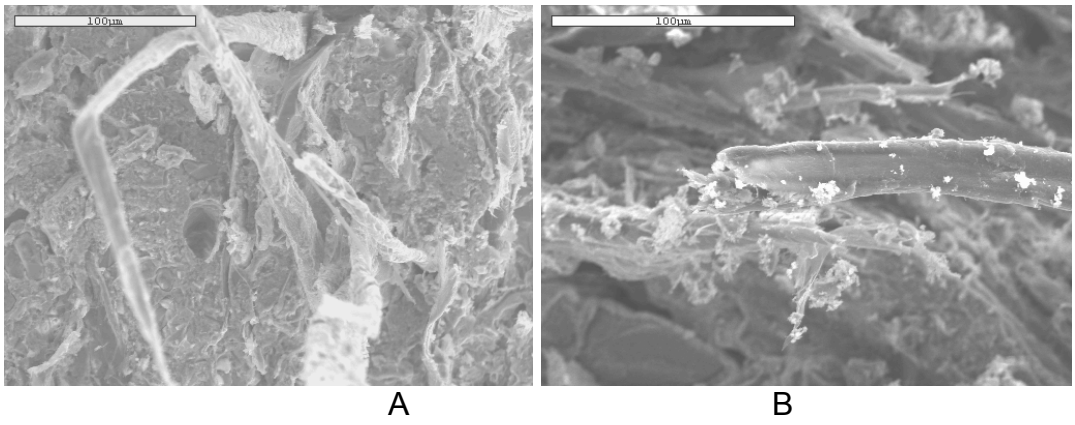

Figure 3-5. Fiber pullout and breakage of specimen SEM3. A. Fiber pullout; B. Fiber breakage.

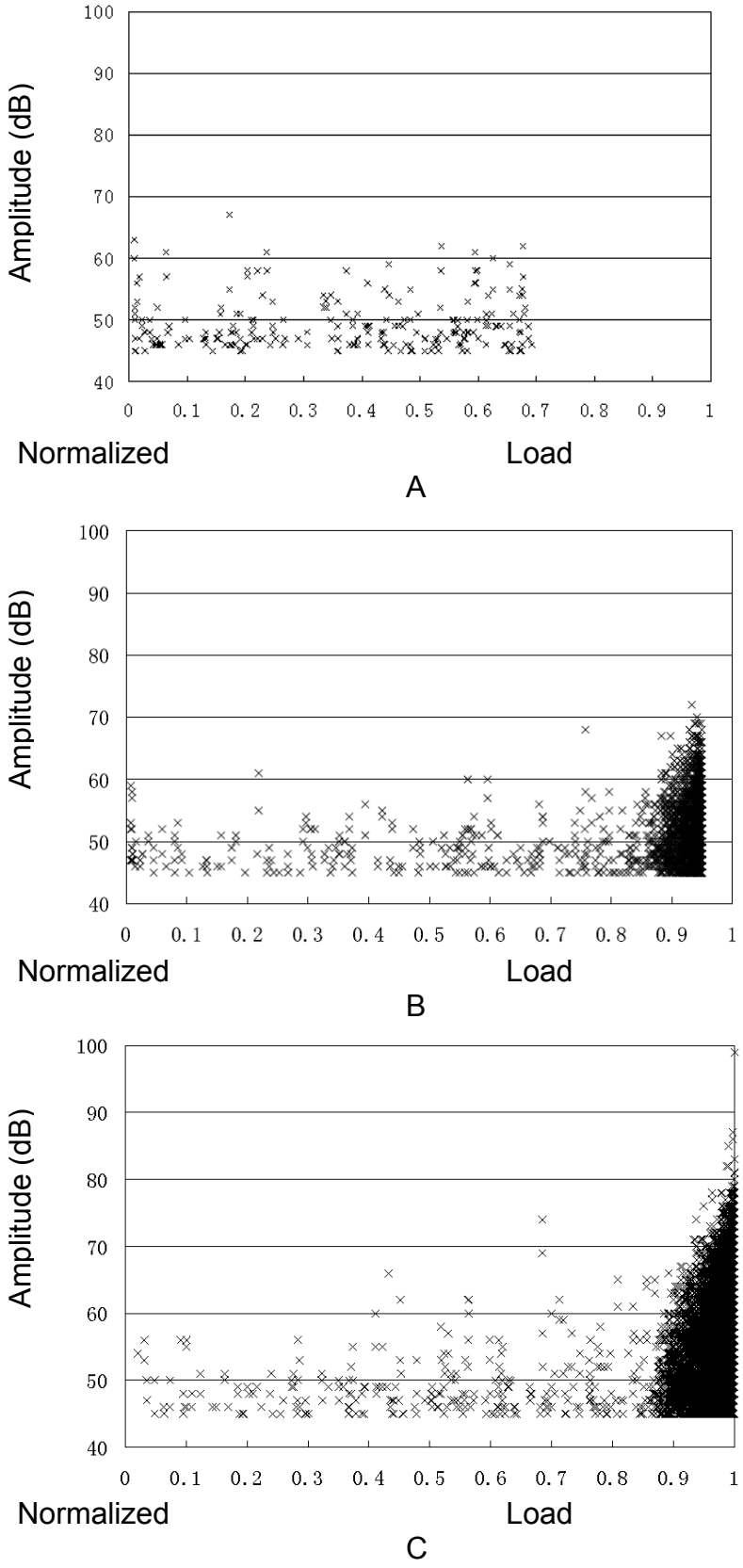

Figure 3-6. AE amplitude versus normalized load A. SEM1; B. SEM2; C. SEM3.

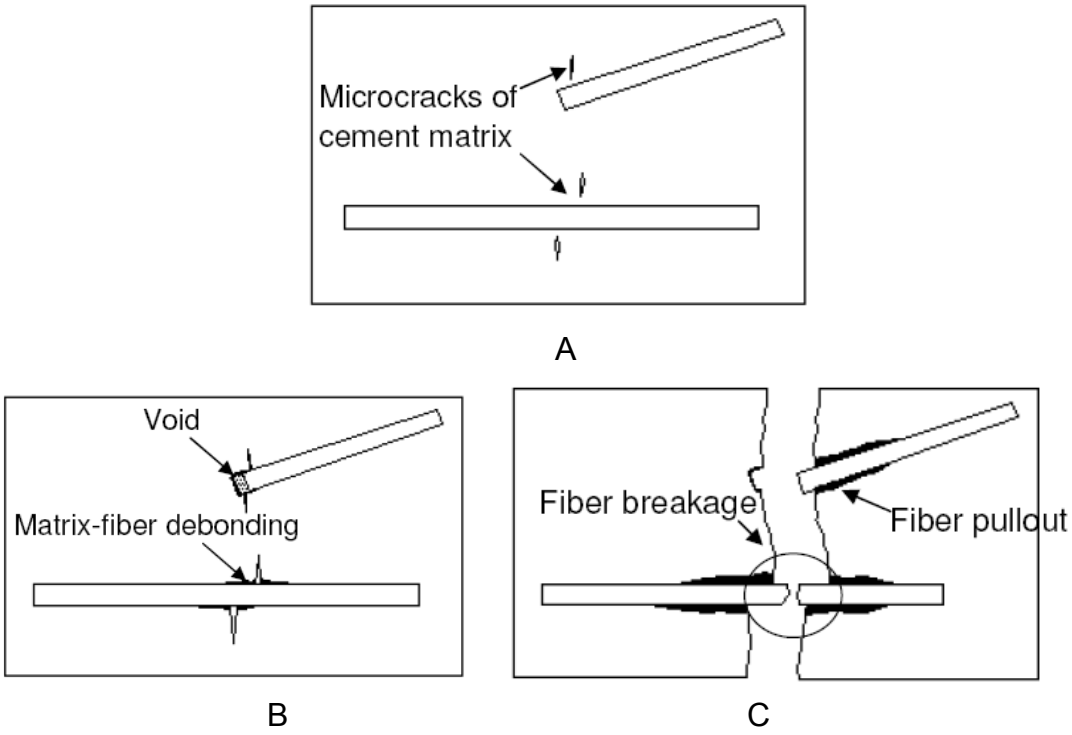

Figure 3-7. Fracture process for CFRC. A. Matrix cracking at early stage; B. Matrix-fiber breakage and fiber pulling out; C. Fiber breakage and complete pull out.

CHAPTER 4
MOISTURE EFFECTS ON CFRC PROPERTIES

The objective of this chapter is to identify the effect of water on CFRC's property. The specimens tested in this chapter are identical to those in Chapter 3 other than they were immersed in water under various conditions. Considering CFRC structure is often exposed to harsh, wet environments, the tests in this section attempt to simulate actual field conditions.

In this chapter, physical and AE results from specimens are plotted together to visualize the dissimilarity created by five different immersion methods. The correlation between AE results and failure mechanisms obtained in Chapter 3 is used to explain the AE results in order to identify the varied failure mechanisms of these treated materials. The mechanical properties are found to correspond with the AE analysis.

Experimental Program

Specimen Preparation

The specimens used were cut with a diamond saw from fiber-reinforced concrete pipe sections commercially provided by Hardie Pipe, Inc. The material properties and manufacturing have been introduced in Chapter 2.

Per ASTM C78, the load was applied at the third point, and the ratio of load span over specimen width was determined to be 3. Therefore, the specimen dimensions were cut to 2 inches by 2 inches by 8 inches long, as shown in Figure 4-1.

The specimens were specially prepared in three different ways. As introduced in Table 4-1, the specimens were designated as CS, meaning control

specimen, which was not treated; S4 and S8, which were saturated in water for 4 and 8 weeks respectively; and WD1, WD5 and WD15, which were exposed to wet/dry cycles of 1, 5 and 15.

The saturated specimens were saturated at room temperature $75 \pm 5^{\circ} F$. After that, the specimens were taken out of water and air dried. The weight of the specimens was taken daily until the mass difference was less than 1% of the previous 24 hours. It was found that after 7 days of drying, the specimens could be considered dry.

The method of determining wetting/drying time is referred to by Mohr (2005). Mass measurement was taken every three hours to monitor the mass loss and gain. If the mass changed below 1% from the prior three hours, the specimens were assumed to be saturated or dry during the wetting or drying cycles. The measured masses are shown in Figure 4-2. It was found that 12 hours of drying and 6 hours of wetting could be considered as a complete wet/dry cycle. Therefore, a wet/dry cycle was designed to be 12 hours drying in an oven space at $149^{\circ} F$, air drying at $75 \pm 5^{\circ} F$ for 6 hours to avoid thermal shock, followed by 6 hours of saturating in water. As mentioned before, the samples were exposed to 1, 5, and 15 wet/dry cycles respectively to compare the mechanical and acoustical properties with control and saturated samples.

Load Procedure

In the third-point bending test, a transverse load is applied to the beam with a span length at least three times (6”) the depth at the one-third point from both

supporting points. The loading was load controlled at a rate of 100 lbs/min until the specimen failed.

Calculation of stresses and deflections

Under the specified load and boundary conditions required in third-point bending test, the formulae for calculating the stress along the failure plane, the deflections at the center and loading point are given in the following equations:

$$\sigma_t = \frac{Pl}{bd^2}$$

$$\Delta \max(at \quad center) = \frac{Pl^3}{56EI}$$

$$\Delta \max(at \quad load \quad point s) = \frac{5Pl^3}{324EI}$$

In which, P is the total load applied on the specimen, l is the distance between two supporting points (6 in.), b is the width of the specimen (2 in.), and d is the depth of the specimen (2 in.).

Testing Facilities

The static third-point bending tests were conducted in the Structural Lab of the Civil and Coastal Engineering Department, University of Florida. The testing machine was an Instron 3384 universal static loading system (Figure 4-3). An LVDT was placed at the center of the specimen's bottom, and connected to National Instrument SCXI-1315 module.

Fracture Mechanism Analysis

The stress versus strain relationships for all specimens are plotted in Figure 4-4. The plots can be clearly divided into two parts. In the first part, the stress strain relationship is linear, or an elastic phase. It signifies the material remains

intact with minor damage. The departure of linearity, on the other hand, is considered the onset of damage during the test. The point between the linear and nonlinear phase is designated as the yield point, P_y. The portion beyond the yield point is referred to as the plastic phase. Figure 4-5A plots AE amplitude versus normalized load for specimen CS with yield point. One can see that before the yield point, the signals are scattered emissions. Their amplitudes are low, around 45 dB to 65 dB. With the conclusions obtained from Chapter 3, the low amplitude AE correlates with cement matrix cracking. Therefore one can conclude that the major damage mode during the elastic portion is matrix cracking. The data also show three middle amplitude hits. This can be explained by local stress concentration due to nonhomogeneity caused by the manufacturing process. The yield point occurs at 88% of the failure load, after which low and middle amplitude AE occurs with an increasing rate of hits. A possible explanation for this portion is with the increasing number and scale of matrix cracking, the fibers begin to pick up stresses redistributed from the matrix. Because of the different moduli, the fibers and matrix have different deformation characteristics. Therefore debonding occurs between the two. This process continues until final failure characteristic of fiber breakage accompanies with high amplitude AE.

The stress versus strain relation of specimen S4, compared with CS, showed an extended elastic phase and very short or no plastic phase in its load deflection plot. The specimen failed abruptly without observing a plastic phase. The S4's yield strength and ultimate strength were on average 13.0% and 4.2%

higher than the CS results (Figure 4-6). It is also worth noting that the difference between the ultimate strength and yield strength of S4 is much smaller than that of CS. These observations implied that the S4 is subjected to more brittle failure than CS.

This phenomenon shows that the 4 weeks saturation in water, functions as an extended period of cement hydration, which increases the cement yield strength. Consequently the cement cracks at a higher stress. If the stress at the point of cracking is higher than the bonding stress between fiber and matrix, stress redistribution does not occur. The fibers are thus unable to delay the propagation of cement cracks, and the whole fiber-reinforced cement material will fail in a brittle manner. This explanation is supported by amplitude versus load in Figure 4-5B, which shows scattered low amplitude AE up until failure, which means the dominant fracture mechanism before the final failure is matrix cracking. It is also observed that there is a lack of middle amplitude AE hits. According to the correlation between AE and failure mechanisms, the occurrence of middle amplitude AE is an indication of fiber/matrix debonding. Therefore the lack of middle amplitude AE signals suggests a lack of fiber/matrix debonding. This conclusion fits well with the discussion on S4's failure mechanism. From this discussion one can suggest that the use of high strength cement might reduce the composite's flexibility. And the bonding ability between fiber and matrix is crucial to its ductility.

On the other hand, with a longer saturation period (8 weeks) CFRC's property changed in another way. The typical result for S8 is more similar to CS.

The yield point occurred at 81%. There was reduced yield strength and a prolonged plastic phase. The S8's yield strength and ultimate strength averaged 26.7% and 10.9% lower than CS. It is proposed that longer exposure to water reduced the yield and ultimate strength of the cement matrix. Therefore in sample S8, the cement matrix cracked at a relatively lower stress than CS, after which stress redistribution occurred between fibers and cement matrix. Instead of cracking abruptly, the fibers helped delay crack propagation. Therefore S8 has a prolonged plastic phase similar to CS. The AE amplitude versus normalized load in Figure 4-6 C also identifies the same procedure. There is an obvious increase in the number of hits and AE amplitude after the yield point at 81% of ultimate load. Before the yield point, only scattered low amplitude AE signals appeared, which implied cement matrix cracking was the dominant damage during this phase. After the yield point, middle amplitude AE signals started to occur and at a higher rate with the progression of damage. This means that during this phase fibers and matrix both were involved in the development of the plastic phase. It is believed that the fibers prolonged final damage and prevented the specimen from an abrupt failure.

Figure 4-5 D to F shows that WD specimens had a smaller yield and ultimate strength and shorter plastic phases than CS. With the increasing number of wet/dry cycles, the specimens displayed more brittle characteristics. The yield points for WD1, WD5 and WD15 occurred at 94%, 93% and 98% respectively. The difference between ultimate and yield strengths, i.e., the additional load the sample can take in plastic phase is reduced with increasing cycles. The

additional strain that the samples can undergo during the plastic phase is also smaller. The addition strain for WD1 was 1.63 milli-strain, or 29.5% of elastic strain. For WD5 it was 0.86 milli-strain (24.4% of elastic strain). Finally for WD15 is 0.15 milli-strain (4.7% of elastic strain).This shows that as the number of wet/dry cycles increased, the material became more brittle. A possible explanation is that wet/dry cycling not only reduces the strength of the cement matrix, but also impacts the bonding between fibers and matrix. It is worth noting that for specimen WD15, the number of middle amplitude AE hits is very small in the nonlinear portion, which means debonding between fibers and matrix does not happen as with the other specimens. This phenomenon is similar to S4, but it is likely caused by another factor. After 15 wet/dry cycles, voids existed within matrix and the interface between the fiber and matrix. Consequently during the test, instead of creating new damages between fiber and matrix, the crack intended to propagate along the existing voids, and the amount of debonding occurring was smaller than specimen CS, WD1 and WD5. It is worth noting that the dramatic increase of AE hits occurred earlier than yield point. Considering the pre-existence of damage within the specimen when the specimen was loaded to a certain level the existing crack surfaces migrated closer to each other, producing friction between the surfaces. It is noted that these AE hits were low amplitude signals, which meant they did not cause significant damage to the specimen.

Conventional AE Data Analysis

In this section conventional AE data are discussed. Conventional AE data are usually referred to as hit, count, energy, signal strength and Historic Index.

These parameters have been used by numerous researchers for locating the "knee" or the onset of significant damage. The cumulative hits, cumulative counts, cumulative energy, cumulative signal strength and Historic Index are all plotted versus load and are shown in Figures 4-6 to 4-10. The knees of these plots are identified by a slope change in the curves. Results from both of the sensors are indicated in the same plot. It is noted that the results from channel 2 of specimen S4 are lower compared to channel 1. Because the same sensors were used in all the tests, it is assumed that the insensitivity was caused by improper mounting.

A summary of the knee of each specimen in all the plots is presented in Table 4-3. The values of yield point of each specimen are compared with the knees.

It is found that the knees estimated from cumulative hits, cumulative counts, cumulative energy and cumulative signal strength versus load are close to the yield points of specimen CS, SR, S8 and WD1. The similarity between the two values shows that AE is able to give the real-time inspection of damage occurrence in loaded structures.

The deviation of knee values from yield points occurred in specimens WD5 and WD15. For WD5, the estimated knees are 82% and 83%, while the yield point occurred at 93% of ultimate load. For WD15, the estimated knees are 86% for cumulative hits, 82% for cumulative counts and energy, and 90% for cumulative signal strength. Compared with the yield point 98%, the AE seems to provide extra warning before final failure. This is caused by the existence of cracks created through a number of wet/dry cycles before the test. The closing of

pre-existed crack surfaces under loading produces AE signals before reaching the yield point.

The knee values provided by the Historic Index are different from the yield points, with the exception of S4 whose yield point is actually a failure point. It is due to the fact that the CFRC material is generally a brittle material, and the signal strength increased exponentially at the end of the damage. Therefore one can observe the onset of final failure, but at the earlier part historic index fluctuates around 1.

Amplitude versus Duration

The amplitude versus duration plot is usually used to evaluate the AE data and eliminate noise (Harvey 2001). It is clearly seen from Figure 4-12 that the AE data recorded is well clustered and very clean. Electromagnetic interference (EMI) is characteristic of very short duration and high amplitude. External noise resulting from mechanical friction is characterized by low amplitude and long duration. These two AE signals were minimal in the test data.

Another observation from the amplitude versus duration plots is that the plots are composed of two clusters of data. The first set is featured by low amplitude, low duration (lower than 1,000 us). The other is typically long duration and most have middle or high amplitudes. For some of the plots, for example specimens S8, WD5 and WD15, the gaps between the two clusters are quite clear.

Figure 4-13A shows AE data for all specimens within the elastic phase. With very few exceptions, the majority of AE data are located in the first duration versus amplitude region as discussed in the previous paragraph. The duration

versus amplitude plots for different number of hits are shown in Figure 4-13B to D. It is clear that with the development of damage, the AE hits are transforming from short duration (<1,000 us) and low amplitude to middle duration (1,000 us to 10,000 us) and amplitude, until shortly before ultimate failure, when the AE hits are featured by long duration (>10,000 us) and high amplitudes.

Amplitude Distribution

Amplitude distribution is a plot of hits versus amplitude. It shows the number of hits each level of amplitude contains. Many researchers have used this plot for AE signature analysis. It has been shown that the plot may have one or more humps and the peak amplitude of each hump characterizes the fracture mechanism.

Figure 4-14 shows the amplitude distribution for all the specimens. AE from both sensors are plotted in one figure. It shows that other than specimen S4, the two sensors recorded similar profiles.

The comparison between results from CS and the other specimens shows the effect of various water treatments. For specimen CS, the amplitude distribution plot has a hump from 45 dB to 60 dB, after which a gradual decreasing, almost linear slope from 60 dB to 75 dB occurs. At amplitudes between 75 dB to 80 dB there's a second linear span. Specimens S8, WD1 and WD5 have similar shapes to CS. The difference between them is that for the latter three specimens the hump contains less amplitude range. For example, specimen WD15 has a hump between 45 dB and 53 dB. The decreasing linear slopes are sharper than CS. At the same time, specimens S8, WD1 and WD5 have a smaller number of hits than CS.

For specimens S4 and WD15, the profiles are different from the others. The plot has one peak at 47 dB, and then the decreasing slope extends to around 60 dB. Both of the two specimens have very few hits at the middle amplitudes, which means an incomplete fracture mechanism is occurring compared to the other specimens. Recalling the correlation between AE amplitude and fracture mechanism, one can say that the missing mechanism is fiber/matrix debonding. Since water treatment is the only difference between specimens CS, S4 and WD15, it is believed to be the cause of the missing of fiber/matrix debonding signature.

Progression of Amplitude Distribution

These plots are a set of amplitude distribution plots of representative specimens at the elastic phase, up to 50%, 75%, 90%, 99% and 100% of ultimate load. Many researchers have used this type of plot to analyze the evolution of fracture mechanisms.

For specimen CS, the plot is linear at the beginning up to 90% of ultimate load. Within this portion, AE hits concentrate at low amplitudes from 45 dB to 55 dB. After that AE starts to occur at a middle amplitude range, and the curve starts to exhibit more peak values. For example, the curve for 99% load has peak values at 46 dB, 55 dB and 69 dB. Specimens S8, WD1 and WD5 have similar shapes to CS. For these samples, the last portion of the curve is related to fiber breakage, which shows a nonlinear relationship.

Cumulative Amplitude Distribution and b-value

It has been researchers' interest to use the slope of the cumulative amplitude distribution plot for AE signature analysis. The plot of a single fracture mechanism should be linear and the slope is unique for each of them.

Figure 4-16 shows the cumulative amplitude distribution for all the specimens. AE from both sensors are plotted in one figure. Other than specimen S4, the two sensors recorded similar profiles. For specimen S4, it was discovered later that the poor sensitivity of sensor 1 resulted from using too much glue to mount it. Therefore the glue attenuated the AE signals and reduced the number it received. However, one can see in Figure 4-16B that the slopes of the two curves are close to one another. This implies that the cumulative amplitude distribution plot is less influenced by attenuation; therefore it can be used as a valid tool for AE signature analysis.

For specimens CS, S8, WD1 and WD5, the plots can be considered approximately bi-linear. This is produced by the complex composition of CFRC and combined fracture mechanisms during its failure.

The plots for specimens S4 and WD15, on the other hand, can be clearly considered as linear. The majority of hits occurred at the low amplitudes, which means the major fracture mechanism is matrix cracking, with fiber breakage occurring only at the end. This means that specimens S4 and WD15 do not have a clear process of fiber/matrix debonding, rather matrix cracking is the dominant fracture mechanism. This agrees with other researchers' conclusions that a single fracture mechanism should have a linear relation.

Progression of Cumulative Amplitude Distribution

Figure 4-17 presents the progression of cumulative amplitude distributions at the various load levels for each specimen. For CS, S8, WD1 and WD5, at the initial stage of loading the curves were linear, while with the development of fracture damage, the curves generally become bi-linear. On the other hand, S4 and WD15 curves are generally a single slope for all damage levels with the only exception at the final failure. Table 4-4 gives the b-values for each of the fracture mechanisms.

Figure 4-18 plots the cumulative amplitude distribution of all specimens in one figure. Specimens CS, S8, WD1 and WD5 have similar shapes, with the only difference being the amount of hits. It is interesting to see that S8 and WD1 have almost exactly the same curve. Considering that the water treatment of WD1 is one wet and dry cycle, and S8 was soaked for eight weeks then dried, it is expected that the water effects influenced their failure mechanisms in a similar way.

Summary

In this chapter, the mechanical property and AE plots of all representative specimens are shown. The significant findings from this chapter are listed as follows.

1. Four weeks saturation in water increases the material's ultimate and yield strength. However, the material also becomes more brittle since the fibers don't delay the crack propagation within the matrix. Eight weeks saturation in water, on the other hand decreases the material's ultimate and yield strength. Wet/dry treatment not only reduces the strength but also makes the material more brittle.
2. Conventional AE analysis proved that AE is a useful tool for detecting internal damage in real time. It was observed that because of existing

damage in specimens WD5 and WD15, conventional AE results produced knee values earlier than the yield point.

3. The duration versus amplitude plot shows that duration evolves with damage levels. The low amplitude AE corresponding to matrix cracking always occurs for short duration. The middle amplitude AE corresponding with matrix/fiber debonding lasts longer. Fiber breakage is generally accompanied by long duration, high amplitude AE hits.

4. It seems that the amplitude distribution analysis provides better results for more ductile specimens. The comparison between the results obtained by various water treatments displayed different fracture mechanisms.

5. The cumulative amplitude distribution and b-value is proved to be an effective method in studying the fracture mechanism. The b-values for different materials also showed different ranges of values. Brittle materials, i.e., S4 and WD15 generally exhibit linear plots while more ductile materials will be bi-linear. The b-values fall within specified ranges for different failure mechanisms.

Table 4-1. Static third-point bending test, sample designation and treatment

Treatment	Designation	Conditions
Control Specimens	CS	Dry, untreated
Saturated in water	S4	4 Weeks
	S8	8 Weeks
Wet/Dry Cycling	WD1	1 cycles
	WD5	5 cycles
	WD15	15 cycles

Table 4-2. Basic properties of representative specimens

Specimen	Total AE hits per sensor	Maximum stress (psi)	Maximum strain $(\times 10^{-3})$
CS	7,524	1,519	5.07
S4	137	1,772	4.62
S8	3,329	1,475	5.98
WD1	3,722	1,355	5.23
WD5	2,069	1,180	4.93
WD15	393	1,058	3.37

Table 4-3 Yield point and knee from cumulative hits, cumulative counts, cumulative energy, cumulative signal strength and Historic Index plots

Specimen	Yield point and onset of significant damage (% of ultimate load)					
	Yield point	Cum hits	Cum counts	Cum energy	Cum signal strength	Historic Index
CS	88	89	89	89	87	97
S4	100	100	100	100	100	100
S8	81	81	82	82	82	99
WD1	94	95	95	96	96	96
WD5	93	82	83	83	82	97
WD15	98	86	82	82	90	99

Table 4-4. Cumulative Amplitude Distribution, b-value

Fracture Mechanism	b-value
Matrix cracking	1.50-2.13
Fiber/matrix debonding	2.96-5.09
Fiber breakage	<1.84 (at high amplitude)

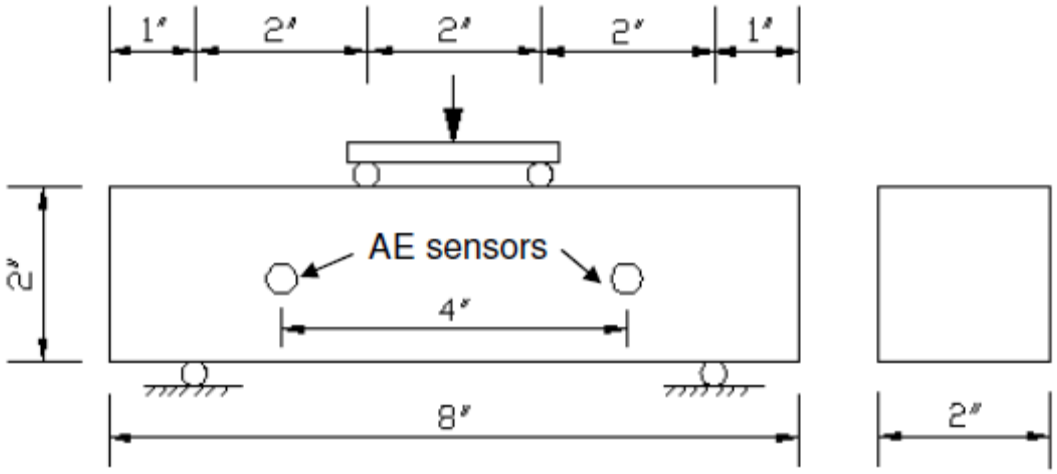

Figure 4-1. Third-point bending test setup

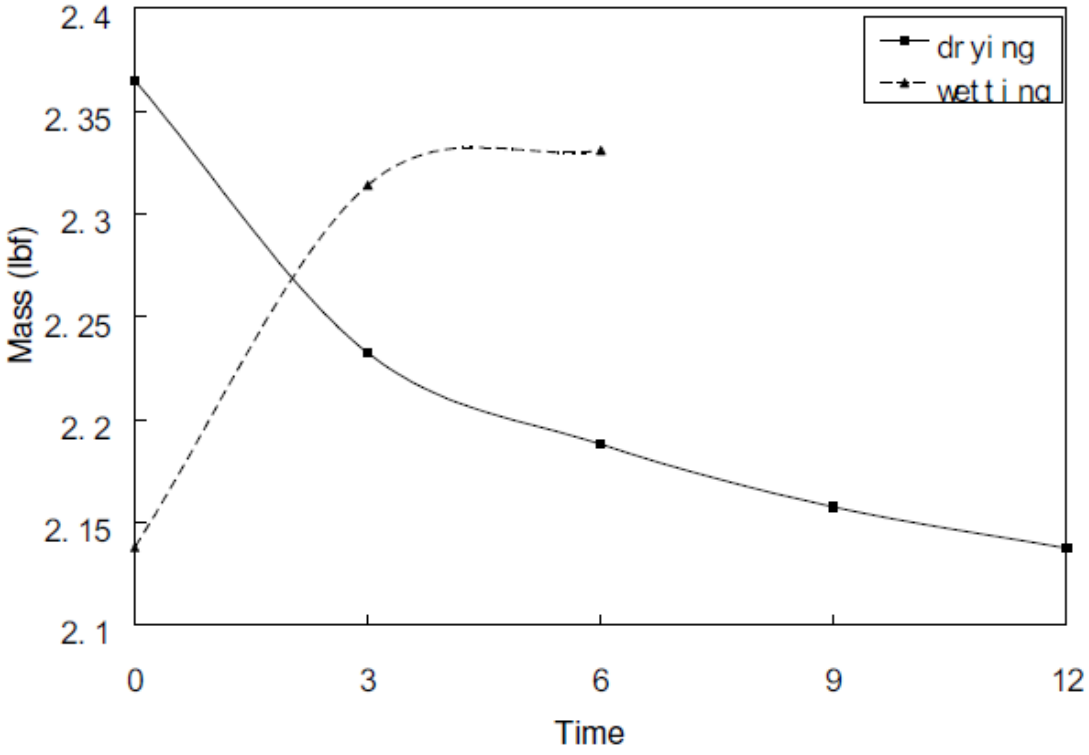

Figure 4-2. Specimen's mass measurement every three hours

Figure 4-3. Static third-point bending test machine, INSTRON 3384.

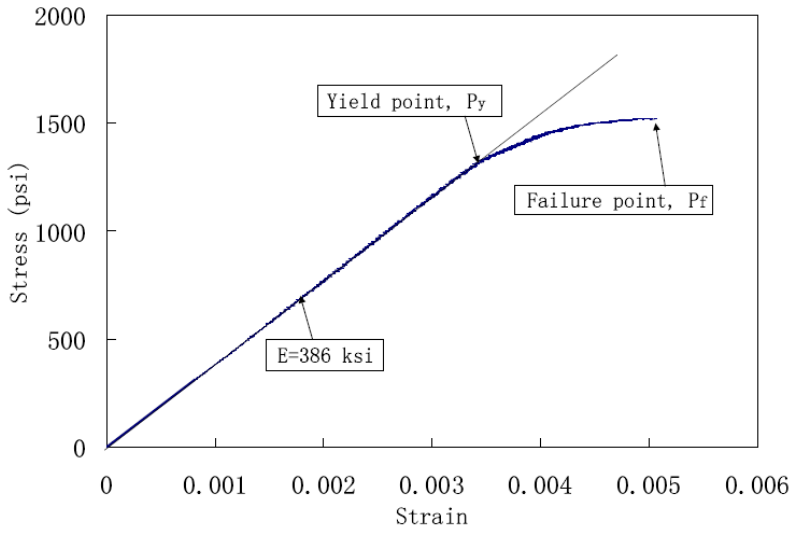
2000
1500
1000
500
0
Stress (psi)
Yield point, Py
Failure point, Pf
E=386 ksi
0
0.001
0.002
0.003
0.004
0.005
0.006
Strain

A

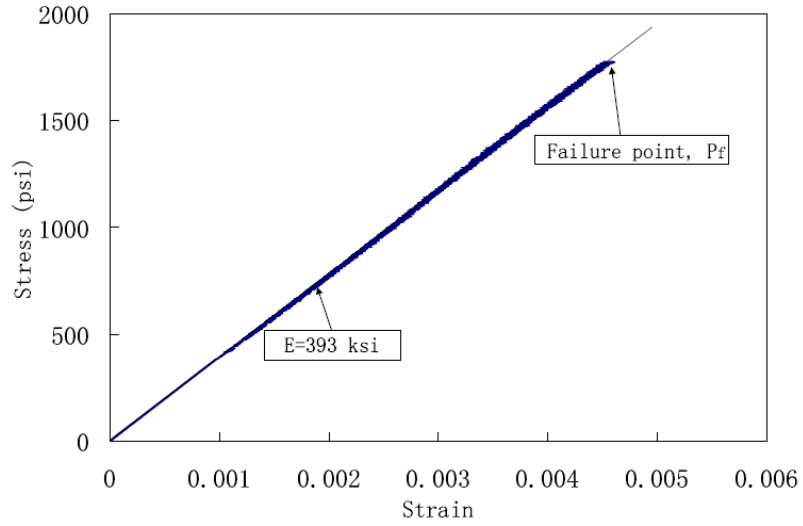
2000
1500
1000
500
0
Stress (psi)
Failure point, Pf
E=393 ksi
0
0.001
0.002
0.003
0.004
0.005
0.006
Strain

B

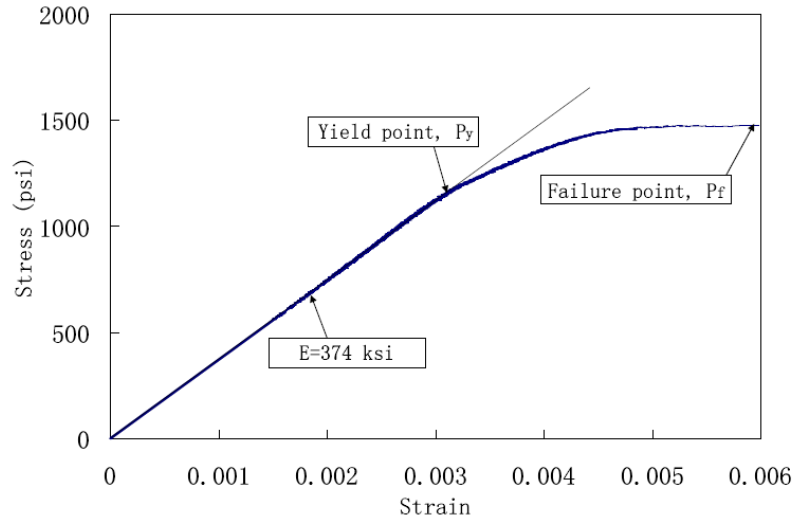
2000
1500
1000
500
0
Stress (psi)
Yield point, Py
Failure point, Pf
E=374 ksi
0
0.001
0.002
0.003
0.004
0.005
0.006
Strain

C

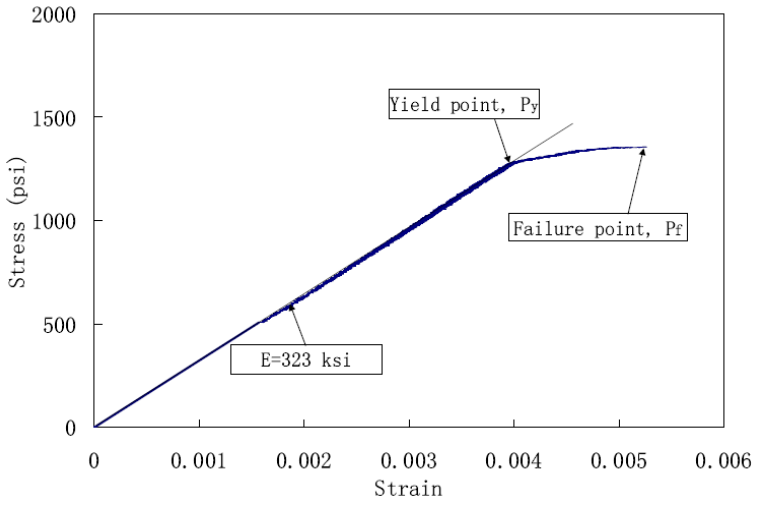

D

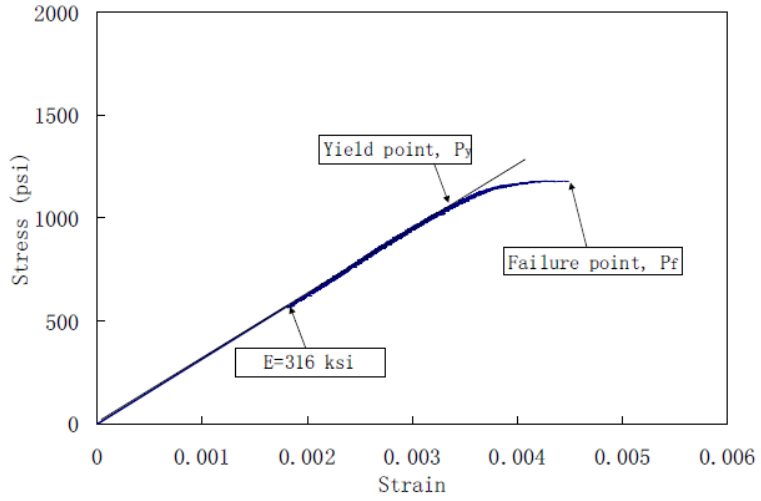

E

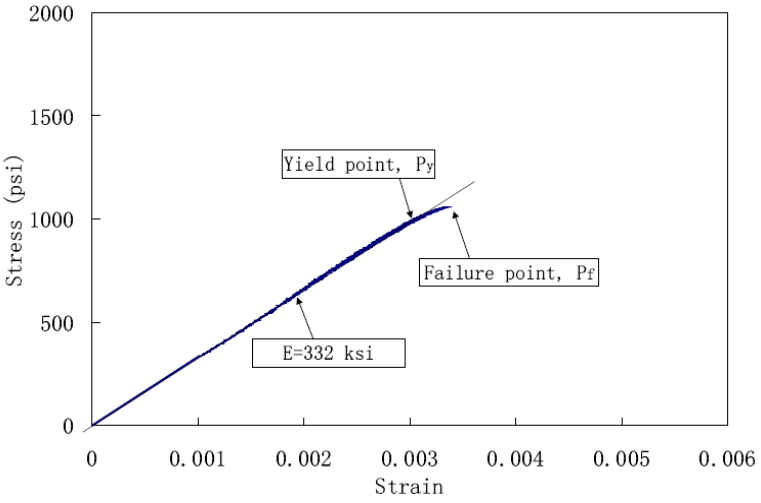

F

Figure 4-4. Stress-strain relation for specimens: A. CS; B. S4; C. S8; D. WD1; E. WD5; F. WD15.

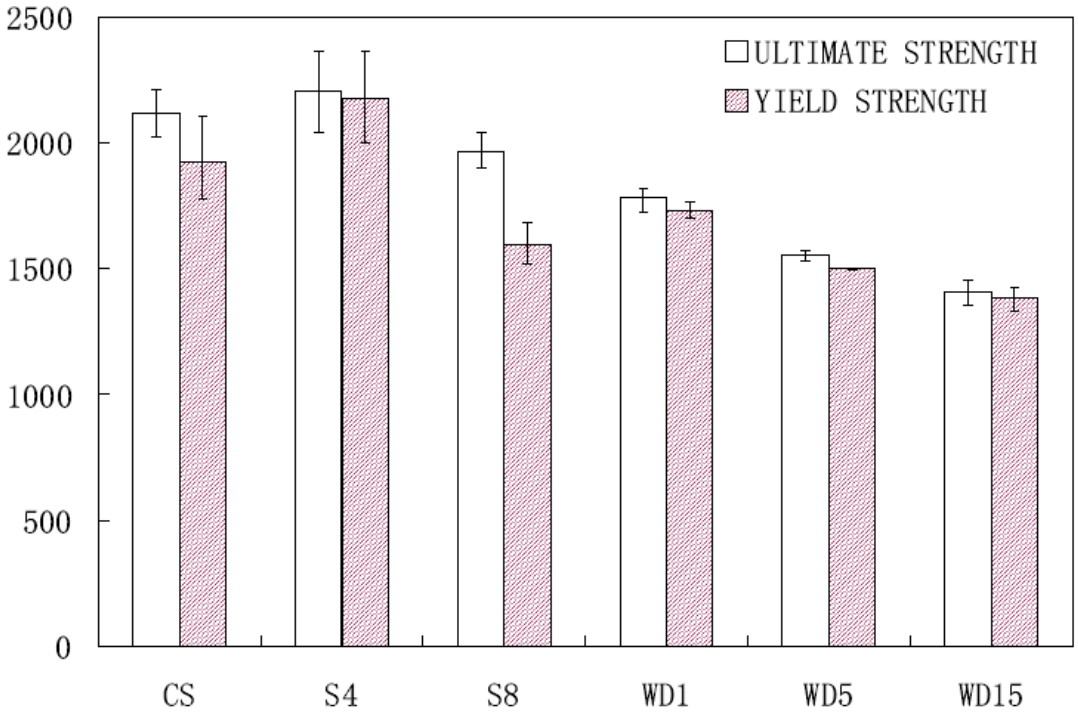

Figure 4-5. Ultimate and yield strength of specimens.

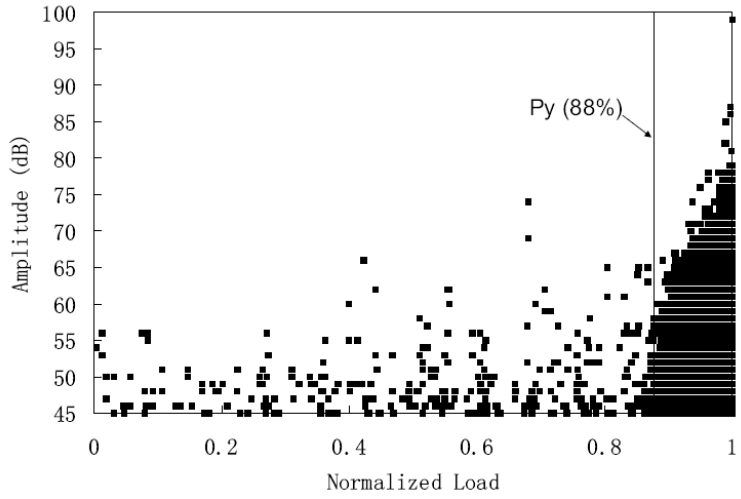
Py (88%)
Amplitude (dB)
Normalized Load

A

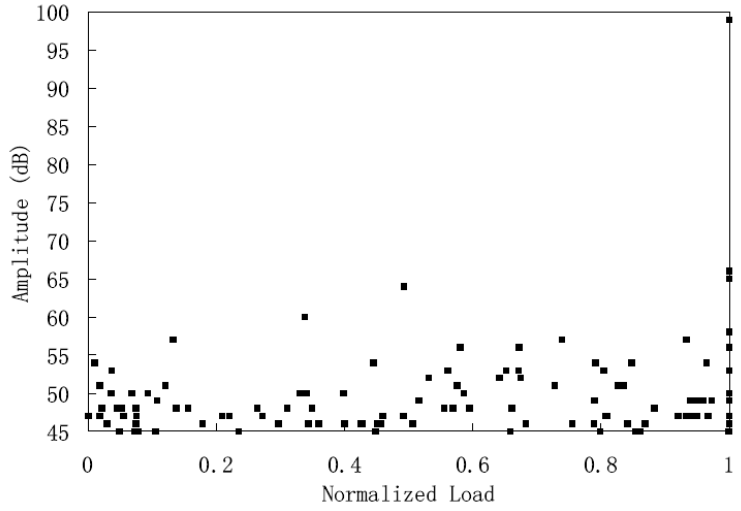
Amplitude (dB)
Normalized Load

B

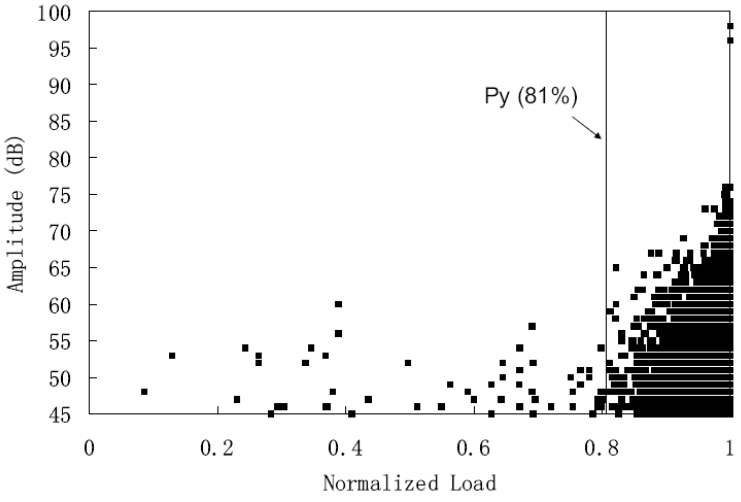
Py (81%)
Amplitude (dB)
Normalized Load

C

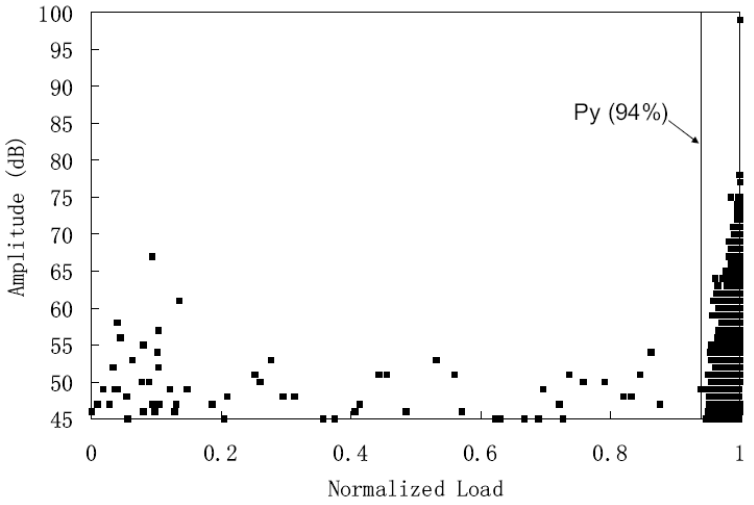

D

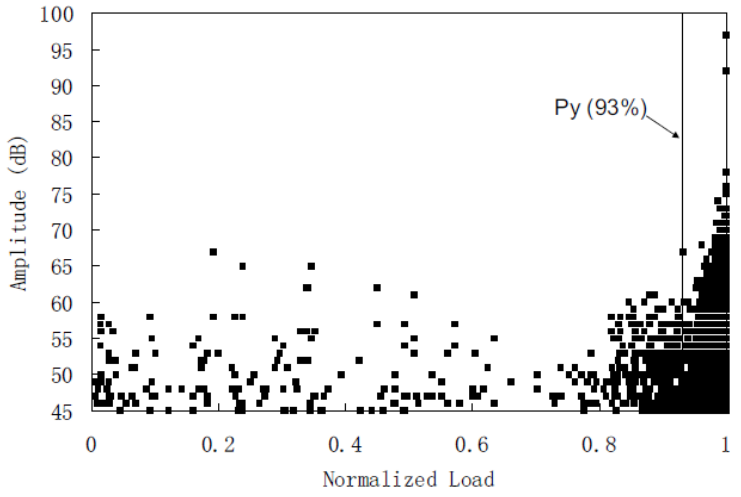

E

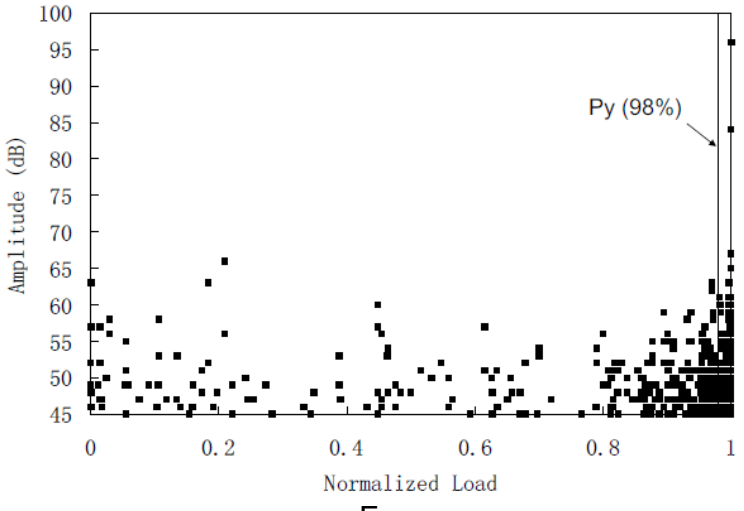

F

Figure 4-6. Amplitude versus normalized load for specimens: A. CS; B. S4; C. S8; D. WD1; E. WD5; F. WD15.

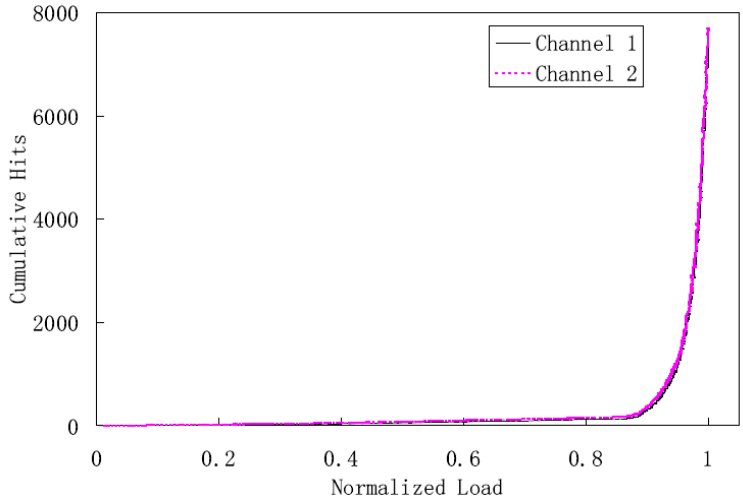
Channel 1
Channel 2
Cumulative Hits
Normalized Load
8000
6000
4000
2000
0
0
0.2
0.4
0.6
0.8
1

A

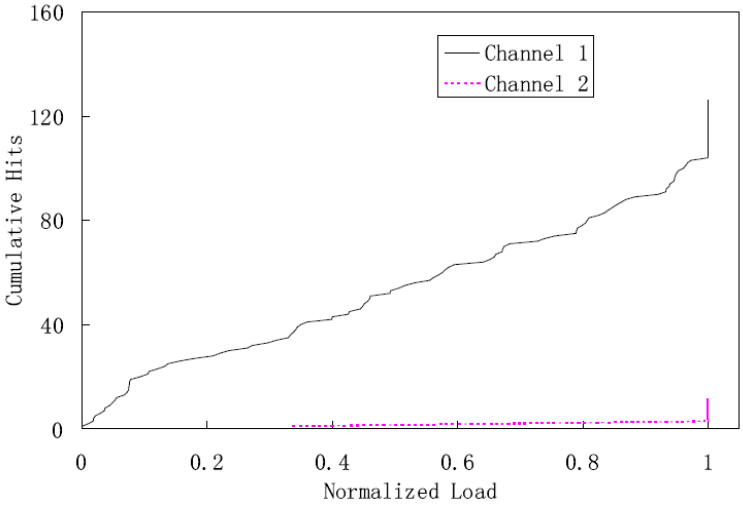
Channel 1
Channel 2
Cumulative Hits
Normalized Load
160
120
80
40
0
0
0.2
0.4
0.6
0.8
1

B

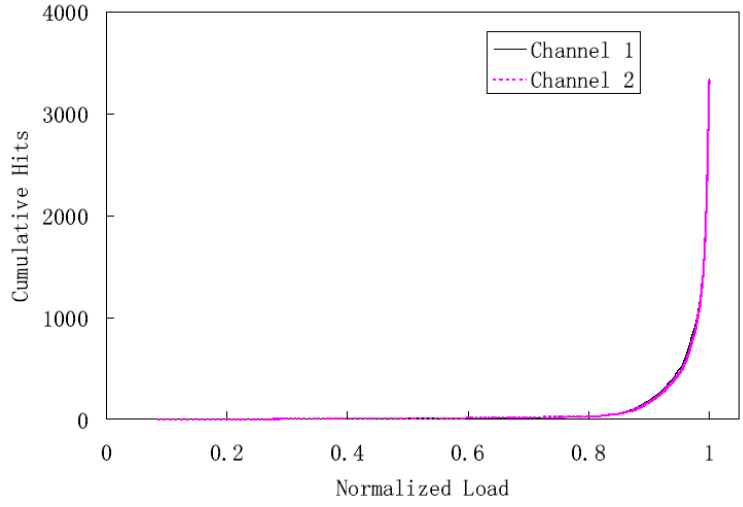
Channel 1
Channel 2
Cumulative Hits
Normalized Load
4000
3000
2000
1000
0
0
0.2
0.4
0.6
0.8
1

C

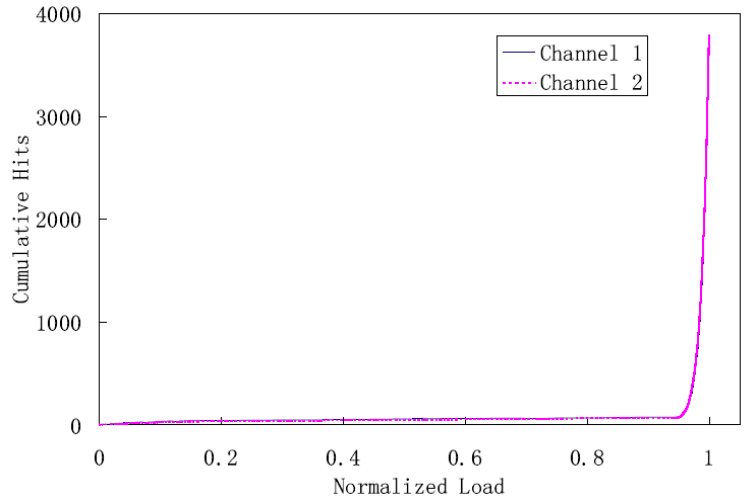

D

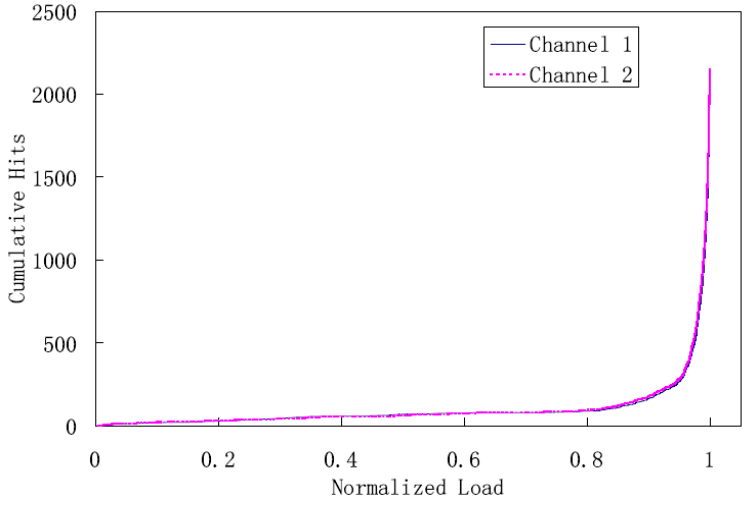

E

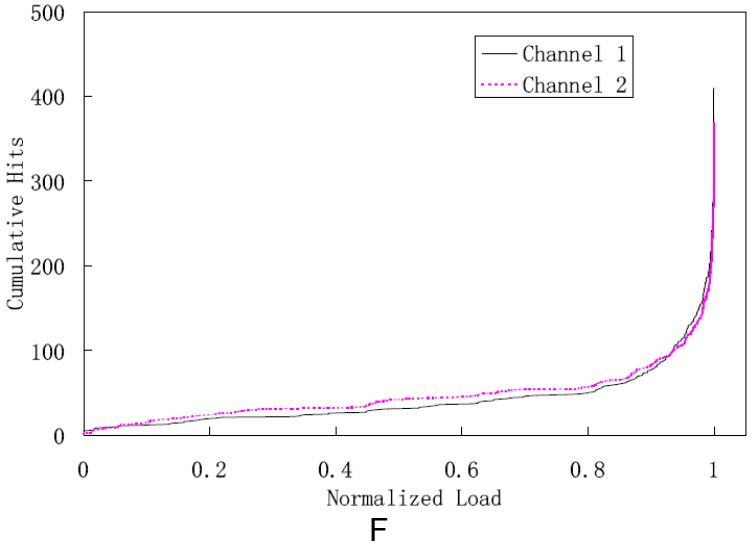

F

Figure 4-7. Cumulative hits versus normalized load for specimens: A. CS; B. S4; C. S8; D. WD1; E. WD5; F. WD15.

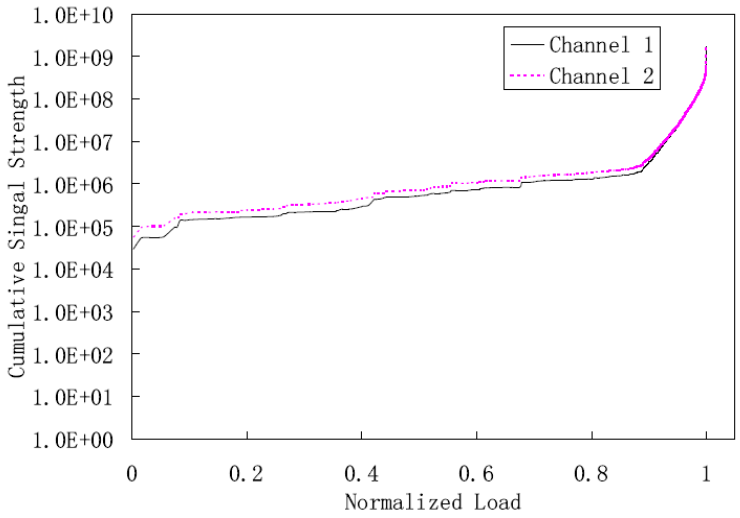
Channel 1
Channel 2
Cumulative Singal Strength
1.0E+10
1.0E+09
1.0E+08
1.0E+07
1.0E+06
1.0E+05
1.0E+04
1.0E+03
1.0E+02
1.0E+01
1.0E+00
0
0.2
0.4
0.6
0.8
1
Normalized Load

A

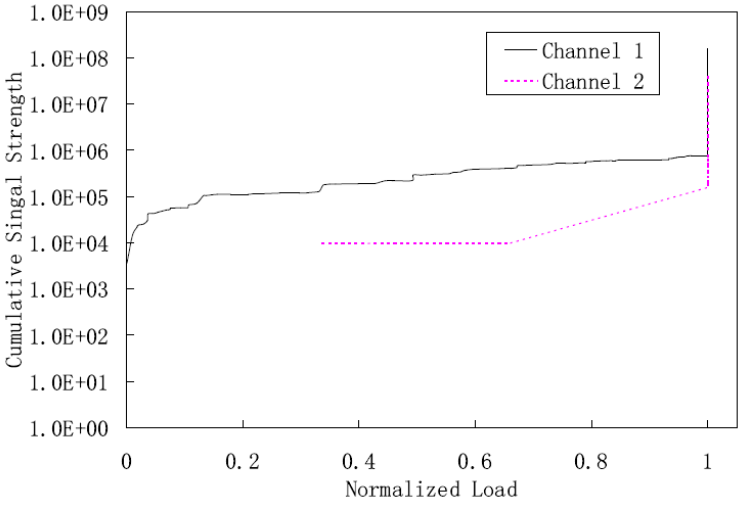
Channel 1
Channel 2
Cumulative Singal Strength
1.0E+09
1.0E+08
1.0E+07
1.0E+06
1.0E+05
1.0E+04
1.0E+03
1.0E+02
1.0E+01
1.0E+00
0
0.2
0.4
0.6
0.8
1
Normalized Load

B

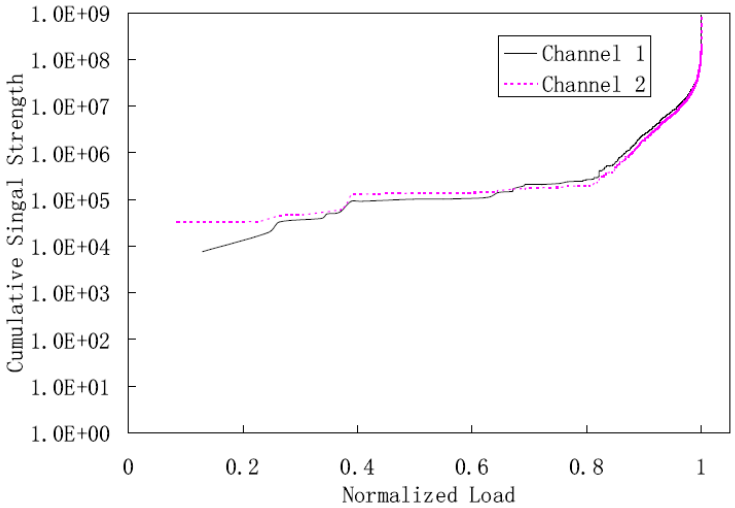
Channel 1
Channel 2
Cumulative Singal Strength
1.0E+09
1.0E+08
1.0E+07
1.0E+06
1.0E+05
1.0E+04
1.0E+03
1.0E+02
1.0E+01
1.0E+00
0
0.2
0.4
0.6
0.8
1
Normalized Load

C

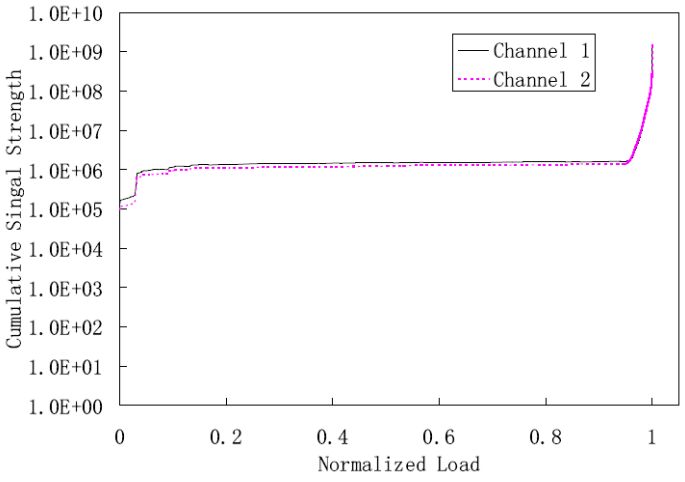

D

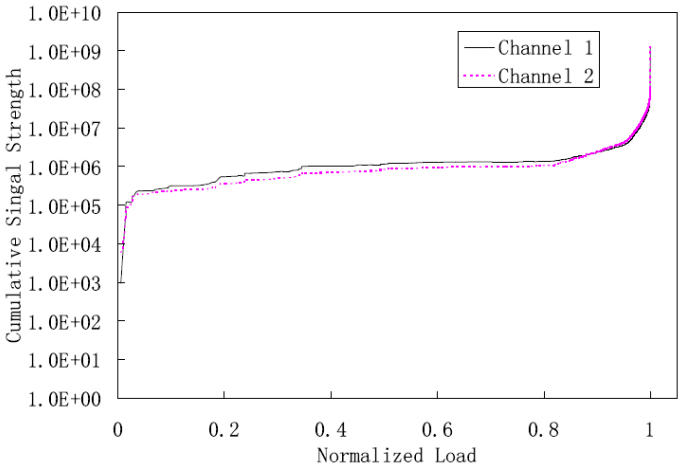

E

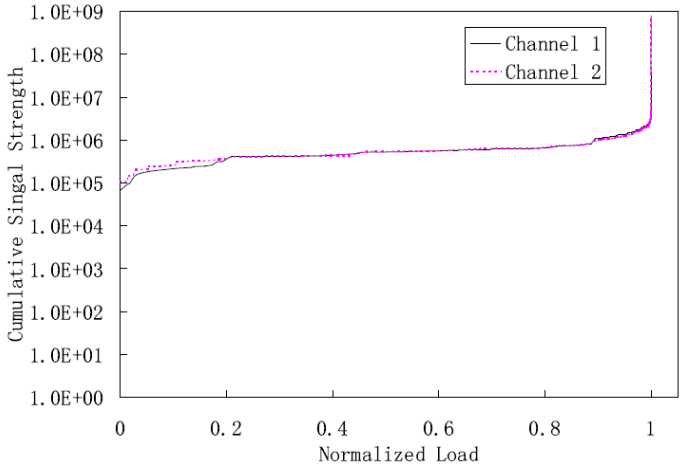

F

Figure 4-8. Cumulative signal strength versus normalized load for specimens: A. CS; B. S4; C. S8; D. WD1; E. WD5; F. WD15.

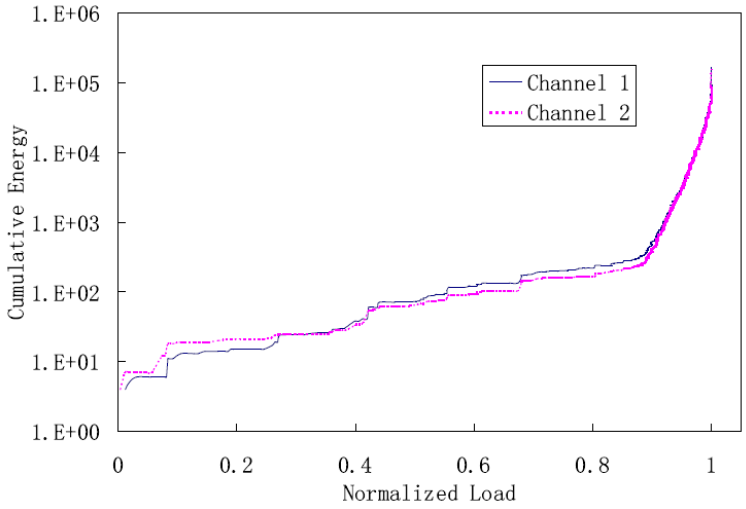
1.E+06
1.E+05
1.E+04
1.E+03
1.E+02
1.E+01
1.E+00
Cumulative Energy
Channel 1
Channel 2
0
0.2
0.4
0.6
0.8
1
Normalized Load

A

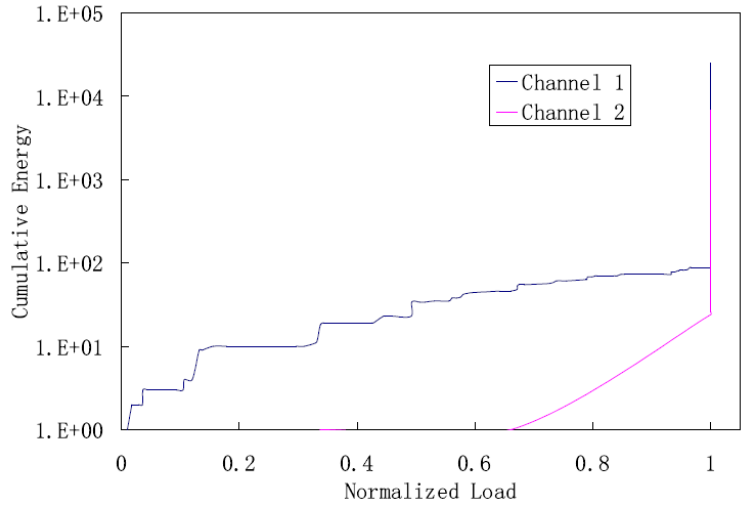
1.E+05
1.E+04
1.E+03
1.E+02
1.E+01
1.E+00
Cumulative Energy
Channel 1
Channel 2
0
0.2
0.4
0.6
0.8
1
Normalized Load

B

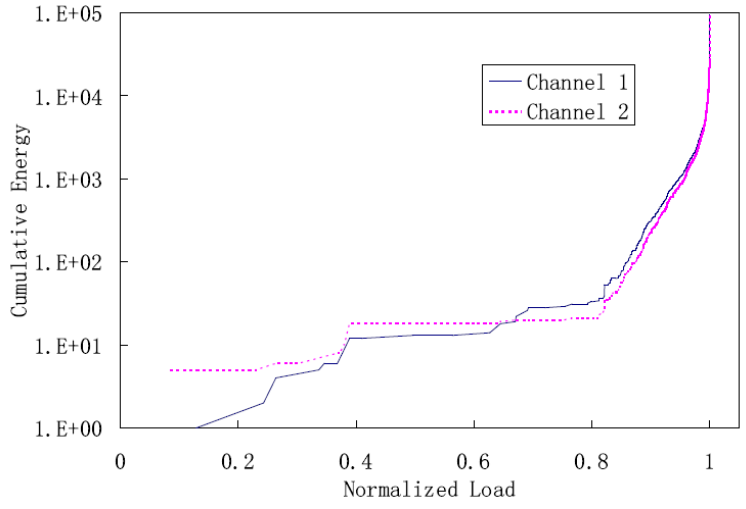
1.E+05
1.E+04
1.E+03
1.E+02
1.E+01
1.E+00
Cumulative Energy
Channel 1
Channel 2
0
0.2
0.4
0.6
0.8
1
Normalized Load

C

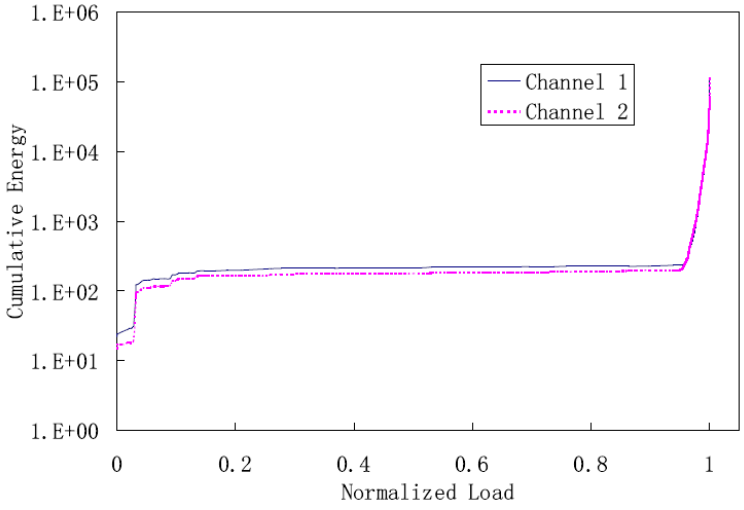

D

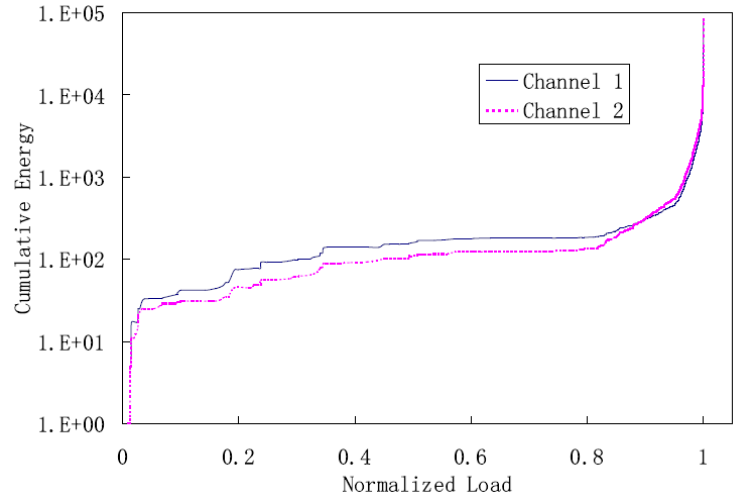

E

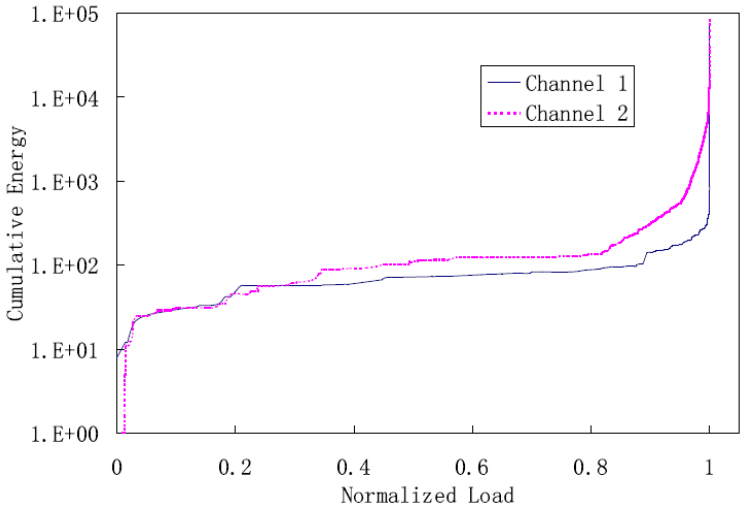

F

Figure 4-9. Cumulative energy versus normalized load for specimens: A. CS; B. S4; C. S8; D. WD1; E. WD5; F. WD15.

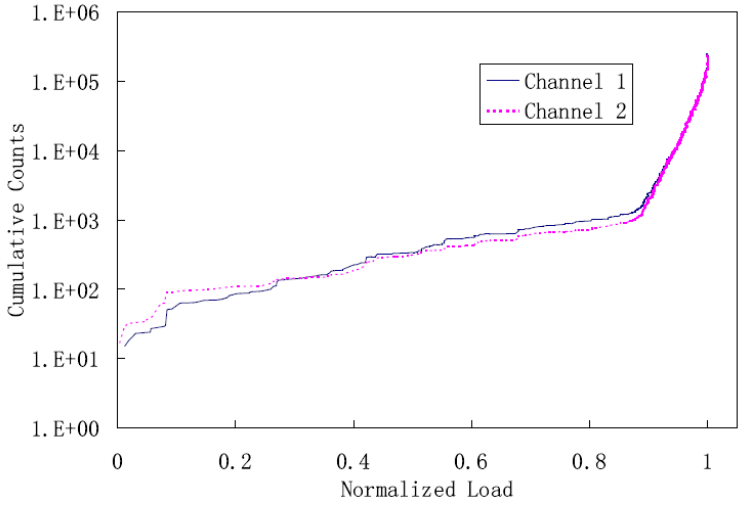
1.E+06
1.E+05
1.E+04
1.E+03
1.E+02
1.E+01
1.E+00
Cumulative Counts
Channel 1
Channel 2
0
0.2
0.4
0.6
0.8
1
Normalized Load

A

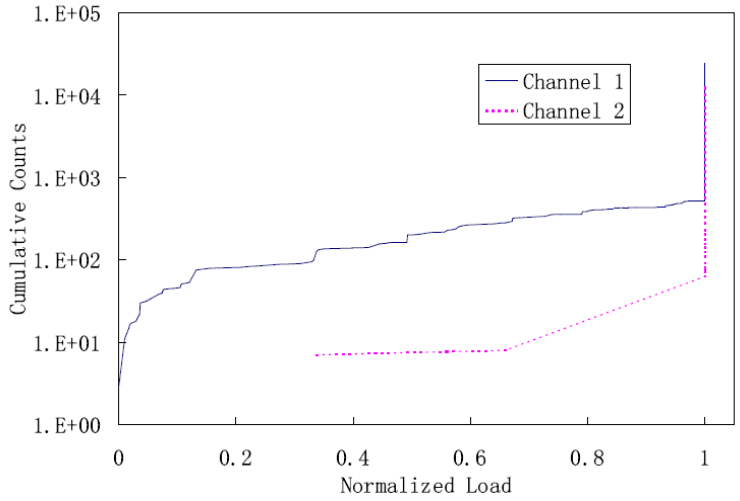
1.E+05
1.E+04
1.E+03
1.E+02
1.E+01
1.E+00
Cumulative Counts
Channel 1
Channel 2
0
0.2
0.4
0.6
0.8
1
Normalized Load

B

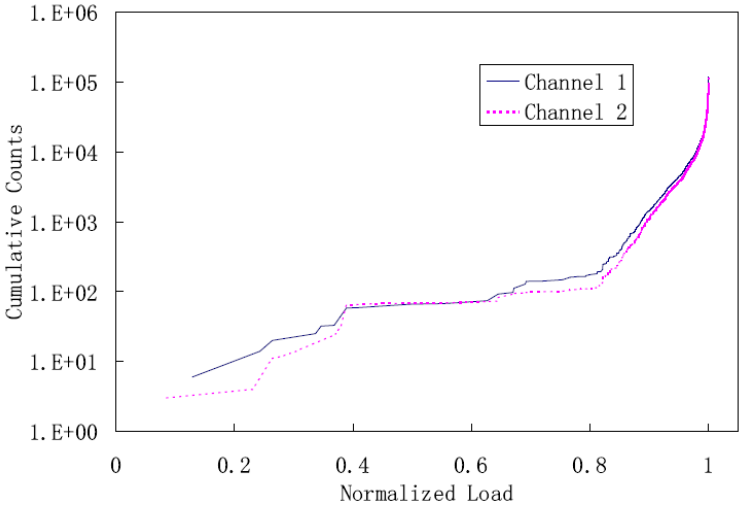
1.E+06
1.E+05
1.E+04
1.E+03
1.E+02
1.E+01
1.E+00
Cumulative Counts
Channel 1
Channel 2
0
0.2
0.4
0.6
0.8
1
Normalized Load

C

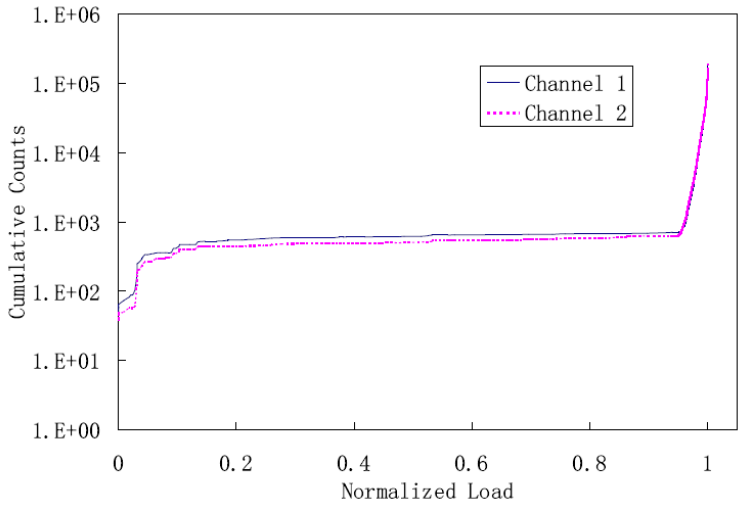

D

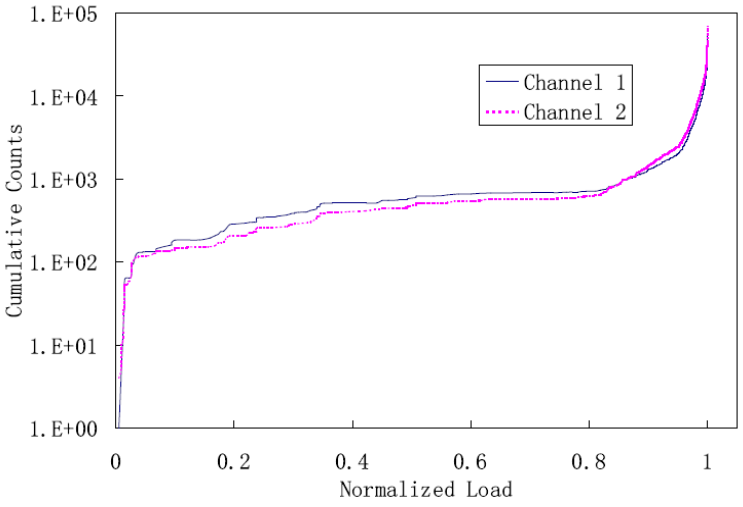

E

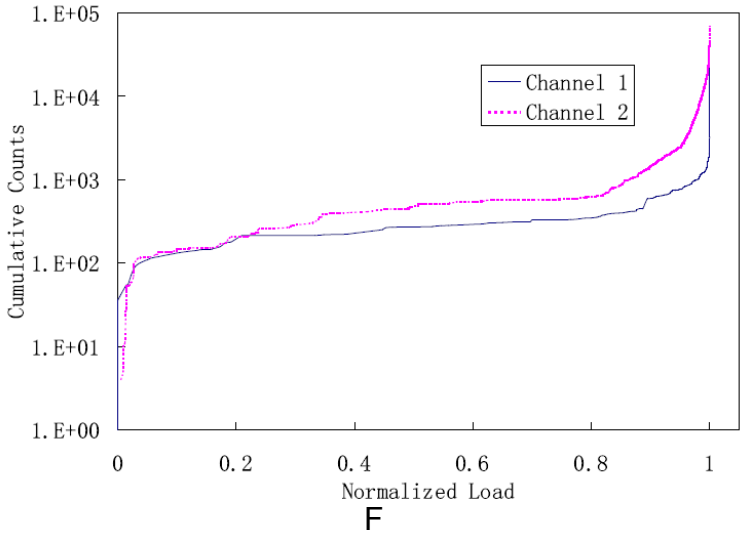

F

Figure 4-10. Cumulative Counts versus normalized load for specimens: A. CS; B. S4; C. S8; D. WD1; E. WD5; F. WD15.

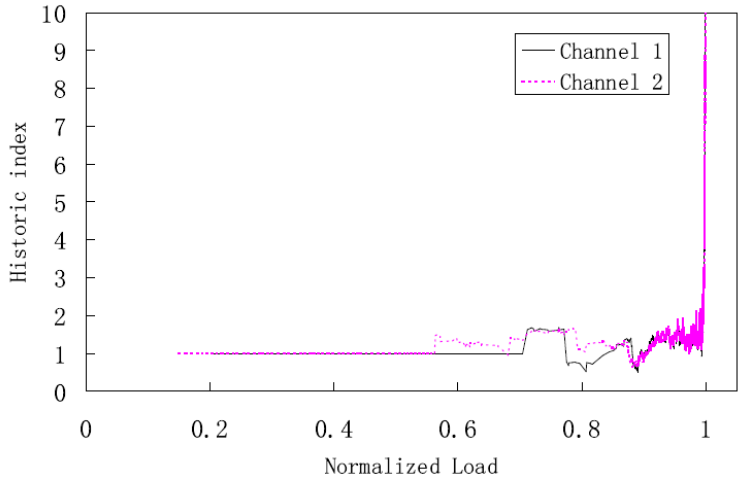
Channel 1
Channel 2
Historic index
Normalized Load
0
1
2
3
4
5
6
7
8
9
10
0
0.2
0.4
0.6
0.8
1

A

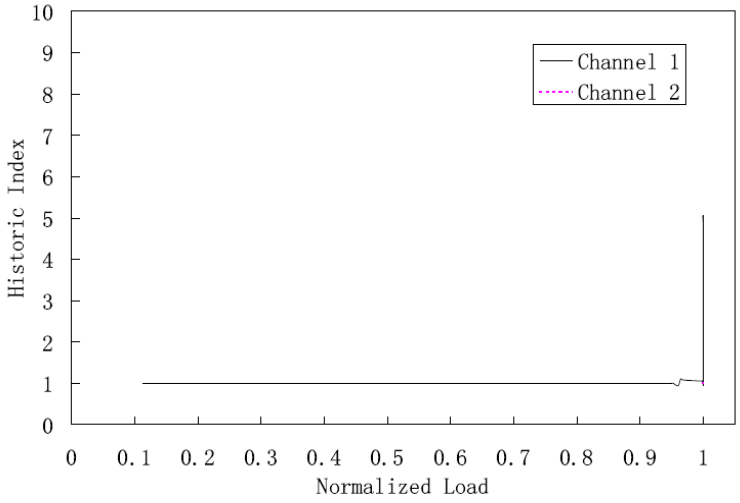
Channel 1
Channel 2
Historic Index
Normalized Load
0
1
2
3
4
5
6
7
8
9
10
0
0.1
0.2
0.3
0.4
0.5
0.6
0.7
0.8
0.9
1

B

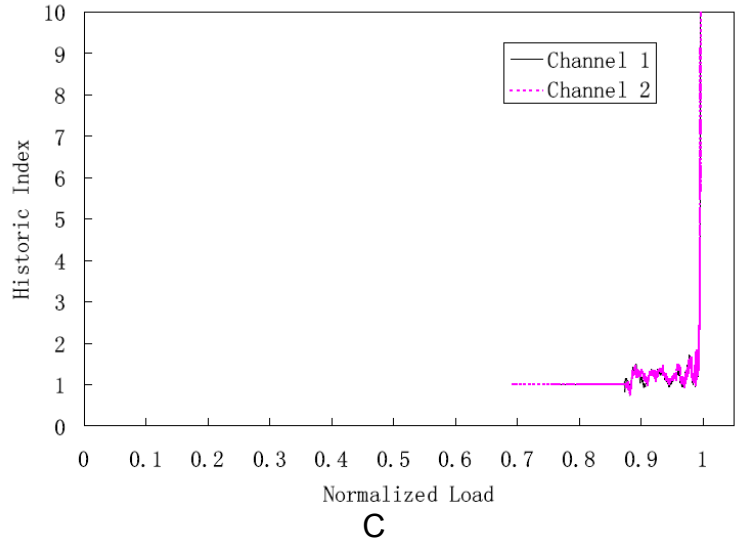
Channel 1
Channel 2
Historic Index
Normalized Load
0
1
2
3
4
5
6
7
8
9
10
0
0.1
0.2
0.3
0.4
0.5
0.6
0.7
0.8
0.9
1

C

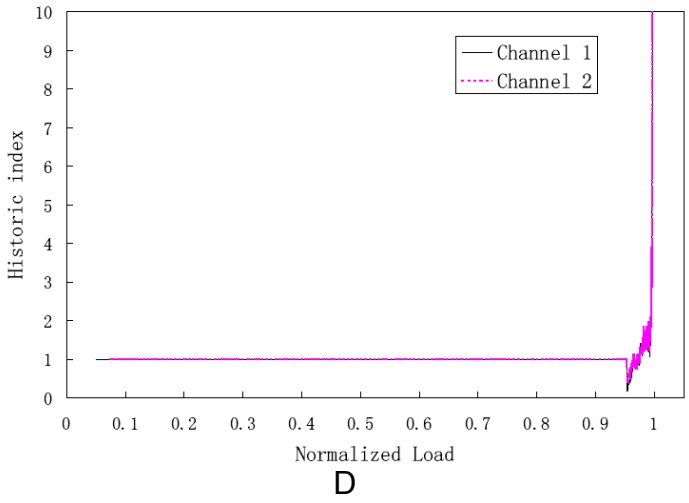

D

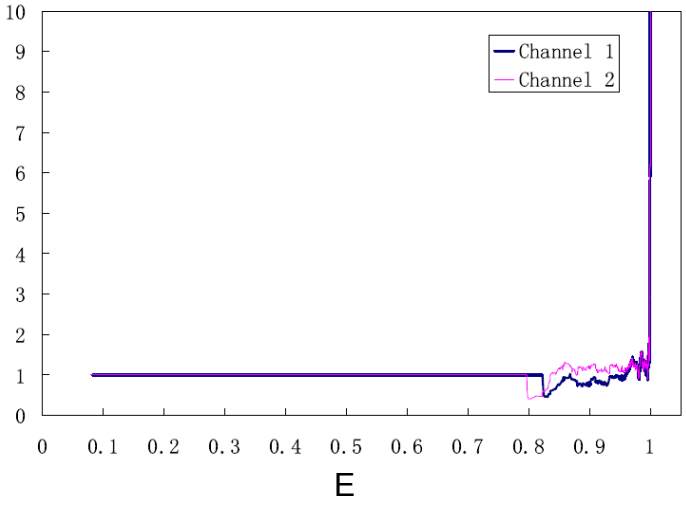

E

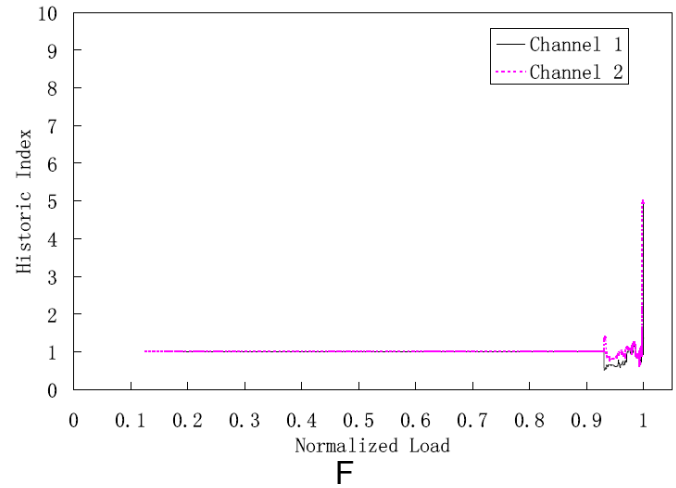

F

Figure 4-11. Historic Index versus normalized load for specimens: A. CS; B. S4; C. S8; D. WD1; E. WD5; F. WD15.

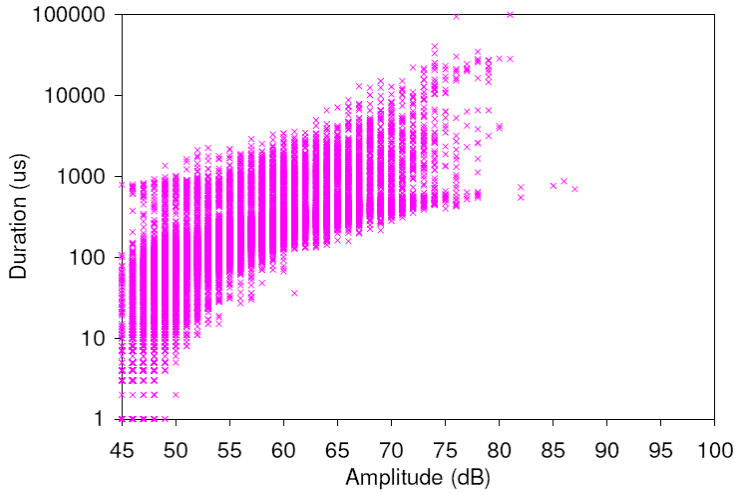
Duration (us)
100000
10000
1000
100
10
1
45 50 55 60 65 70 75 80 85 90 95 100
Amplitude (dB)

A

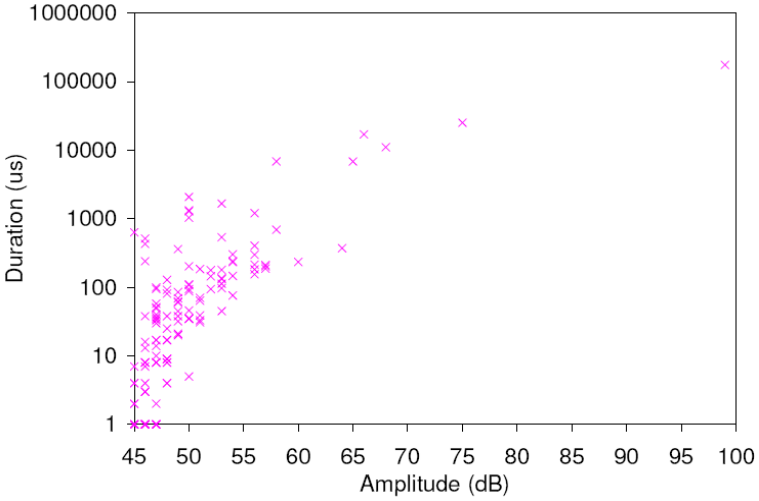
Duration (us)
1000000
100000
10000
1000
100
10
1
45 50 55 60 65 70 75 80 85 90 95 100
Amplitude (dB)

B

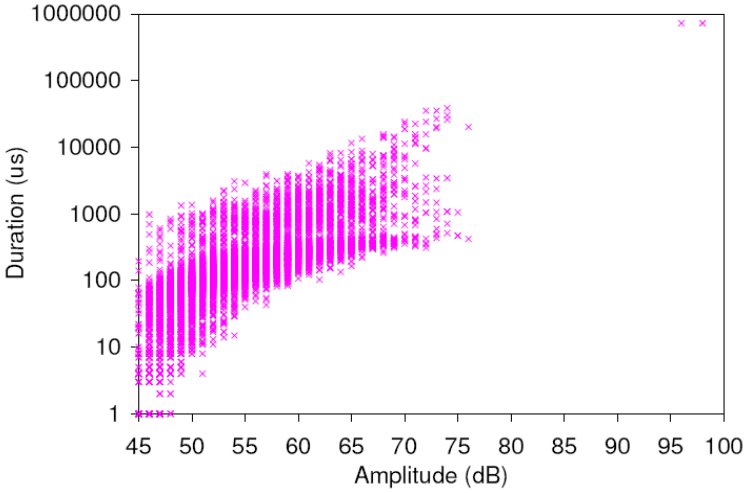
Duration (us)
1000000
100000
10000
1000
100
10
1
45 50 55 60 65 70 75 80 85 90 95 100
Amplitude (dB)

C

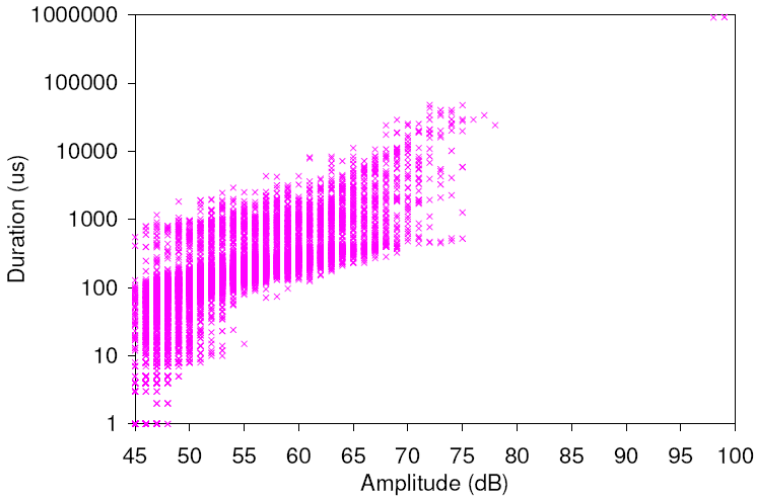

D

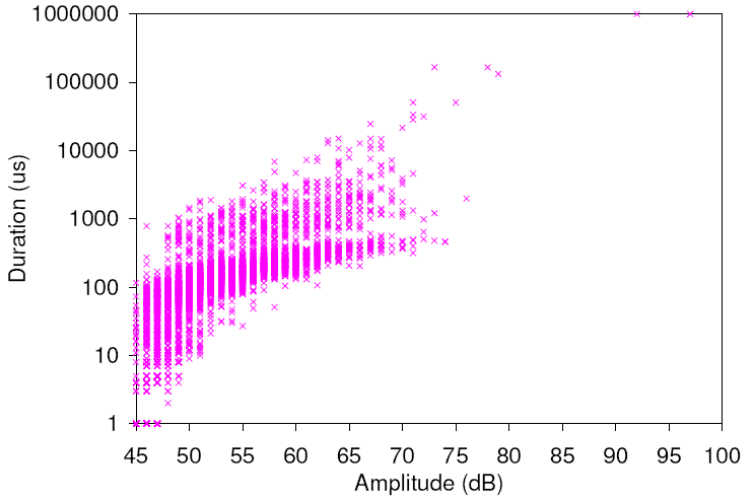

E

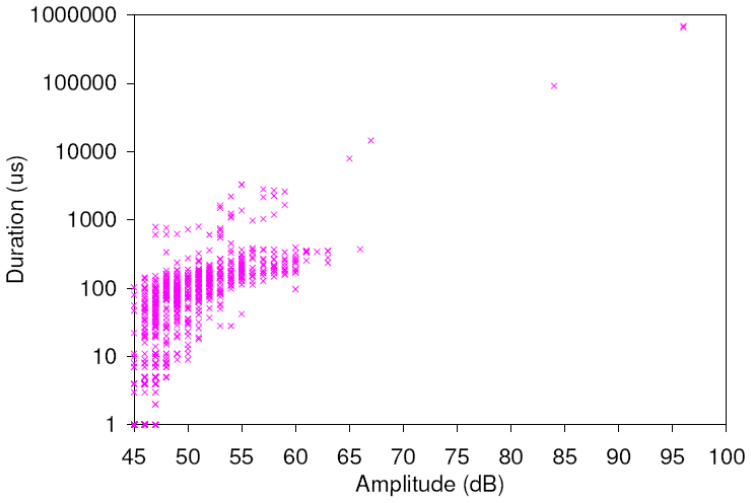

F

Figure 4-12. Duration versus amplitude for specimens: A. CS; B. S4; C. S8; D. WD1; E. WD5; F. WD15.

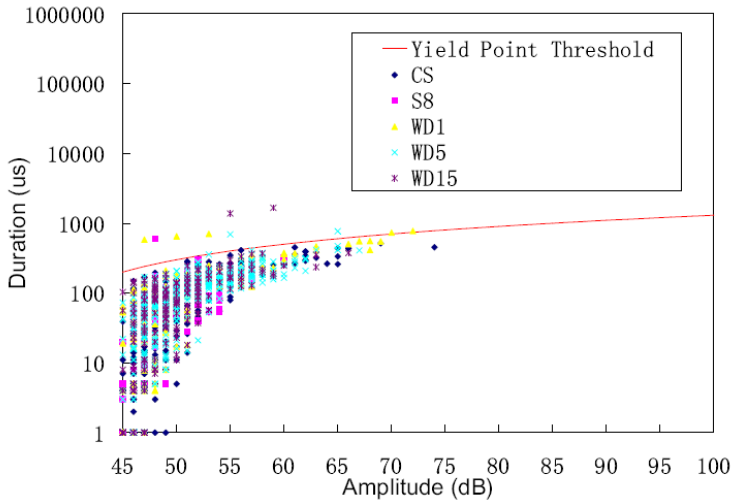
Yield Point Threshold
CS
S8
WD1
WD5
WD15
Duration (us)
Amplitude (dB)
1000000
100000
10000
1000
100
10
1
45 50 55 60 65 70 75 80 85 90 95 100

A

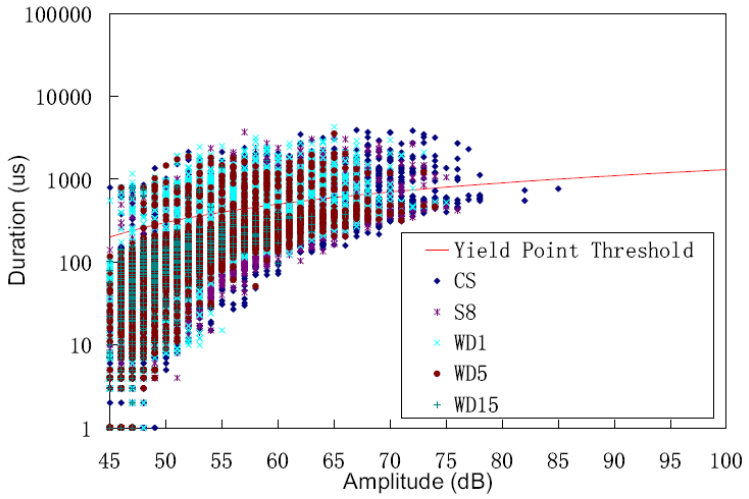
Yield Point Threshold
CS
S8
WD1
WD5
WD15
Duration (us)
Amplitude (dB)
100000
10000
1000
100
10
1
45 50 55 60 65 70 75 80 85 90 95 100

B

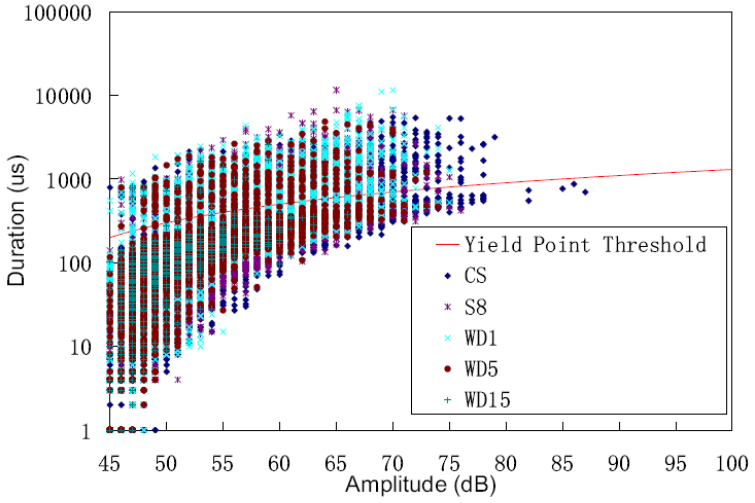
Yield Point Threshold
CS
S8
WD1
WD5
WD15
Duration (us)
Amplitude (dB)
100000
10000
1000
100
10
1
45 50 55 60 65 70 75 80 85 90 95 100

C

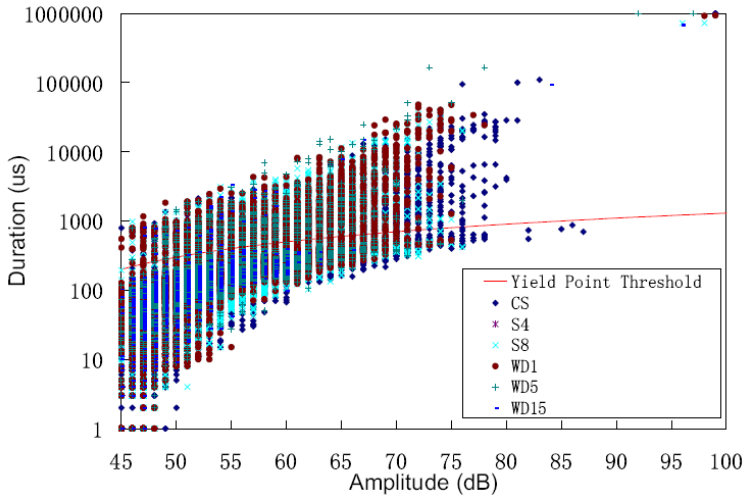

D

Figure 4-13. Duration versus amplitude for specimens; A. Elataic phase B. Up to 80% total hits; C. Up to 90% total hits; D. Total hits.

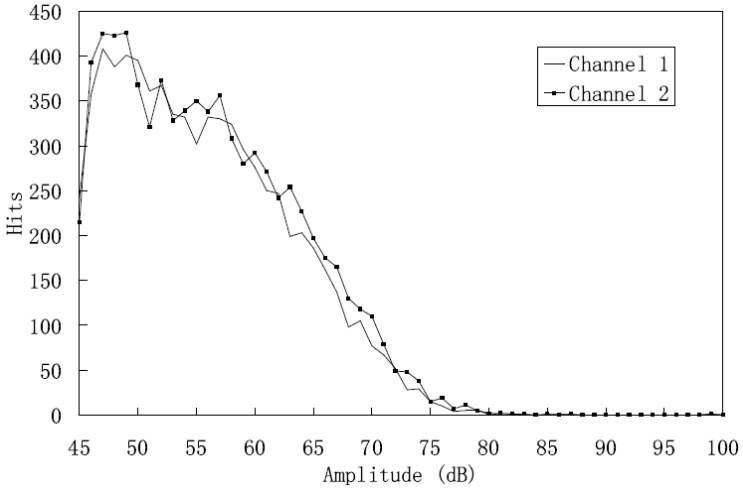

A

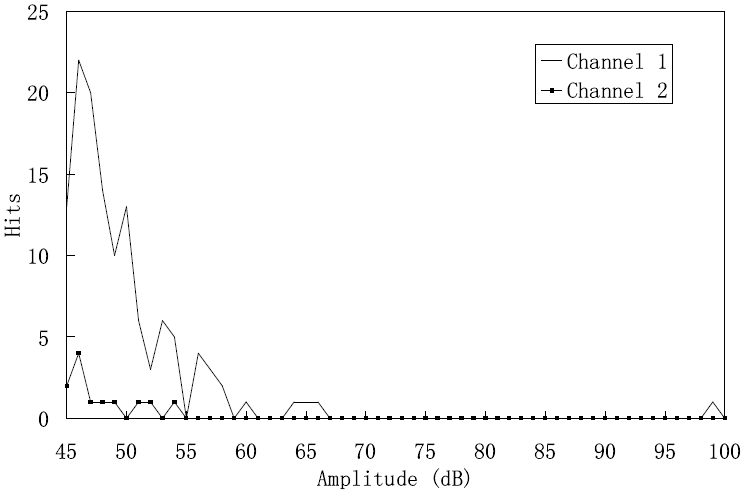

B

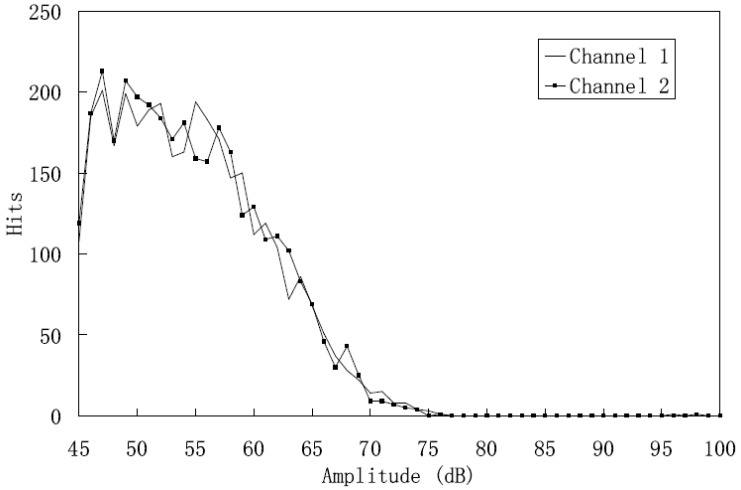
Channel 1
Channel 2
Hits
Amplitude (dB)
0
50
100
150
200
250
45
50
55
60
65
70
75
80
85
90
95
100

C

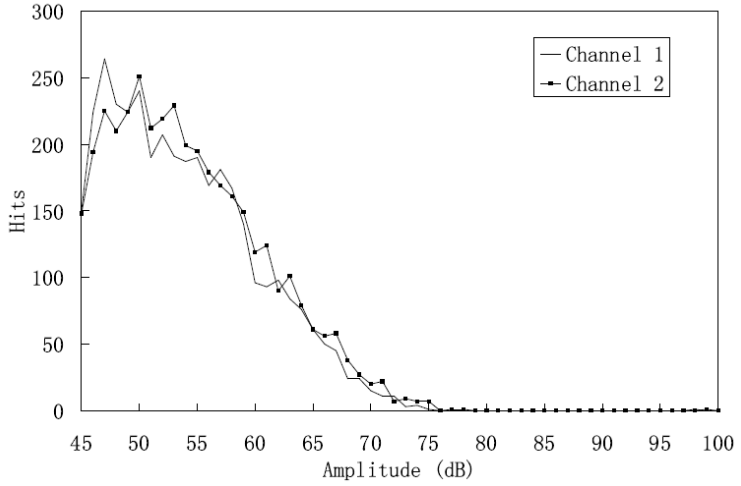
Channel 1
Channel 2
Hits
Amplitude (dB)
0
50
100
150
200
250
300
45
50
55
60
65
70
75
80
85
90
95
100

D

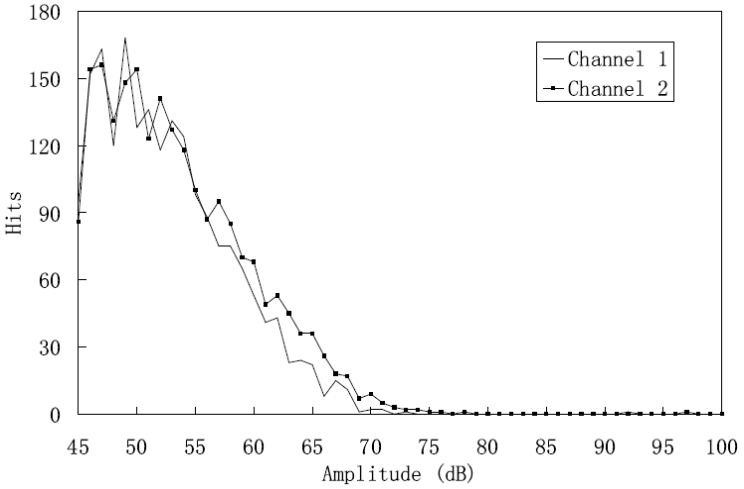
Channel 1
Channel 2
Hits
Amplitude (dB)
0
30
60
90
120
150
180
45
50
55
60
65
70
75
80
85
90
95
100

E

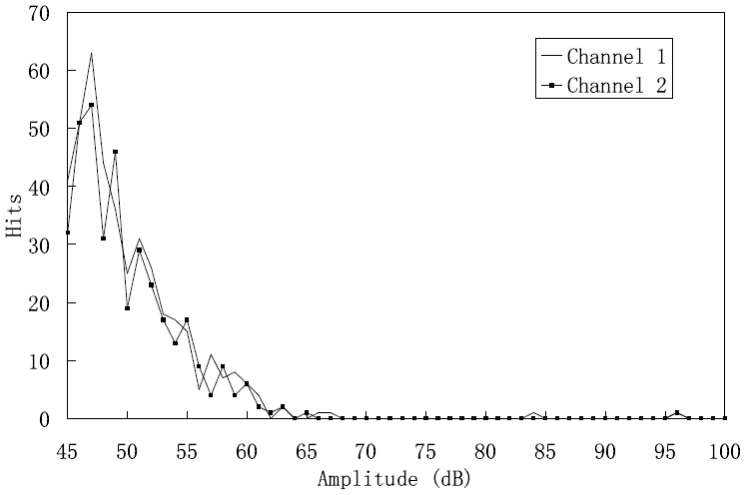

F

Figure 4-14. Amplitude distribution for specimens: A. CS; B. S4; C. S8; D. WD1; E. WD5; F. WD15.

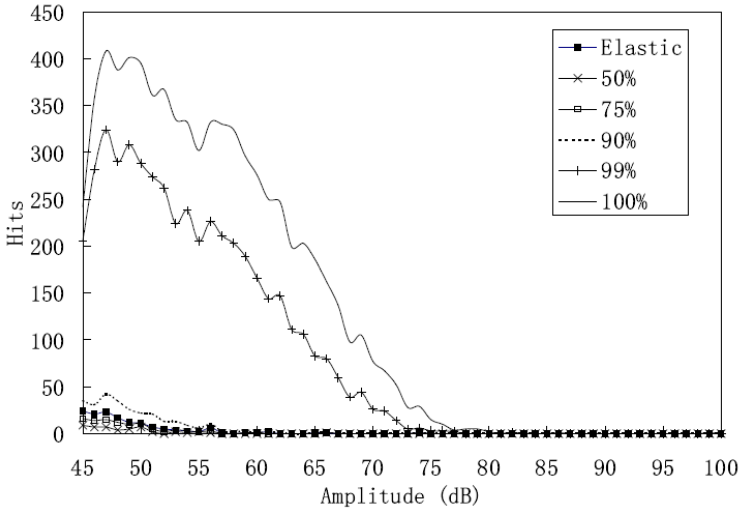
Elastic
50%
75%
90%
99%
100%
Hits
Amplitude (dB)

A

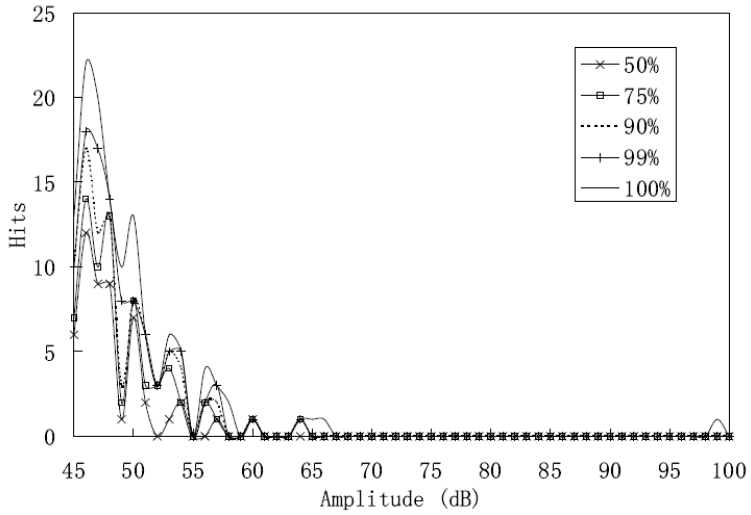
50%
75%
90%
99%
100%
Hits
Amplitude (dB)

B

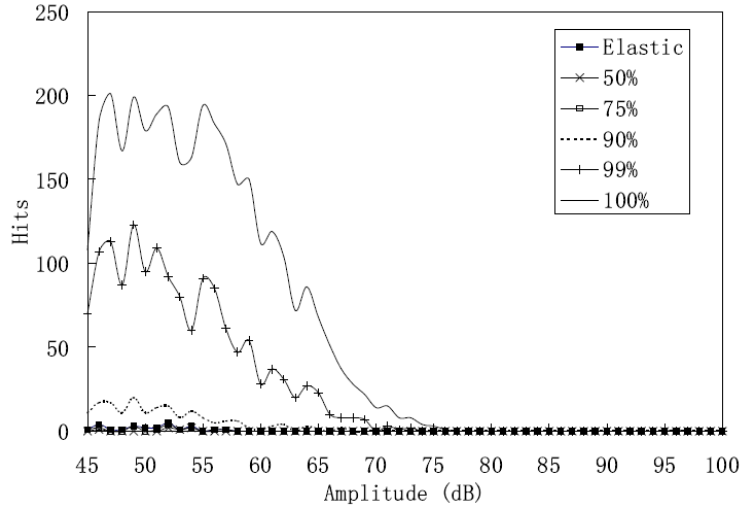
Elastic
50%
75%
90%
99%
100%
Hits
Amplitude (dB)

C

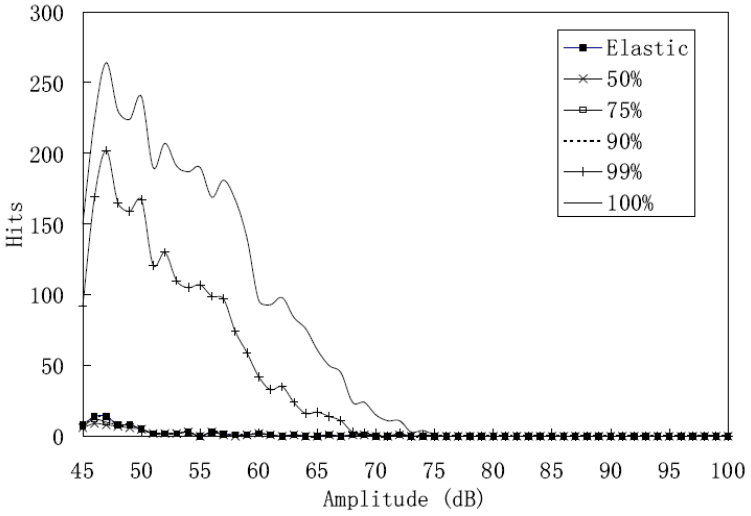

D

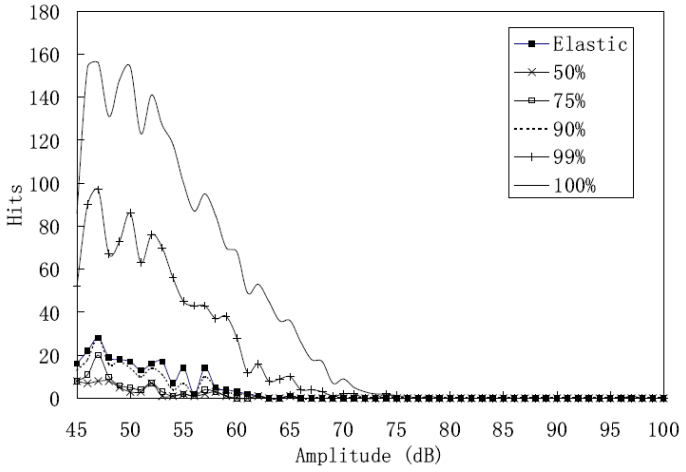

E

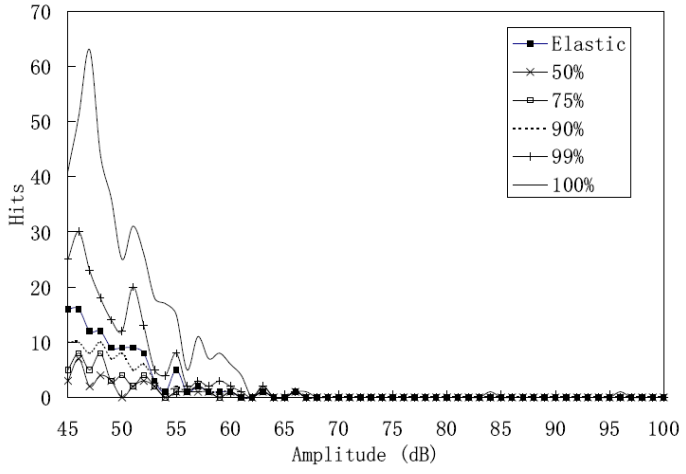

F

Figure 4-15. Progression of amplitude distribution for specimens: A. CS; B. S4; C. S8; D. WD1; E. WD5; F. WD15.

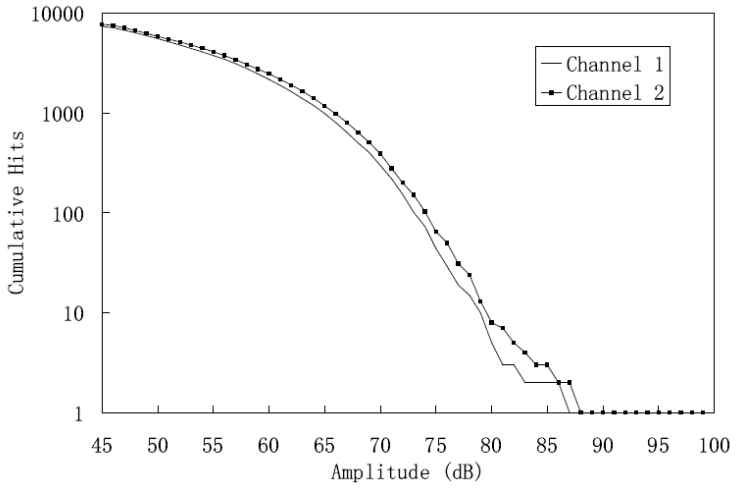
10000
1000
100
10
1
Cumulative Hits
Channel 1
Channel 2
45 50 55 60 65 70 75 80 85 90 95 100
Amplitude (dB)

A

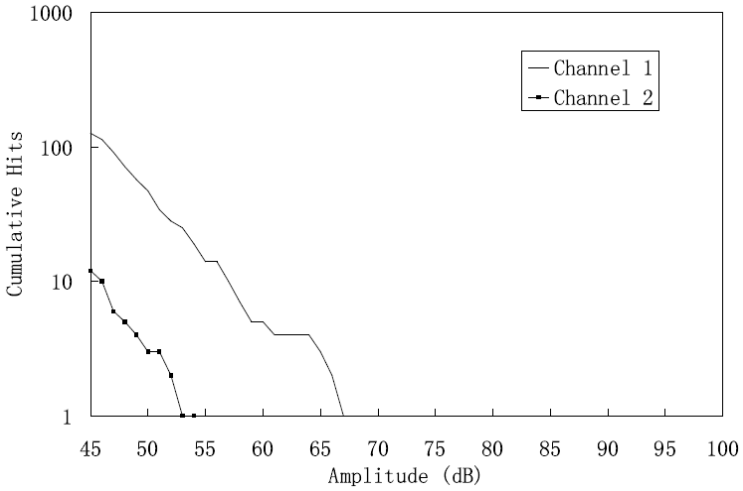
1000
100
10
1
Cumulative Hits
Channel 1
Channel 2
45 50 55 60 65 70 75 80 85 90 95 100
Amplitude (dB)

B

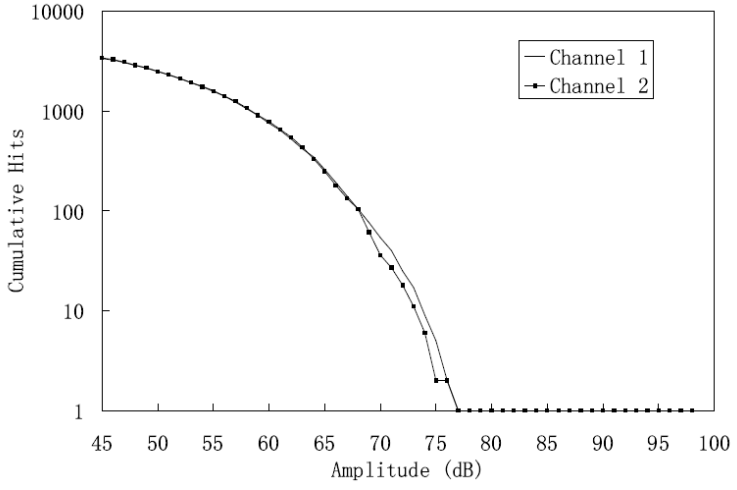
10000
1000
100
10
1
Cumulative Hits
Channel 1
Channel 2
45 50 55 60 65 70 75 80 85 90 95 100
Amplitude (dB)

C

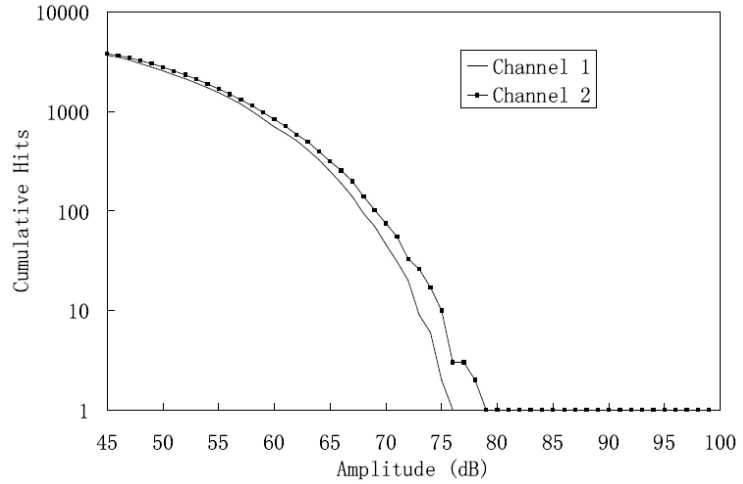

D

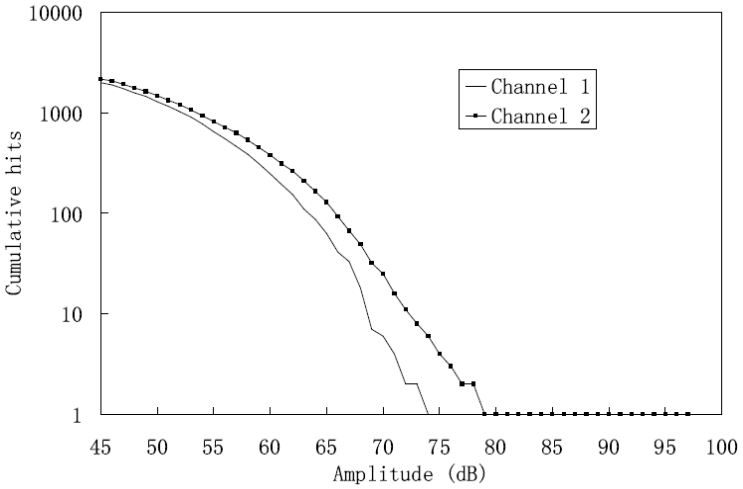

E

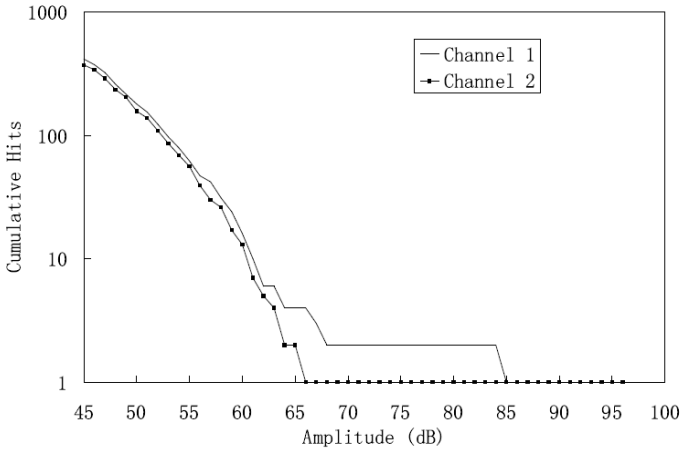

F

Figure 4-16. Cumulative amplitude distribution for specimens: A. CS; B. S4; C. S8; D. WD1; E. WD5; F. WD15.

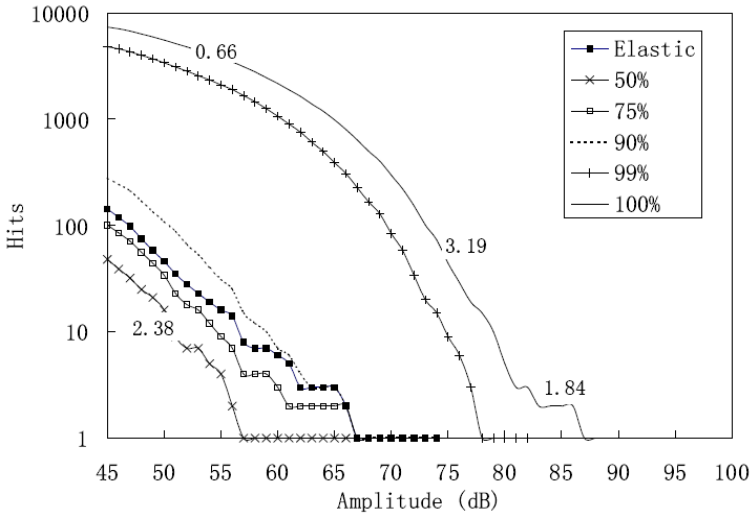
10000
1000
100
10
1
Hits
0.66
3.19
2.38
1.84
Elastic
50%
75%
90%
99%
100%
45 50 55 60 65 70 75 80 85 90 95 100
Amplitude (dB)

A

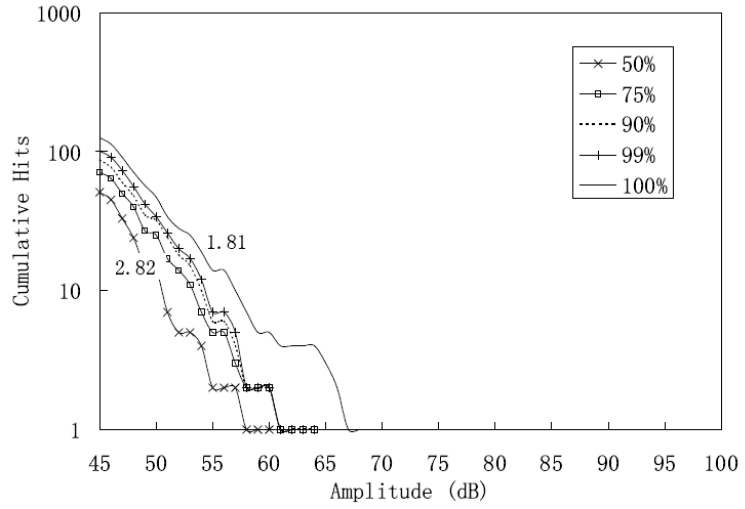
1000
100
10
1
Cumulative Hits
1.81
2.82
50%
75%
90%
99%
100%
45 50 55 60 65 70 75 80 85 90 95 100
Amplitude (dB)

B

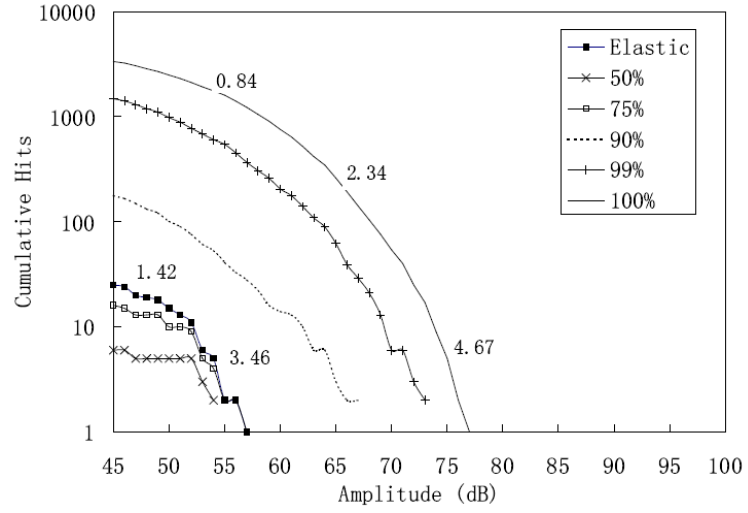
10000
1000
100
10
1
Cumulative Hits
0.84
2.34
1.42
3.46
4.67
Elastic
50%
75%
90%
99%
100%
45 50 55 60 65 70 75 80 85 90 95 100
Amplitude (dB)

C

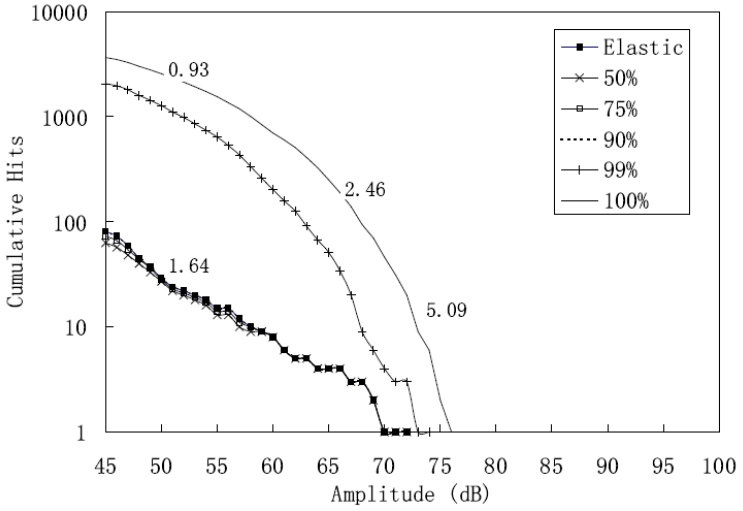

D

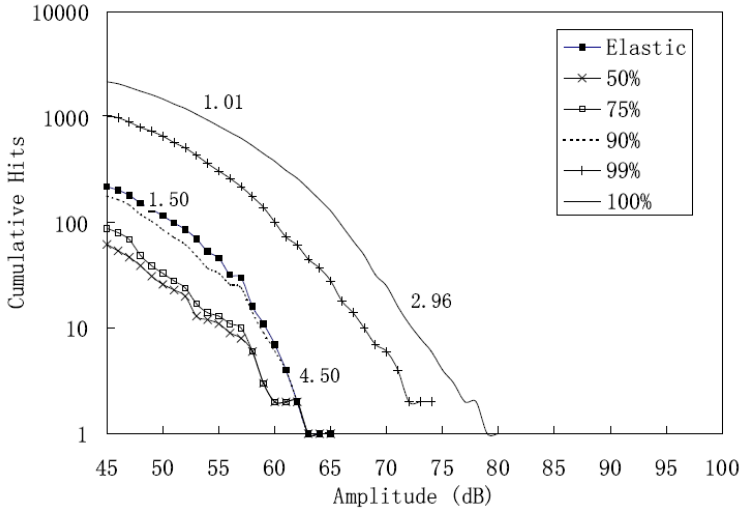

E

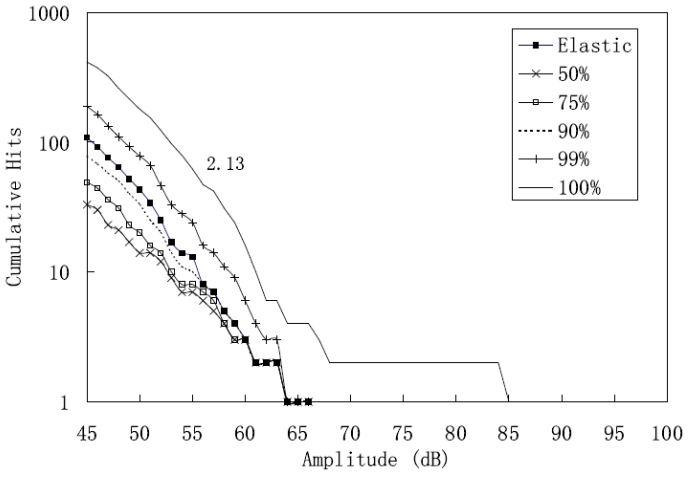

F

Figure 4-17. Progression of cumulative amplitude distribution for specimens: A. CS; B. S4; C. S8; D. WD1; E. WD5; F. WD15.

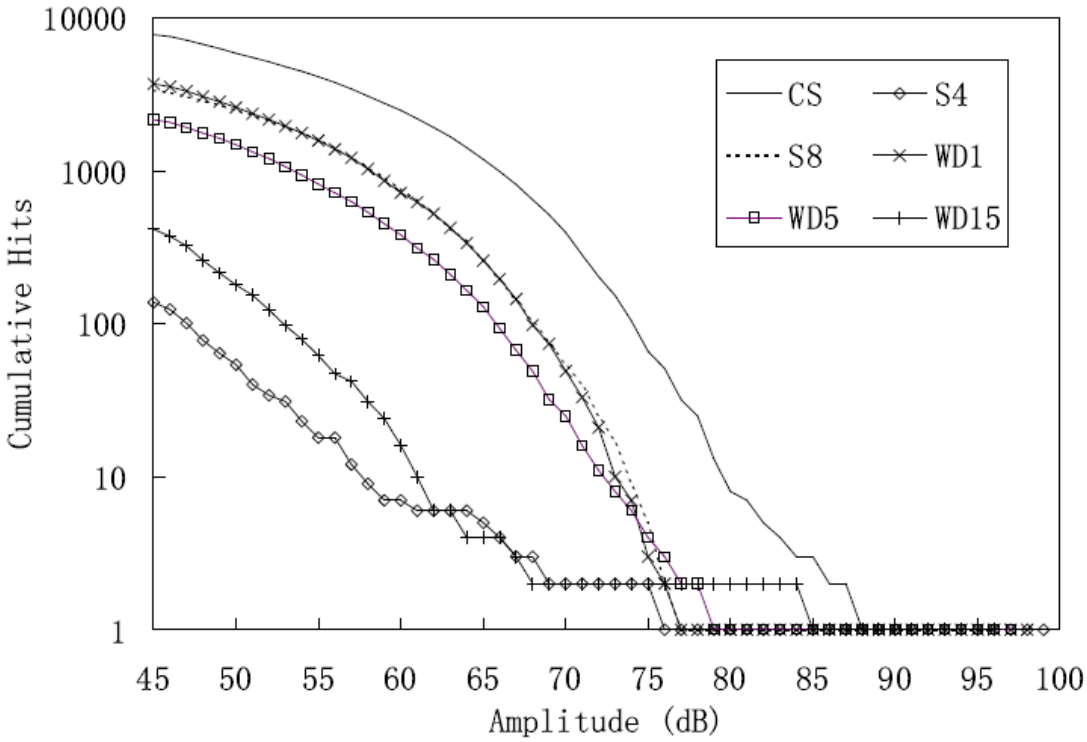

Figure 4-18. Comparison of cumulative amplitude distribution for all specimens.

CHAPTER 5
FATIGUE PROPERTY OF CFRC

The objective of this chapter is to identify the effect of cyclic loading on CFRC's property and to identify the onset of significant damage under various loading conditions using AE. Both mechanical and AE results are discussed and compared.

Experimental Program

Specimens Preparation

The specimens used in fatigue third-point bending test were the same dimensions as those in static bending test, that is, 2 inches by 2 inches by 8 inches long. Only dry specimens were studied in this experimental program.

Load Procedure

The loading was load controlled at the frequencies shown in Table 5-1. A hidden frequency was used for lower maximum fatigue loads in order to save testing time. The load ratio, which is the ratio of minimum to maximum load, was set at 0.05.

Testing Facilities

The fatigue bending tests were conducted at the state of Florida Material Research Park in Gainesville. The testing machine used was an MTS 244 loading system (Figure 5-1). The control system for the machine provided the number of cycles, time, load and deflection at the loading points. The experimental setup is shown in Figure 5-2.

CFRC Fatigue Life

Five fatigue tests were conducted with the maximum fatigue loads to be 2,000 lbs, 1,800 lbs, 1,700 lbs, 1,600 and 1,500 lbs. The number of cycles for each load is given in Table 5-2. The AE results will be discussed for the load of 2,000 lbs, 1,800 lbs and 1,600 lbs loads.

Identification of AE Resulting from Friction

AE signals resulting from friction is a common problem with AE inspection during fatigue tests. Typically the friction mechanisms are believed to come from the closure of crack surfaces at certain level stress levels. Friction between surfaces creates AE signals which follow certain rules. The friction starts at a particular point and continues, repeating at the same load level on every cycle. The friction AE usually contrasts with emission from new damage which increases as failure approaches.

In our research, friction was found to exist as well. Figure 5-3, 5-4 and 5-5 show the 3-D plots of amplitude, number of cycles and loading percentage for every cycle. The load reached its maximum value at 50% of each cycle, after which it dropped to a minimum and began another cycle. It can be seen from the plots that friction emissions repeated themselves at particular loads during each cycle, with some occurring at the unloading stage.

The plot of amplitude versus time for each test is given in Figure 5-6. Table 5-3 shows the number of hits resulting from friction and damage development. One can see the number of friction AE at 2,000 lbs test was much less than the number at the 1,800 and 1,600 lbs loads. In the 2,000 lbs test, damage initiated and developed at a much higher rate than for other tests. The cyclic loads altered

the existing crack surfaces during each cycle, therefore very little friction occurred. In the 1,800 and 1,600 lbs tests, a “steady state” existed while damage accumulated until the final failure phase. During this period, the existing cracks opened and closed under cyclic loads, where the friction generated AE signals were created.

The friction data were not related directly to damage development; therefore they were eliminated from valid data.

Mechanical Parameters to Identify the Damage Process

The stress versus strain relationship for the 2,000 lbs fatigue testing is plotted in Figure 5-7. One cycle is highlighted in this plot. The definition of secant modulus is designated as E in the plot. Secant modulus is the slope of the line connecting the origin and a given point on the stress-strain curve, or the ratio of nominal stress to corresponding strain at any specified point on the stress-strain curve expressed in force per unit area. The secant modulus was calculated for each cycle, and is shown in Figure 5-8.

From Figure 5-8 we can see that the secant modulus goes through an increasing phase, a steady phase and then drops at the final failure phase. The secant modulus change is believed to indicate the corresponding material damage levels. The AE amplitude is also shown in the same plots, and one can see that the final failure phase is accompanied by an increase in AE hits and amplitude. In Figure 5-8A, the changing of secant modulus covers all the fatigue testing, meaning the development of damage continues throughout the entire loading process. Therefore the AE signal shows a steady increase in the number of hits and their amplitudes.

Figure 5-8B shows the secant modulus development curve. For the first part of the curve, the secant modulus slowly increases until it reaches 90% of the fatigue test. It then becomes relatively linear at a much steeper slope. Corresponding to the development of damage shown in the secant modulus curve, for the first part of the test, there is only scattered AE. The amplitudes of most signals are also low before the final failure phase, which means the majority of the internal damage is due to matrix cracking. At the final phase, AE shows an increase in both the number of hits and amplitude. High amplitude AE occurs, which indicates final failure of the material.

It is noted in Figure 5-8C that the secant modulus curve for 1,600 lbs maximum load has sudden decrease after 15% of the cycles. The drop then returns back to its original shape. On the other hand, at the same moment of this decrease one observes a burst of AE hits, which implies that internal damage has occurred. Note that the peak amplitude of these AE hits is 71 dB, which indicates that the damage involves cement matrix cracking and fiber/matrix debonding, without developing fiber breakage. A possible explanation of this phenomenon is that the localized stress has been created due to the inhomogeneity of the material. At the location where the cement matrix cracks, debonding between fiber and matrix occurs. The stress is then redistributed by the fiber to cement matrix to stronger matrix. Because the material is generally intact, the stress redistribution is successful. As a result, the secant modulus returns to its normal trend. The initiation of the final failure phase, where the

secant modulus curve begins to decrease, occurs around 80% of the completed test. It is obvious that this process is accompanied by higher amplitude AE.

Conventional AE Analysis

In this section the conventional AE data are discussed. Same as in Chapter 4, conventional AE data are referred to as hit, count, energy, signal strength and Historic Index. The cumulative hits versus normalized cycles, cumulative counts versus normalized cycles, cumulative energy versus normalized cycles, cumulative signal strength versus normalized cycles and Historic Index versus load are plotted in Figures 5-9 to 5-11.

Maximum Load = 2,000 lbs

The plot of cumulative hits shows a steady increase. This means the damage occurs and develops continuously throughout the testing process. It was found that the cumulative counts, energy and signal strength plots have different shapes compared to cumulative hits. They are initially low but start to increase exponentially around 60% of the complete test. The reason for this difference is due to the definitions of energy, signal strength and count. For example, for cumulative counts, the number of counts per hit increases as final failure approaches. Therefore the cumulative counts, energy and signal strength are more representative of the final failure phase, while the plot of cumulative hits better displays the whole progress. The Historic Index plot begins its increase around 80%.

Maximum Load = 1,800 lbs

The conventional AE plots are given in Figure 5-10. They show an abrupt increase around 90% of its fatigue life, and the position obviously correlates with the knee position of the secant modulus.

Maximum Load = 1,600 lbs

The plots indicate two knee positions. One is at the local damage level shown in Figure 5-8C. The other one is around 80%, which corresponds to the onset of final failure.

Amplitude Distribution Analysis

Amplitude distribution is the plot of hit numbers versus amplitude. It shows the number of hits each level of amplitude contains. Many researchers have used this plot for AE signature analysis. It has been shown that the plot may show one or more humps with the peak amplitude of each hump characterizing the fracture mechanism.

Figure 5-16 shows the amplitude distribution for the 2,000 lbs fatigue test. AE from both of the sensors are plotted in one figure. Two channels yield similar profiles, and the peak amplitude occurs at 47 dB, 49 dB, 56 dB, 67 dB and 70 dB. The progression of amplitude distribution is shown in Figure 5-17. It shows that the amplitude distribution curves for 80%, 90%, 95% and 100% of fatigue life show similar shapes, meaning that at 80% of fatigue test, the damage within the specimen has been undergoing damage including cement matrix cracking and fiber/matrix debonding. Fiber breakage occurs at the final failure phase.

The similar conclusion can be drawn from the progression of cumulative amplitude distribution plot. The 50% curve is linear and concentrates in low

amplitude range, which means the main damage mechanism is matrix cracking. The 80%, 90%, and 95% curves show similar profiles. At the amplitude between 65 and 75 dB, one can see the slope of the line, which is also known as b-value, is approximately 3.86. At the final failure phase, due to the involvement of fiber breakage, the 100% curve deviates at the high amplitude range with a corresponding b-value of 1.59.

The progression of amplitude distribution for 1,800 lbs is shown in Figure 5-21. The majority of hits occur during the last 5% of the fatigue test. The same observation can be made in Figure 5-23, which shows the progression of cumulative amplitude distribution. Until 95% of the fatigue life, the majority of hits are concentrated within the amplitude range of 45 dB and 65 dB. The linear shape of the curves up to 95% and a b-value of 1.90 indicate that the main fracture mechanism is cement matrix cracking. After that fibers start to exhibit damage. The b-value of 4.35 at the 60 dB to 70 dB range on the 99% curve proves our observation in another way. At the end of the test, fiber breakage occurs and produces a b-value of 1.59 at high amplitude range.

For the 1,600 lbs fatigue test, the most hits occur during the last 10% of the test. The cumulative amplitude distribution in Figure 5-27 shows that before 80% of its fatigue life, the major fracture mechanism is cement matrix cracking. After that, the fibers start to incur in damage, and the b-value of 3.18 is within the fiber/matrix debonding range. At the end of test, a b-value of 1.76 indicates the onset of final failure.

Summary

In this chapter, the mechanical property and AE plots during fatigue testing with different maximum fatigue loads is discussed. The significant findings from this chapter are as follows.

1. AE signals resulting from mechanical friction were separated from damage induced AE signals.

2. The secant modulus during fatigue testing usually undergoes an increasing phase, followed by a constant then falling phase. Changing of secant modulus is an indication of damage level within the specimen.

3. Conventional AE analysis shows that AE is useful in detecting internal damage in real time.

4. The amplitude distribution analysis shows that for short cycle fatigue tests, such as the 2,000 lbs fatigue test, the damage is distributed over the entire fatigue test. For high cycle fatigue tests, for example 1,800 lbs and 1,600 lbs tests, the damage is found to be more concentrated in the last 10% of their fatigue life.

5. The cumulative amplitude distribution and b-value was shown to be an effective method to study the fracture mechanism with the b-values for different materials showing different ranges of values. The b-values obtained during fatigue testing are found to be within the same range as in Chapter 4.

Table 5-1. Fatigue third-point bending test, load frequency

Maximum Load (lbs)	Load Frequency (Hz)
1,500	20
1,600	20
1,700	20
1,800	10
2,000	5

Table 5-2. The fatigue life under different loads.

Maximum Fatigue Load	Cycles
2,000	758
1,800	37,552
1,700	119,314
1,600	169,603
1,500	1,602,995

Table 5-3. The number of friction and valid AE hits for representative tests.

Fatigue test	Number of valid AE data	Number of friction hits
2,000	6,666	185
1,800	23,971	57,134
1,600	62,434	172,784

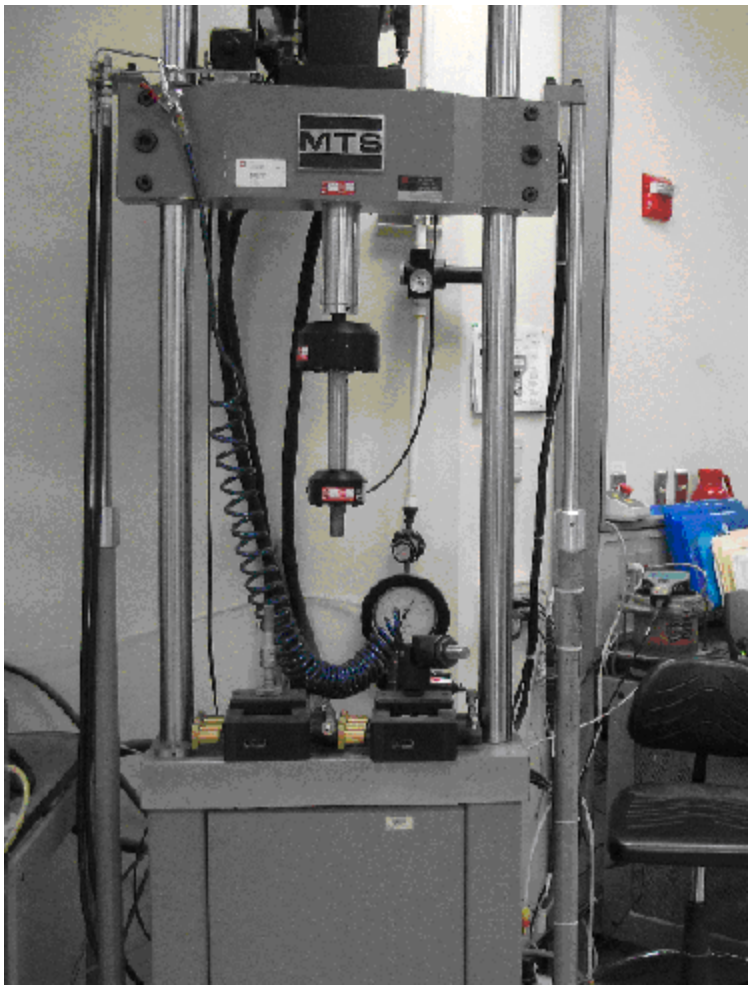

Figure 5-1. Fatigue third-point bending test, MTS 244

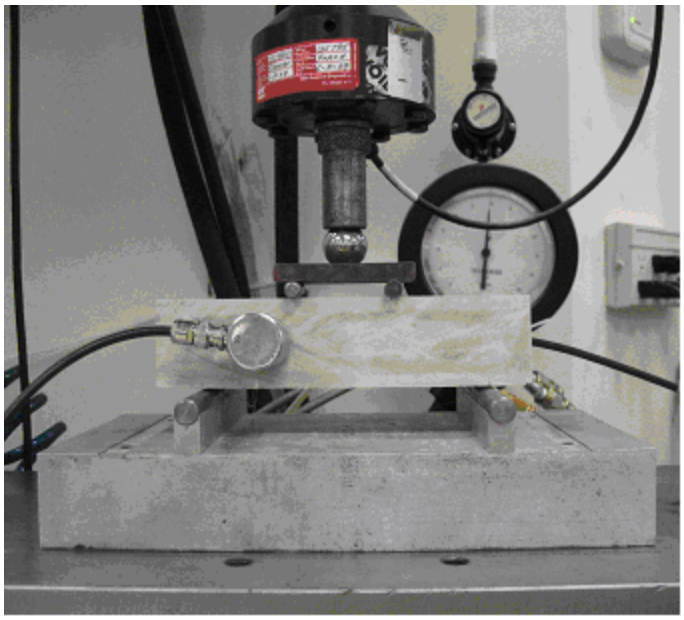

Figure 5-2. Fatigue third-point bending test setup.

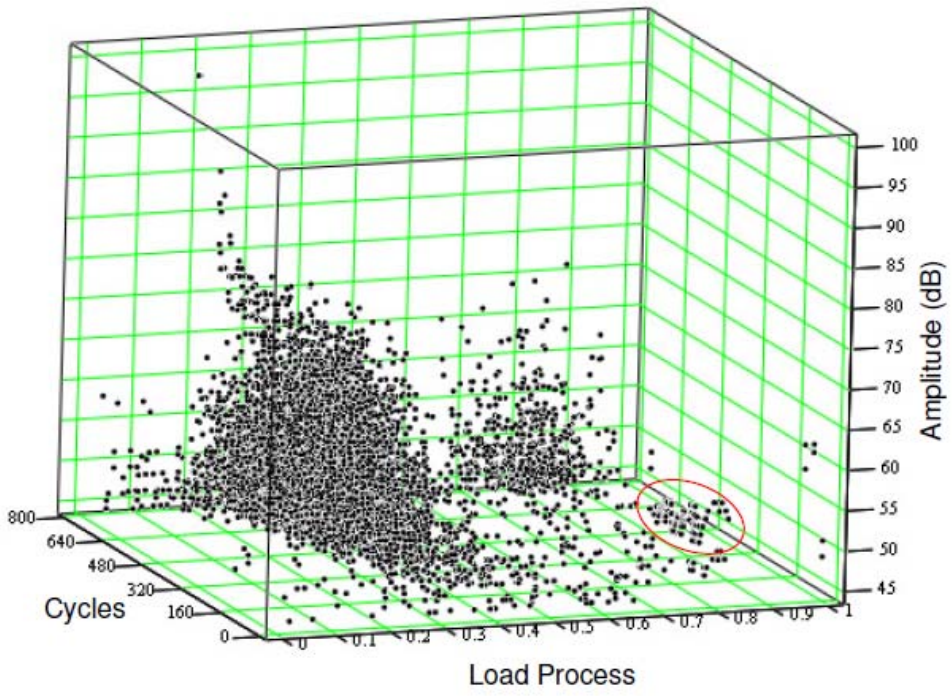

A

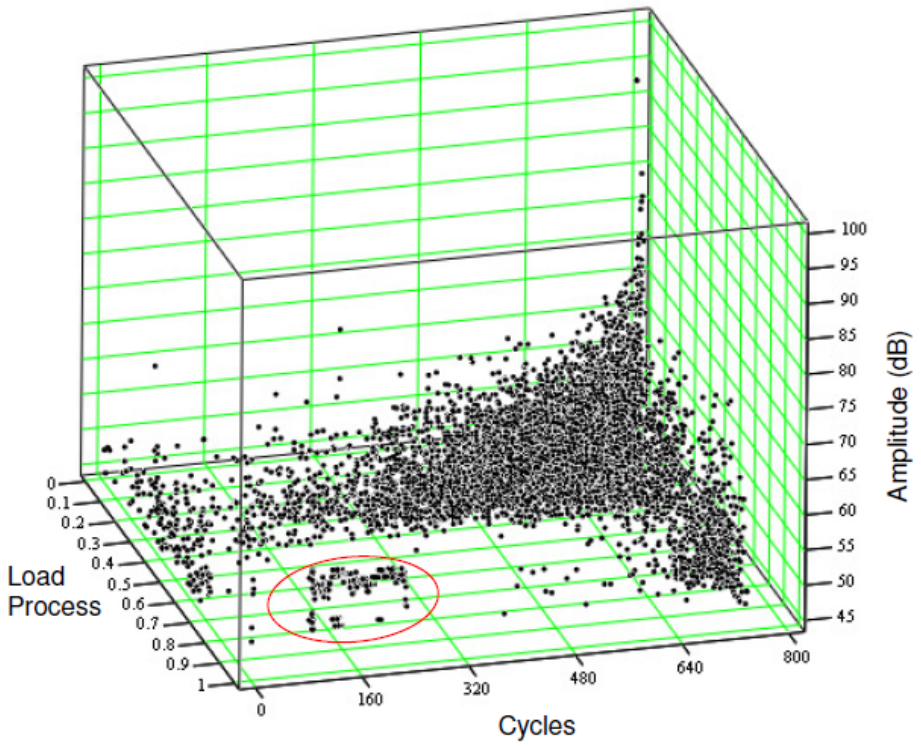

B

Figure 5-3. Identification of friction data, maximum fatigue load = 2,000 lbs.

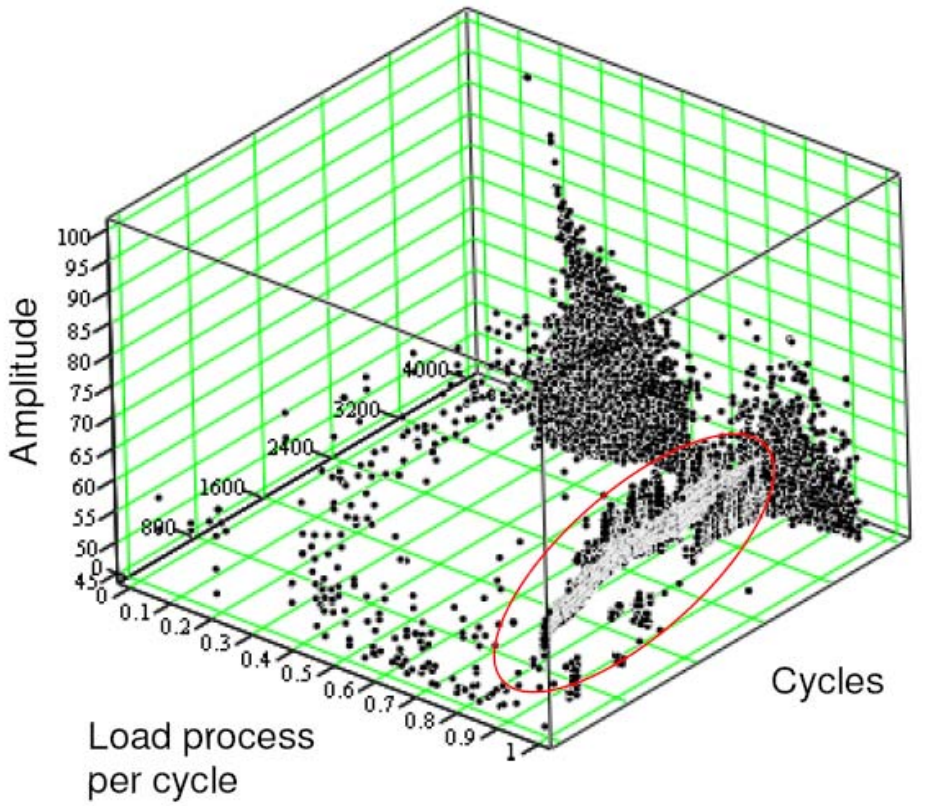

A

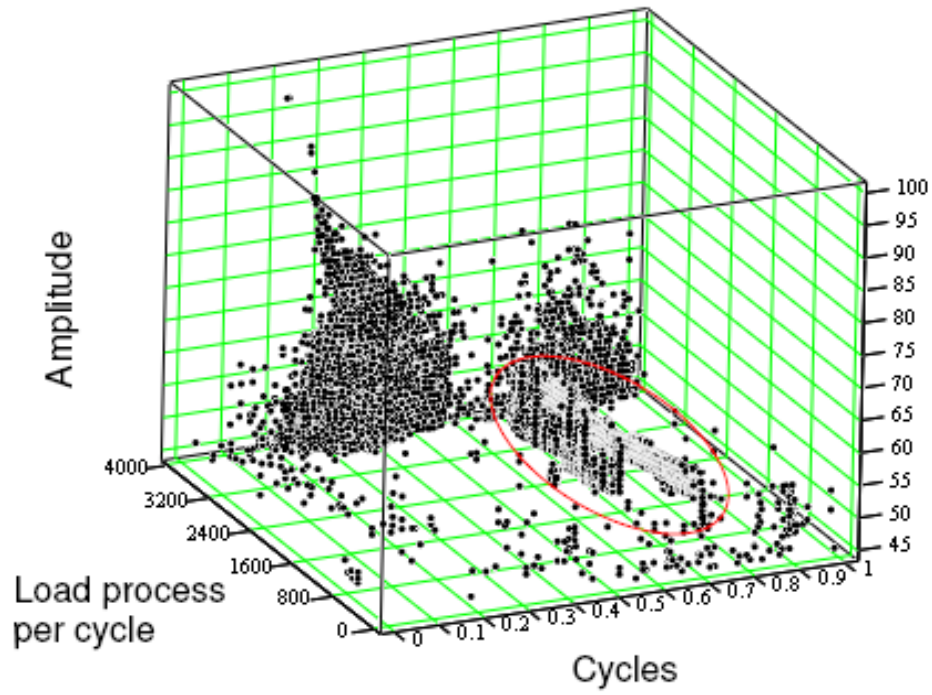

B

Figure 5-4. Identification of friction data, maximum fatigue load = 1,800 lbs.

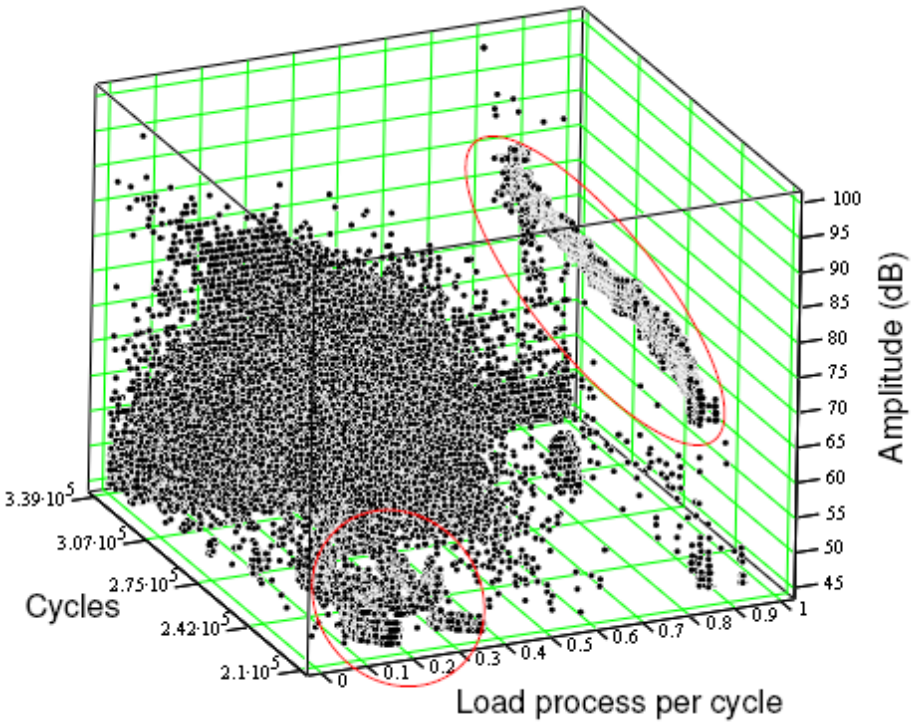

A

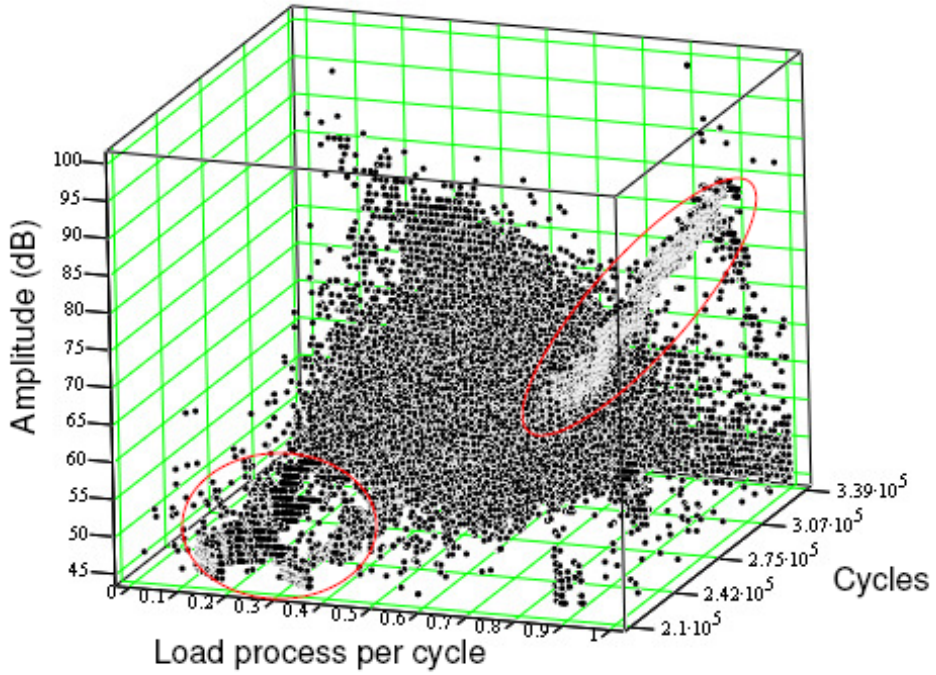

B

Figure 5-5. Identification of friction data, maximum fatigue load = 1,600 lbs.

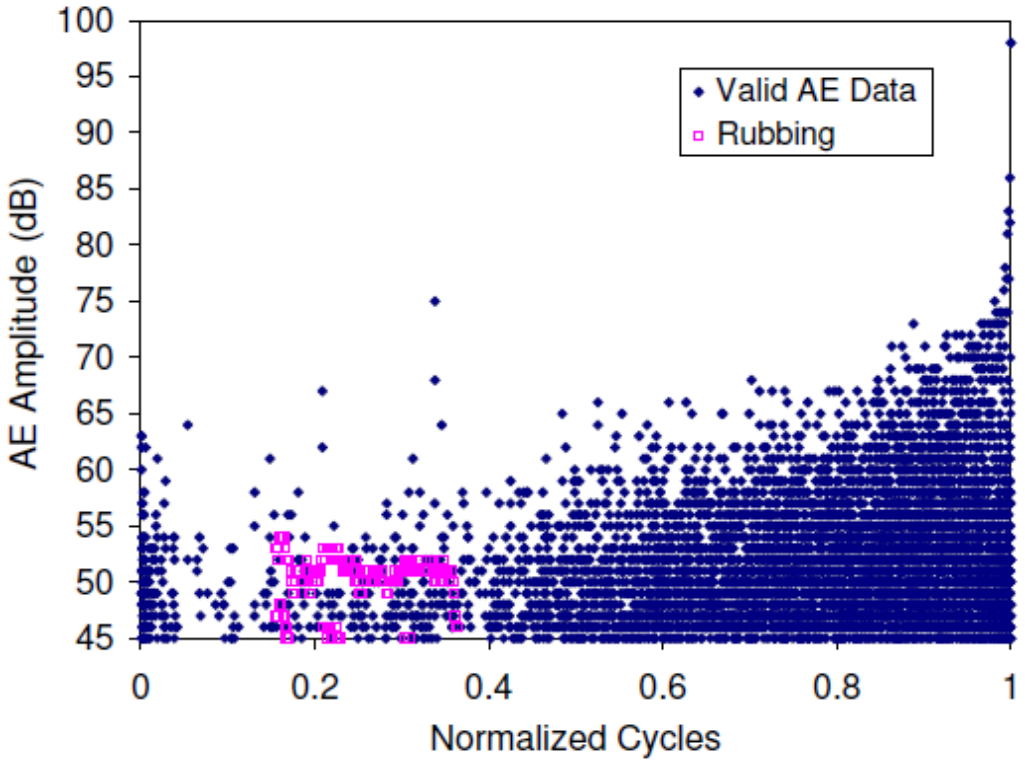
Valid AE Data
Rubbing
AE Amplitude (dB)
100
95
90
85
80
75
70
65
60
55
50
45
0
0.2
0.4
0.6
0.8
1
Normalized Cycles

A

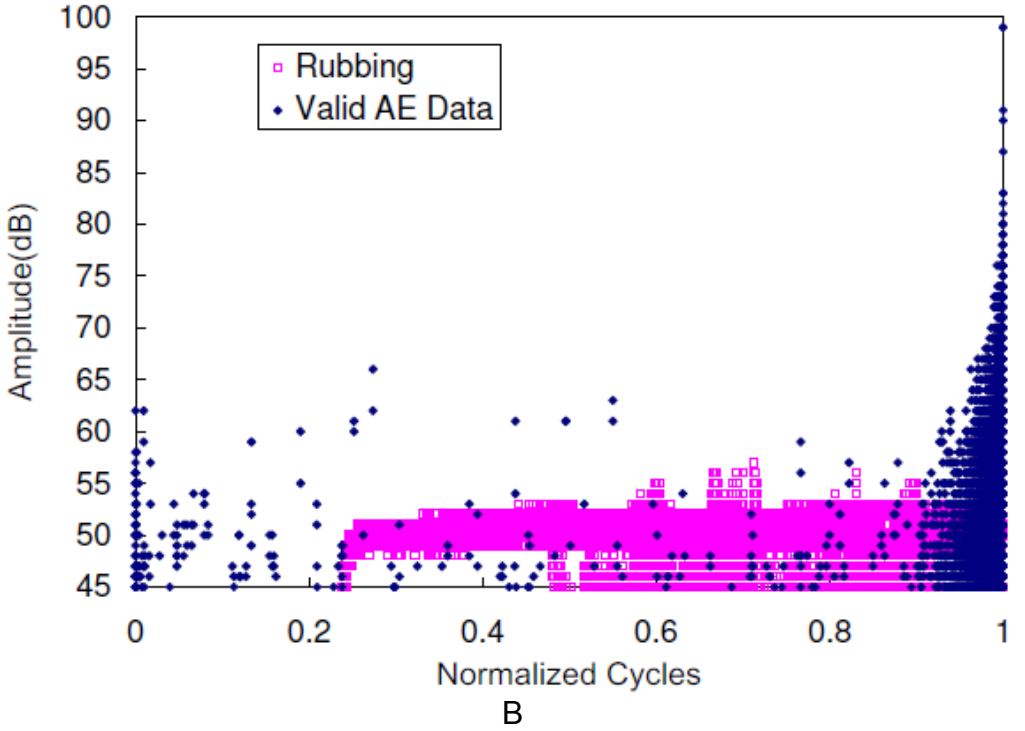
Rubbing
Valid AE Data
Amplitude(dB)
100
95
90
85
80
75
70
65
60
55
50
45
0
0.2
0.4
0.6
0.8
1
Normalized Cycles

B

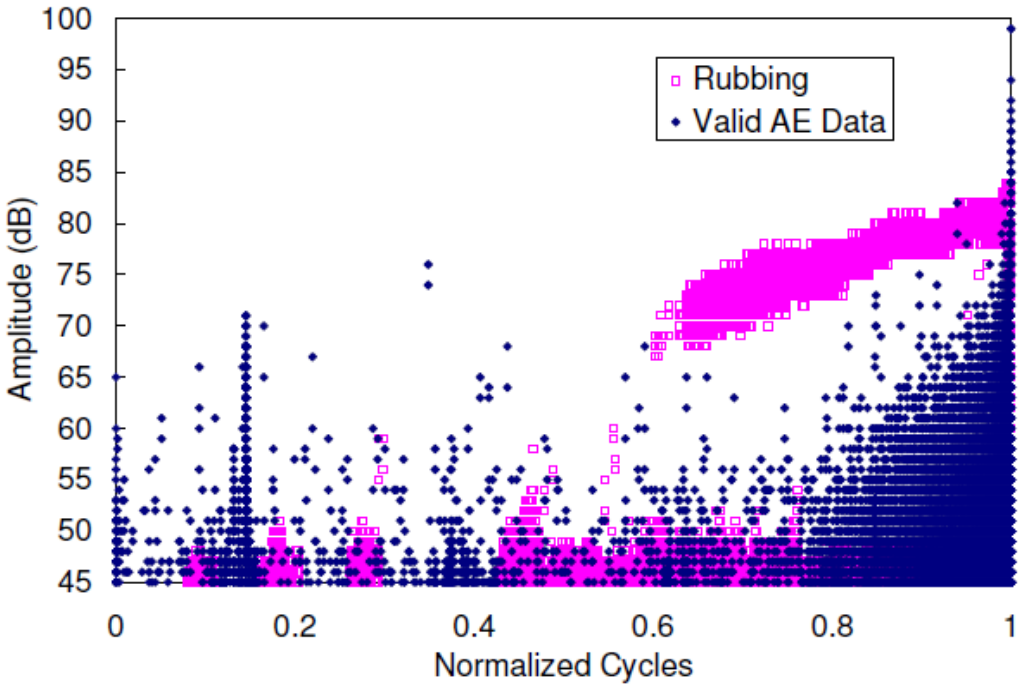

C

Figure 5-6. Amplitude versus normalized cycles with identified friction AE A. maximum load = 2,000 lbs; B. maximum load = 1,800 lbs; C. maximum load = 1,600 lbs.

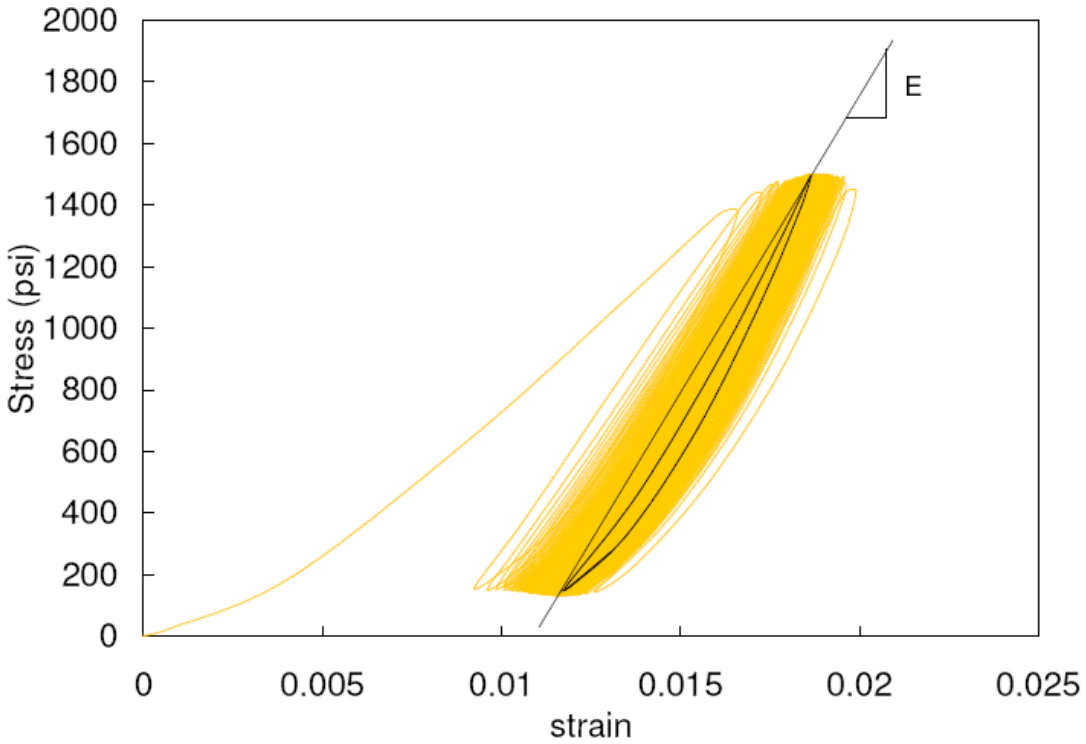

Figure 5-7. Example of stress-strain relation and secant E, maximum load = 2,000 lbs

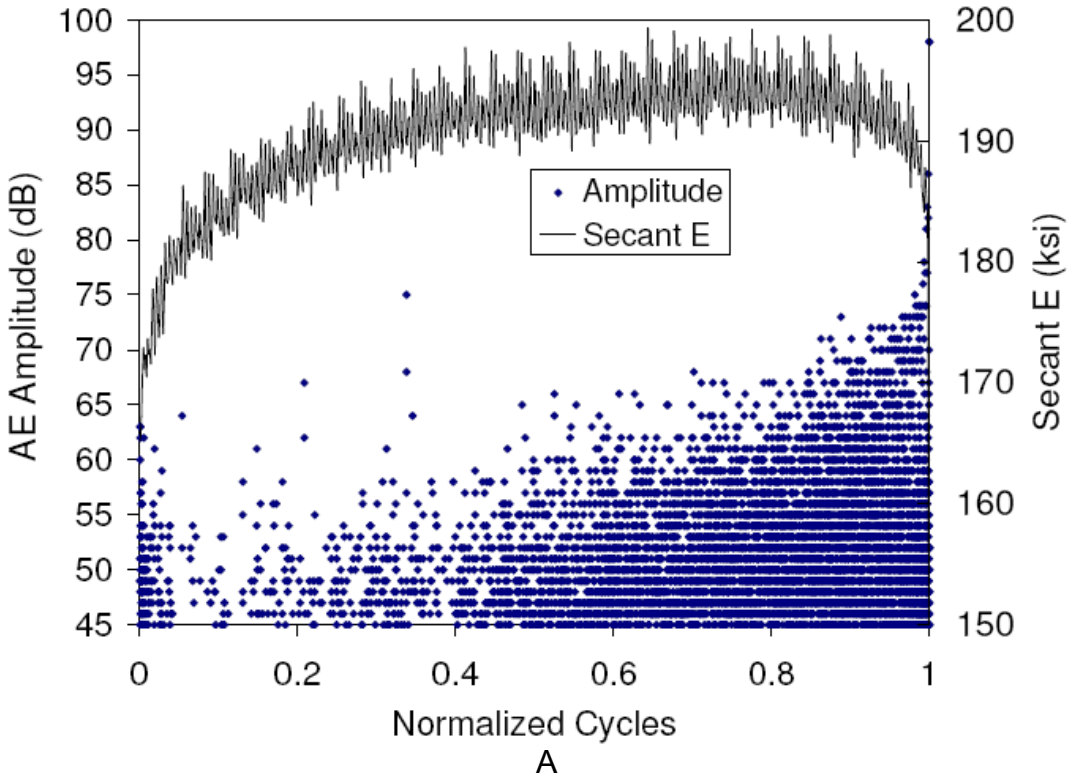
AE Amplitude (dB)
Secant E (ksi)
Amplitude
Secant E
Normalized Cycles
100
95
90
85
80
75
70
65
60
55
50
45
200
190
180
170
160
150
0
0.2
0.4
0.6
0.8
1

A

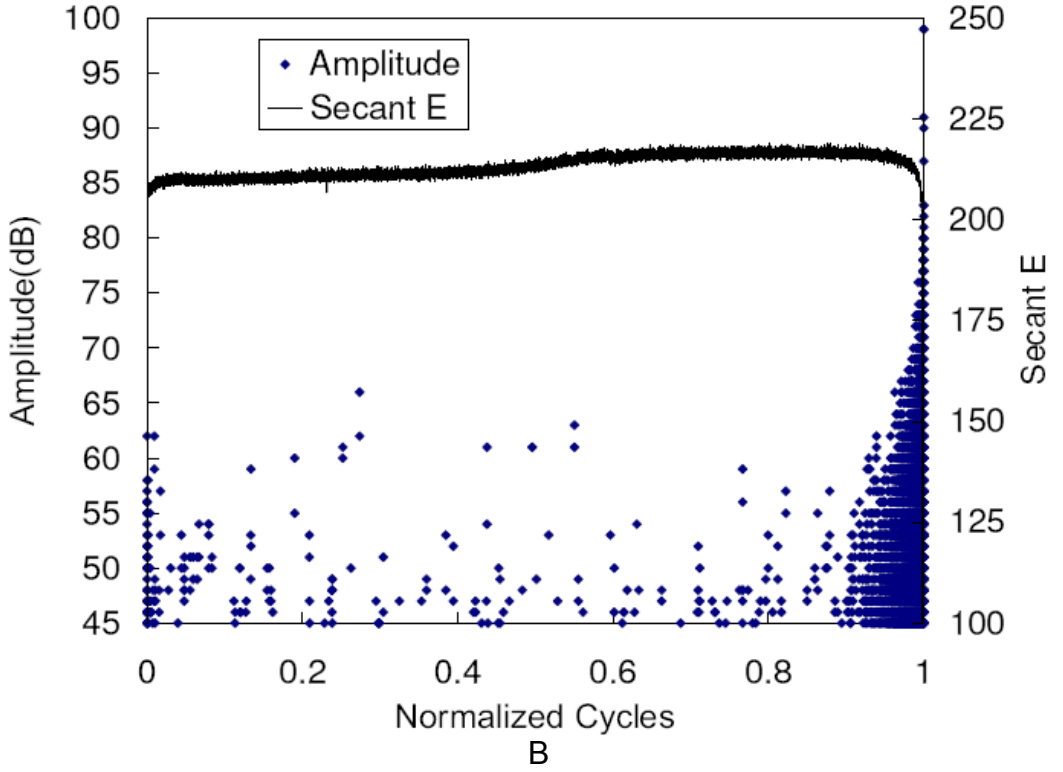
Amplitude(dB)
Secant E
Amplitude
Secant E
Normalized Cycles
100
95
90
85
80
75
70
65
60
55
50
45
250
225
200
175
150
125
100
0
0.2
0.4
0.6
0.8
1

B

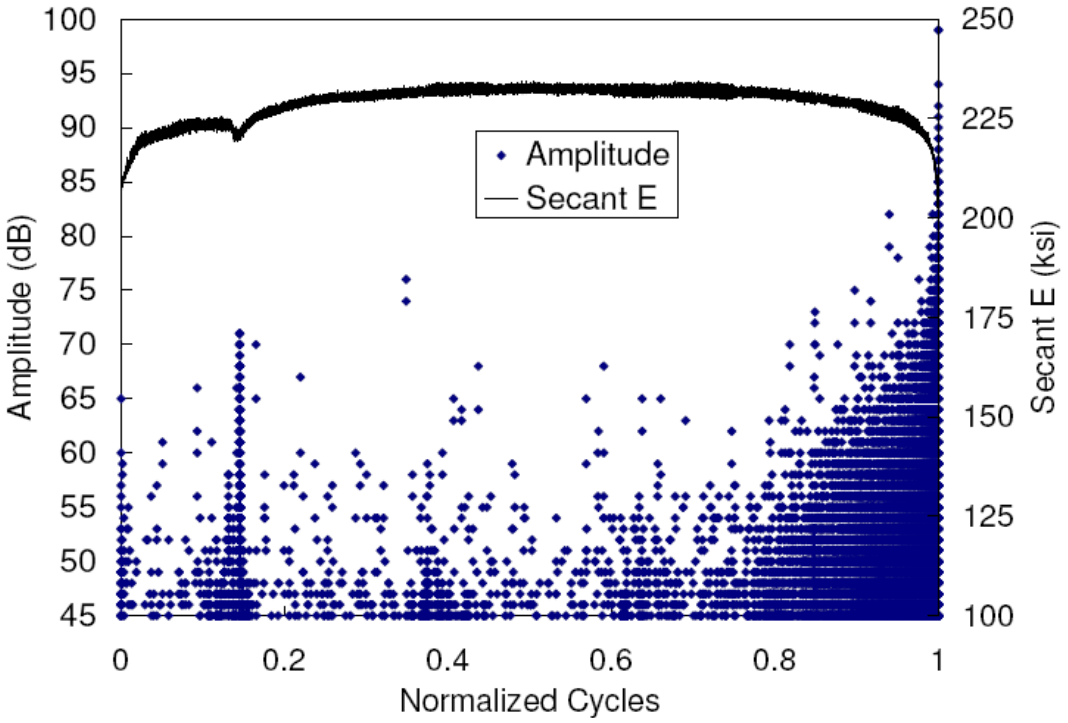

C

Figure 5-8. Amplitude and secant modulus versus normalized cycles. A. maximum load = 2,000 lbs; B. maximum load = 1,800 lbs; C. maximum load = 1,600 lbs.

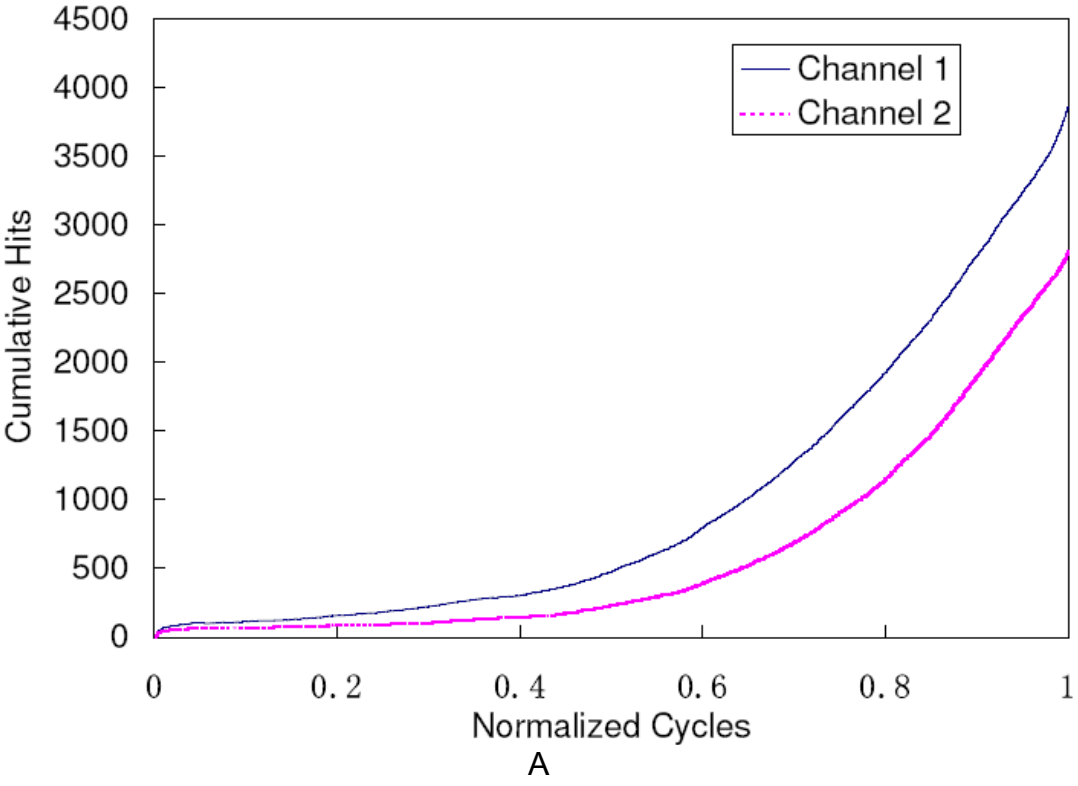

A

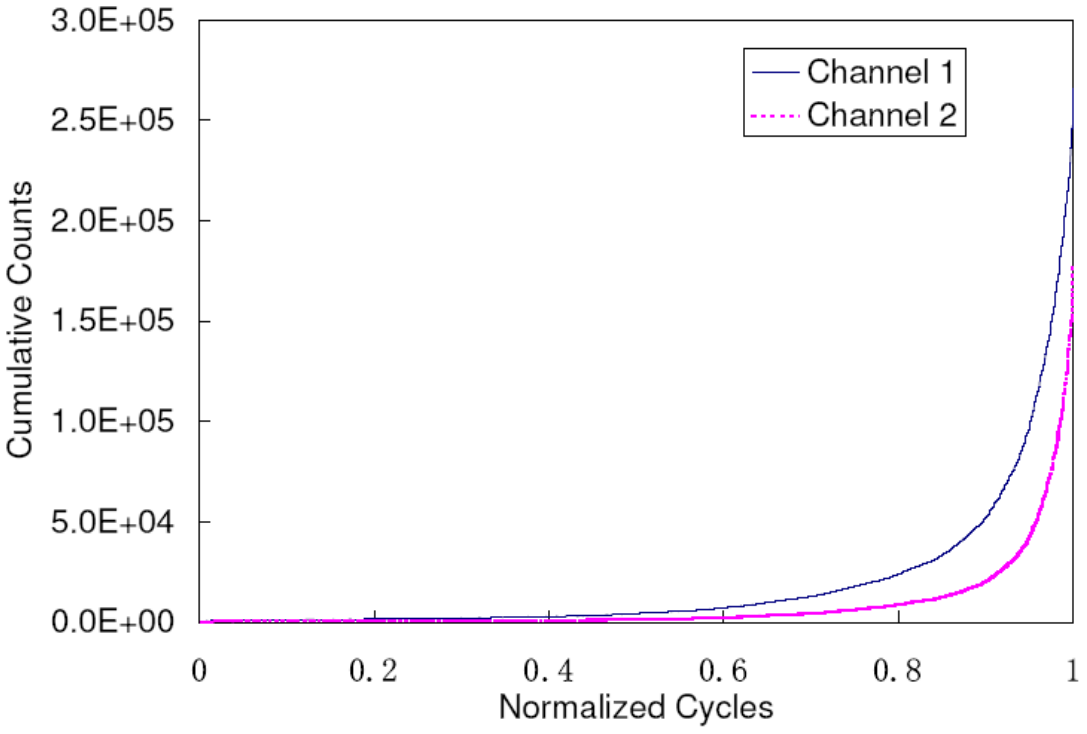
3.0E+05
2.5E+05
2.0E+05
1.5E+05
1.0E+05
5.0E+04
0.0E+00
Cumulative Counts
Channel 1
Channel 2
0
0.2
0.4
0.6
0.8
1
Normalized Cycles

B

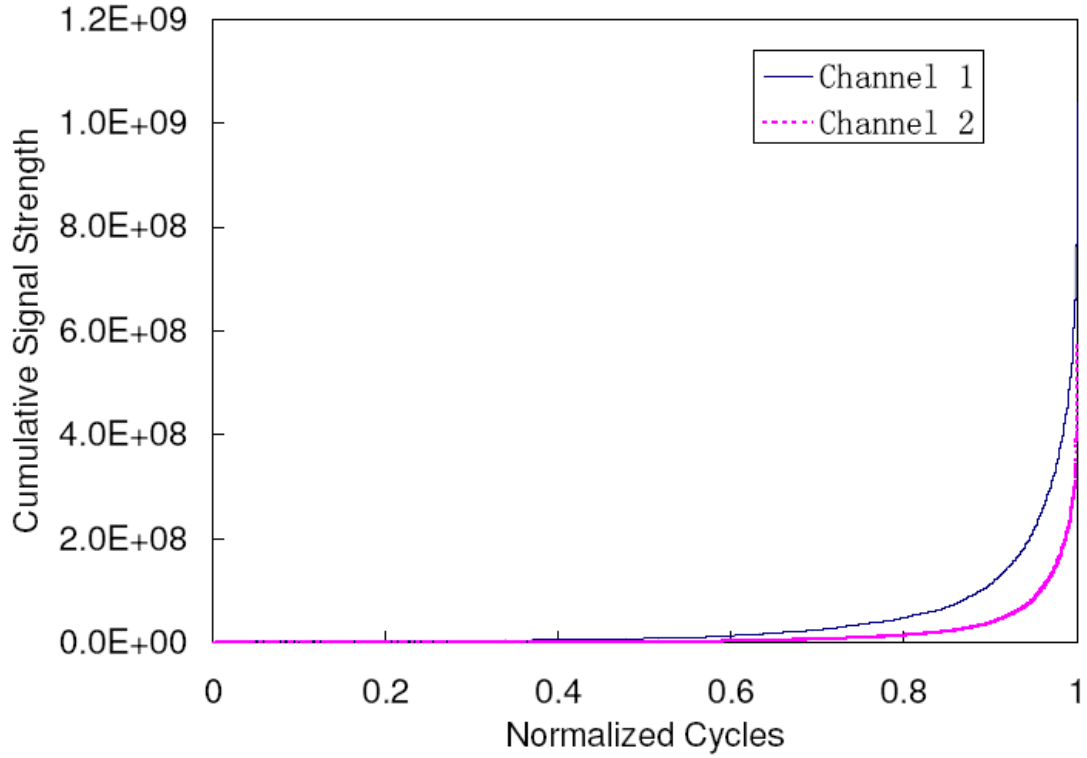
1.2E+09
1.0E+09
8.0E+08
6.0E+08
4.0E+08
2.0E+08
0.0E+00
Cumulative Signal Strength
Channel 1
Channel 2
0
0.2
0.4
0.6
0.8
1
Normalized Cycles

C

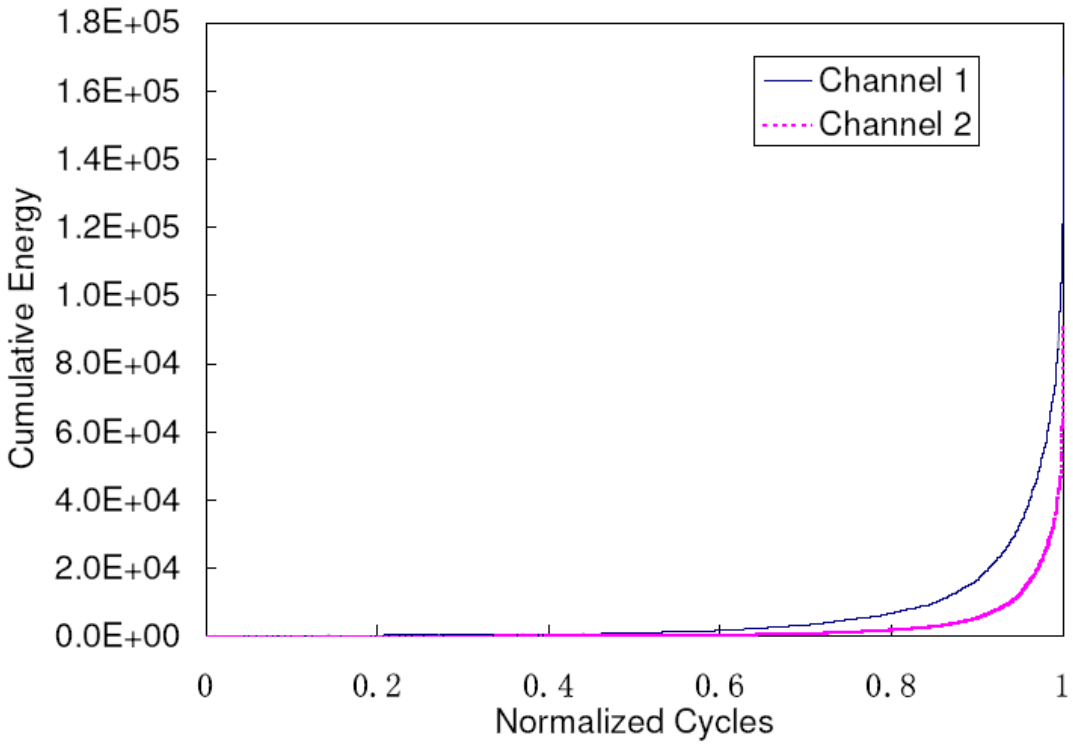

D

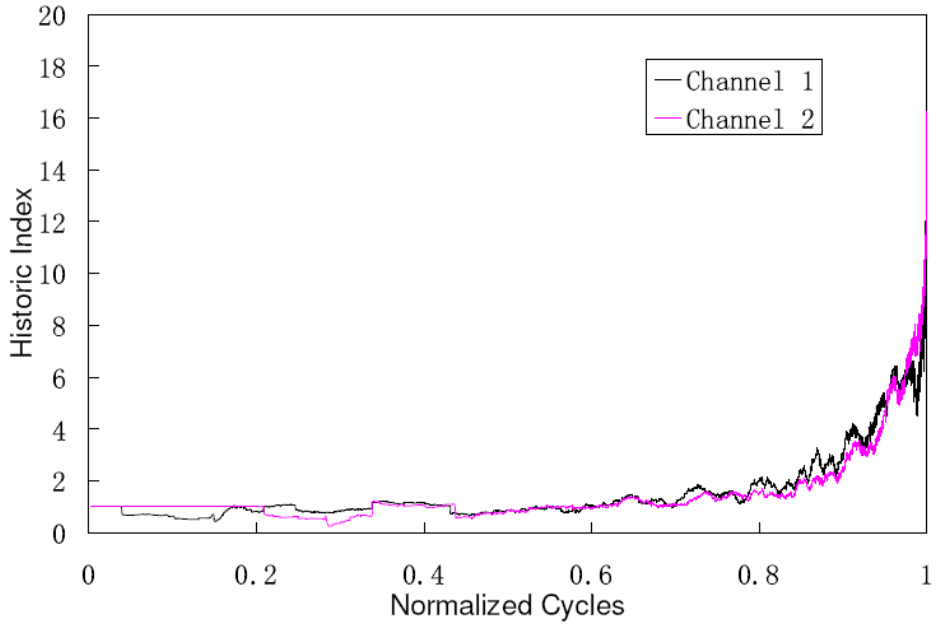

E

Figure 5-9. Conventional AE results for fatigue test with maximum load 2,000 lbs. A. Cumulative hits versus normalized cycles; B. Cumulative counts versus normalized cycles; C. Cumulative signal strength versus normalized cycles; D. Cumulative energy versus normalized cycles; E. Historic index versus normalized cycles.

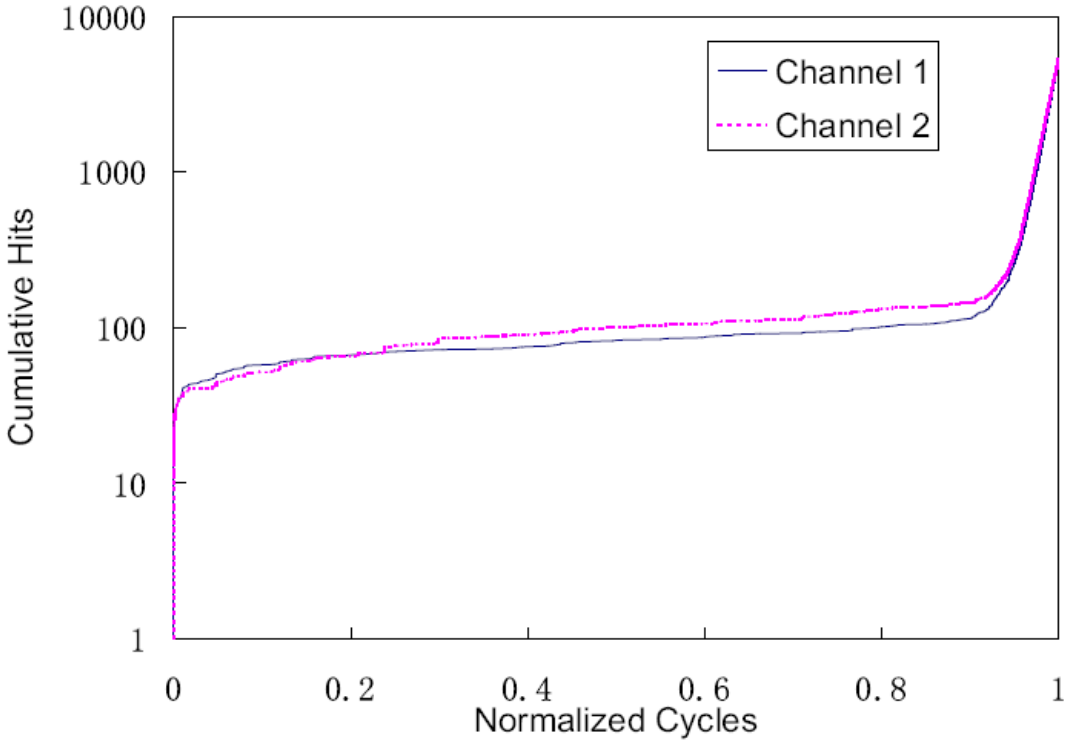
10000
1000
100
10
1
Cumulative Hits
Channel 1
Channel 2
0
0. 2
0. 4
0. 6
0. 8
1
Normalized Cycles

A

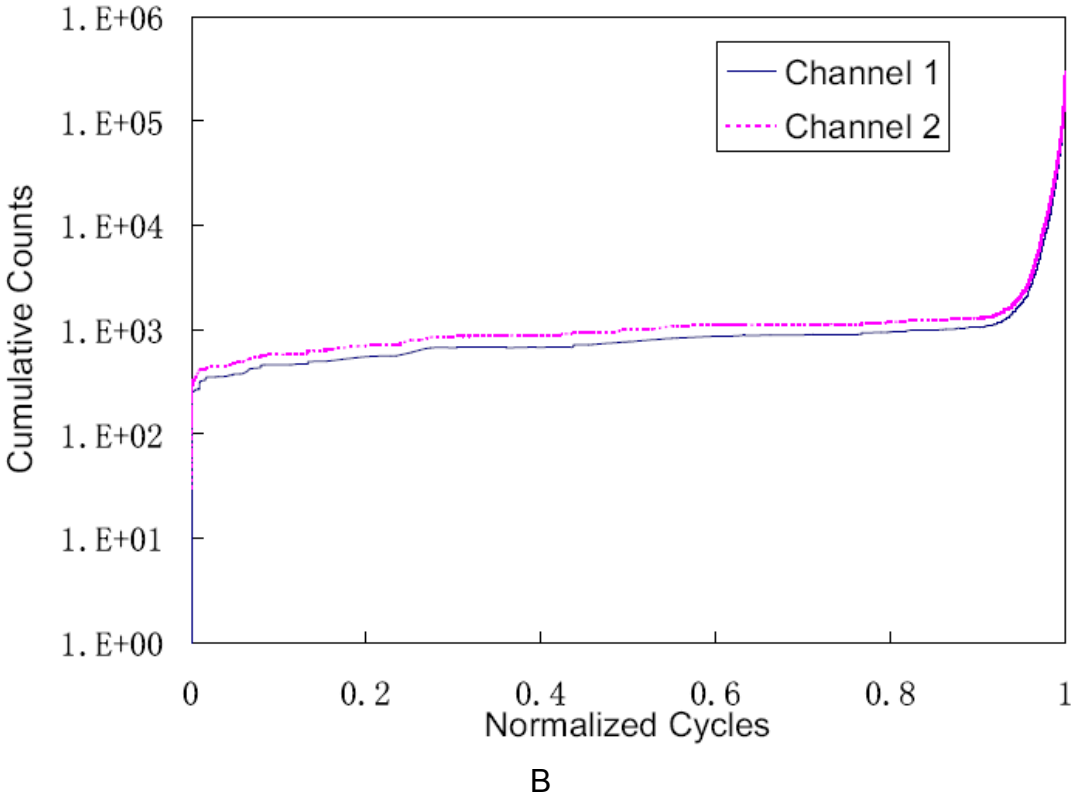
1. E+06
1. E+05
1. E+04
1. E+03
1. E+02
1. E+01
1. E+00
Cumulative Counts
Channel 1
Channel 2
0
0. 2
0. 4
0. 6
0. 8
1
Normalized Cycles

B

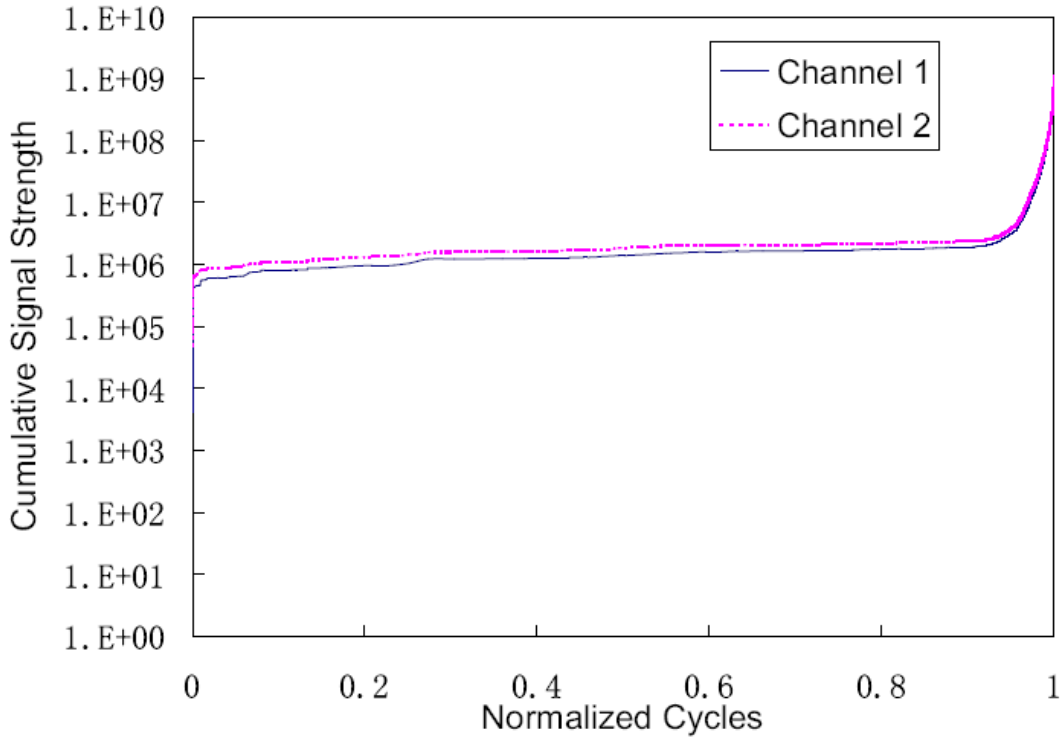
1. E+10
1. E+09
1. E+08
1. E+07
1. E+06
1. E+05
1. E+04
1. E+03
1. E+02
1. E+01
1. E+00
Cumulative Signal Strength
Channel 1
Channel 2
0
0. 2
0. 4
0. 6
0. 8
1
Normalized Cycles

C

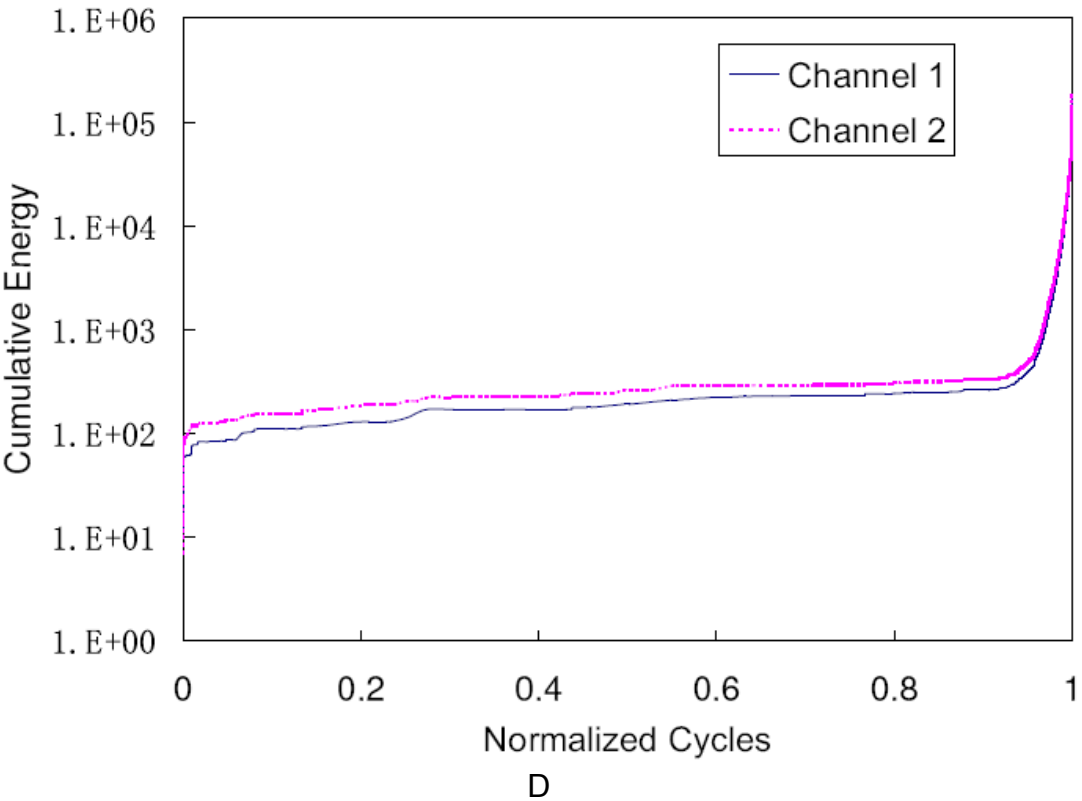
1. E+06
1. E+05
1. E+04
1. E+03
1. E+02
1. E+01
1. E+00
Cumulative Energy
Channel 1
Channel 2
0
0.2
0.4
0.6
0.8
1
Normalized Cycles

D

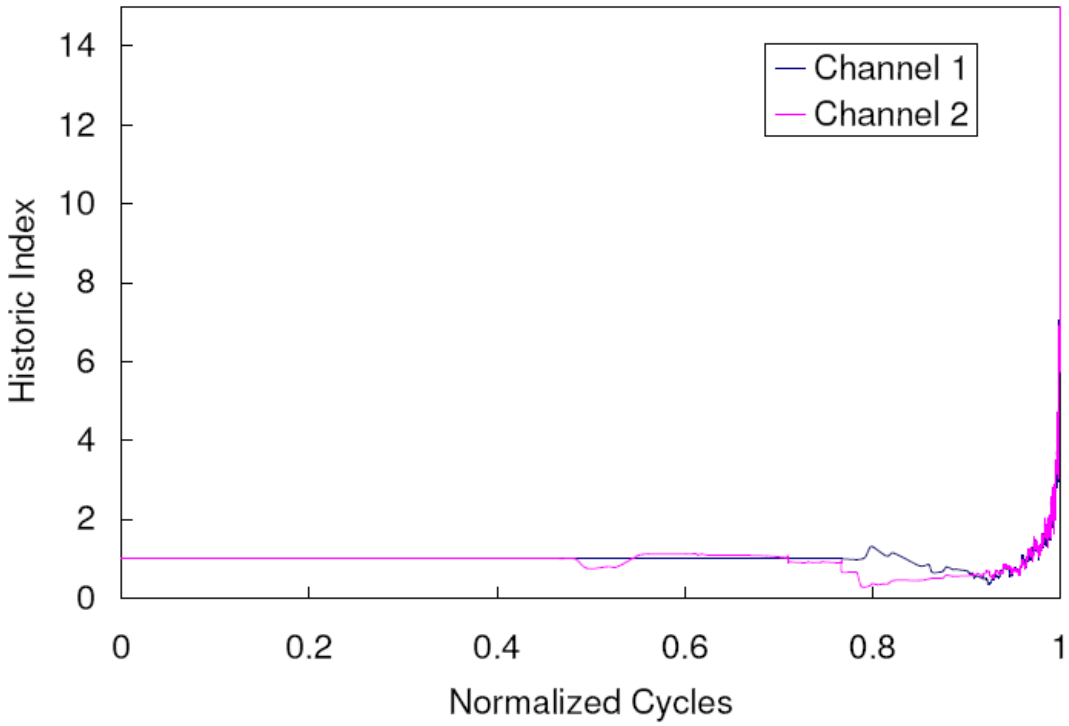

E

Figure 5-10. Conventional AE results for fatigue test with maximum load 1,800 lbs. A. Cumulative hits versus normalized cycles; B. Cumulative counts versus normalized cycles; C. Cumulative signal strength versus normalized cycles; D. Cumulative energy versus normalized cycles; E. Historic index versus normalized cycles.

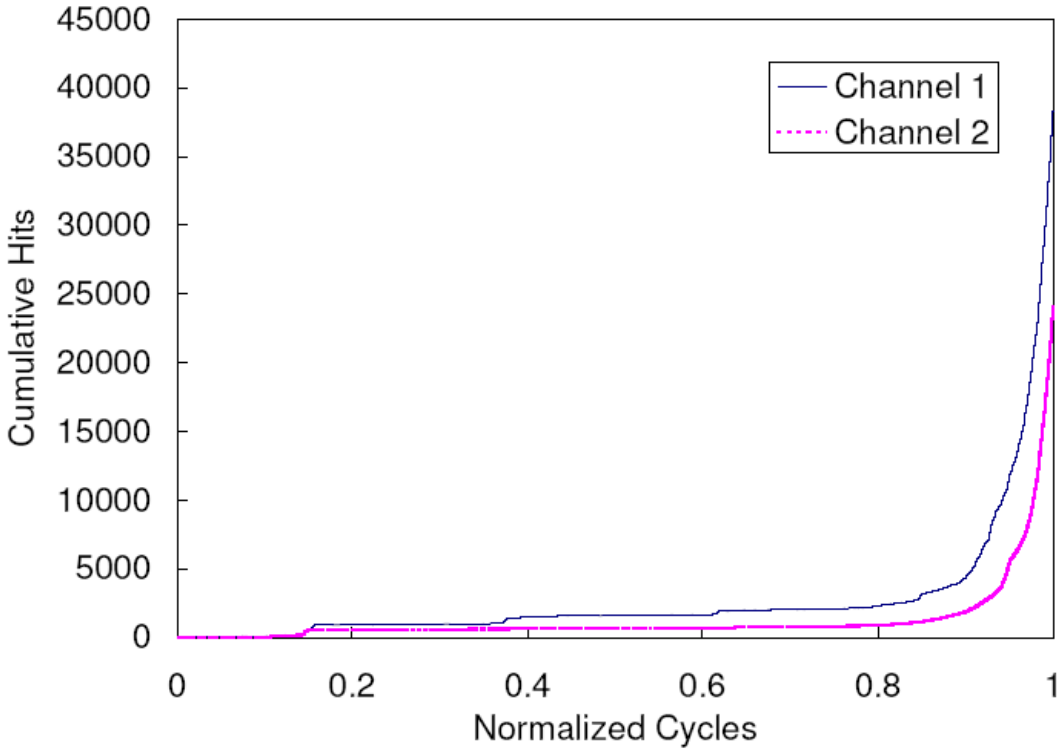
45000
40000
35000
30000
25000
20000
15000
10000
5000
0
Cumulative Hits
0
0.2
0.4
0.6
0.8
1
Normalized Cycles
Channel 1
Channel 2

A

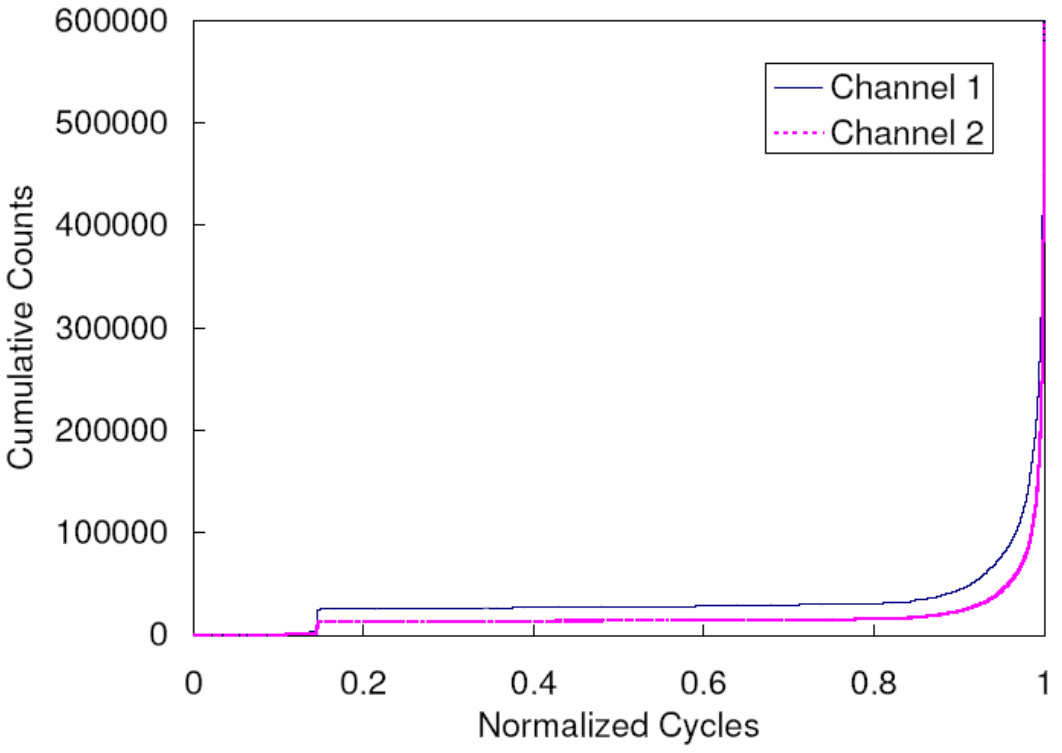
600000
500000
400000
300000
200000
100000
0
Cumulative Counts
0
0.2
0.4
0.6
0.8
1
Normalized Cycles
Channel 1
Channel 2

B

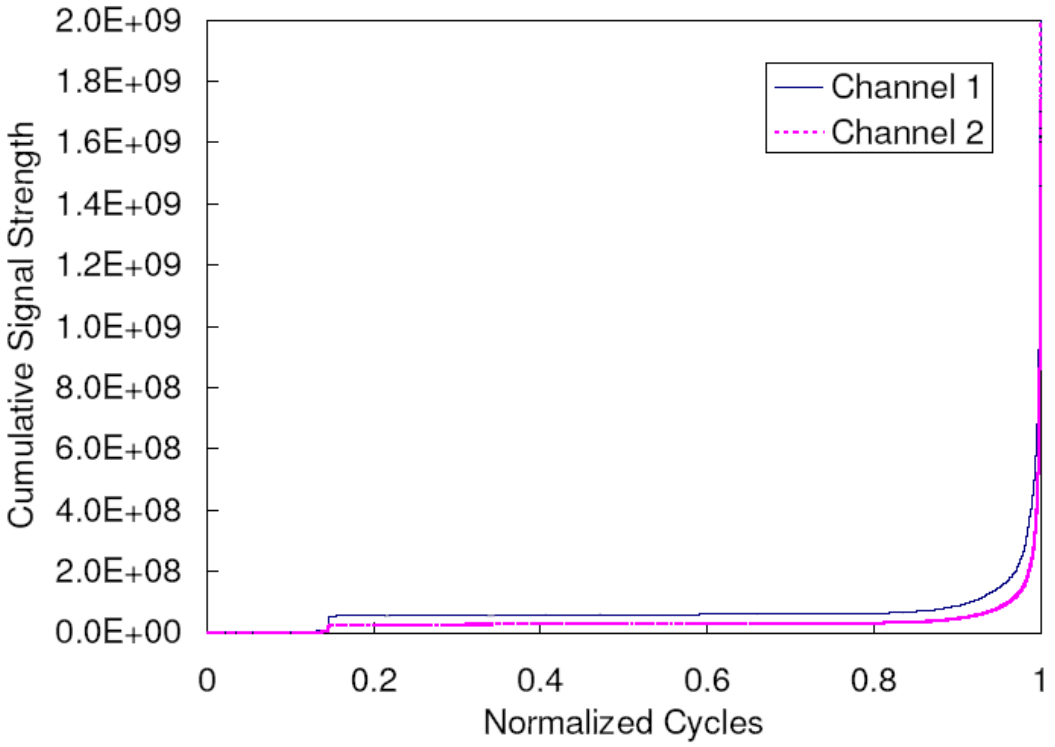
Cumulative Signal Strength
2.0E+09
1.8E+09
1.6E+09
1.4E+09
1.2E+09
1.0E+09
8.0E+08
6.0E+08
4.0E+08
2.0E+08
0.0E+00
0
0.2
0.4
0.6
0.8
1
Normalized Cycles
Channel 1
Channel 2

C

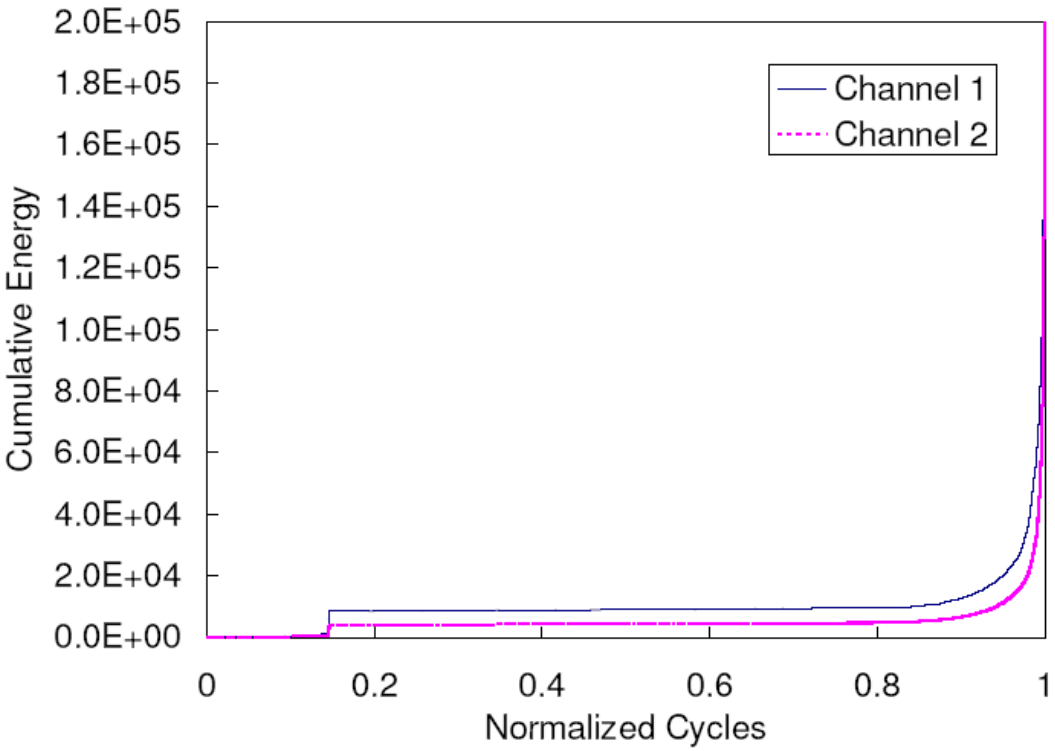
Cumulative Energy
2.0E+05
1.8E+05
1.6E+05
1.4E+05
1.2E+05
1.0E+05
8.0E+04
6.0E+04
4.0E+04
2.0E+04
0.0E+00
0
0.2
0.4
0.6
0.8
1
Normalized Cycles
Channel 1
Channel 2

D

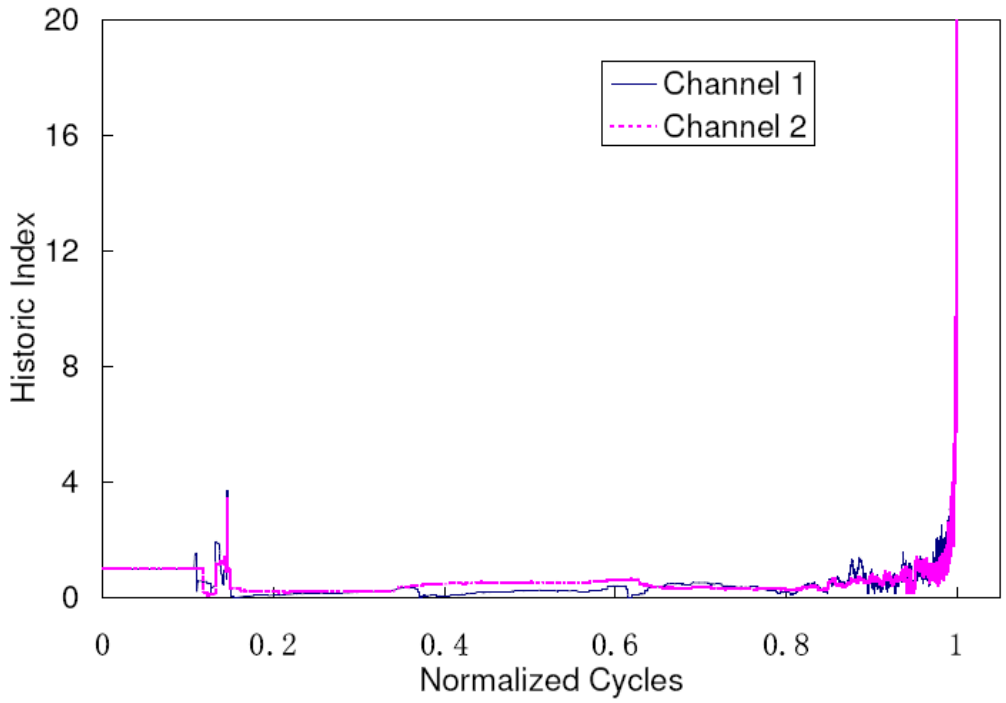

E

Figure 5-11. Conventional AE results for fatigue test with maximum load 1,600 lbs. A. Cumulative hits versus normalized cycles; B. Cumulative counts versus normalized cycles; C. Cumulative signal strength versus normalized cycles; D. Cumulative energy versus normalized cycles; E. Historic index versus normalized cycles.

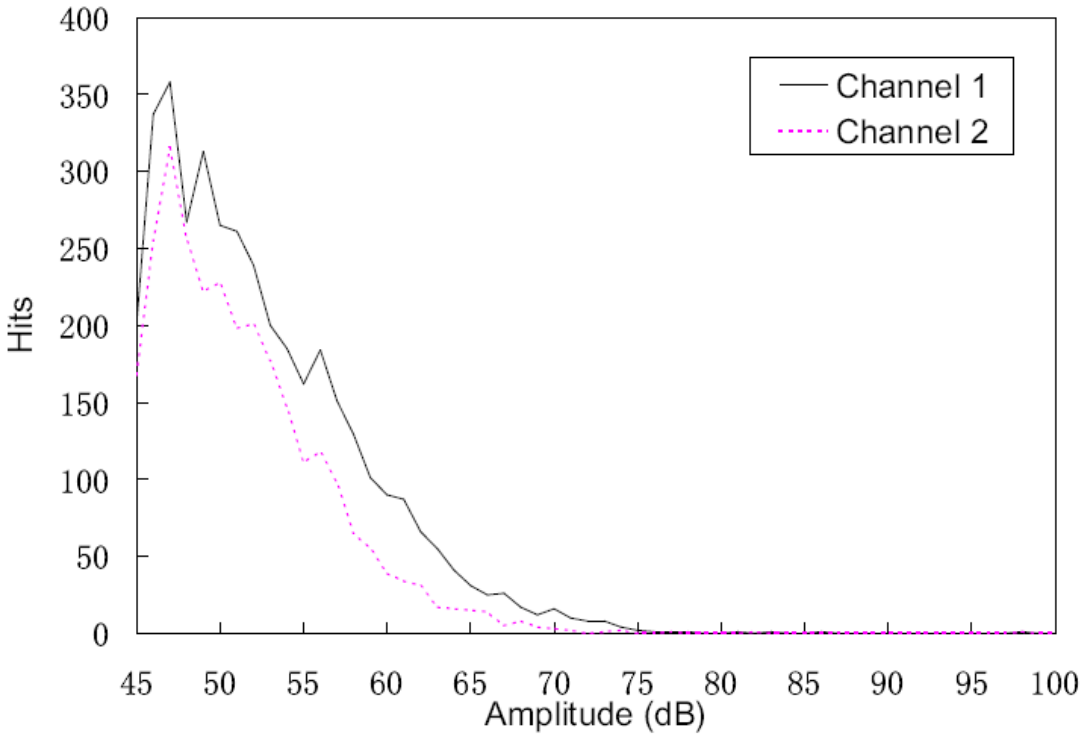

Figure 5-12. Amplitude distribution fatigue test with maximum load 2,000 lbs.

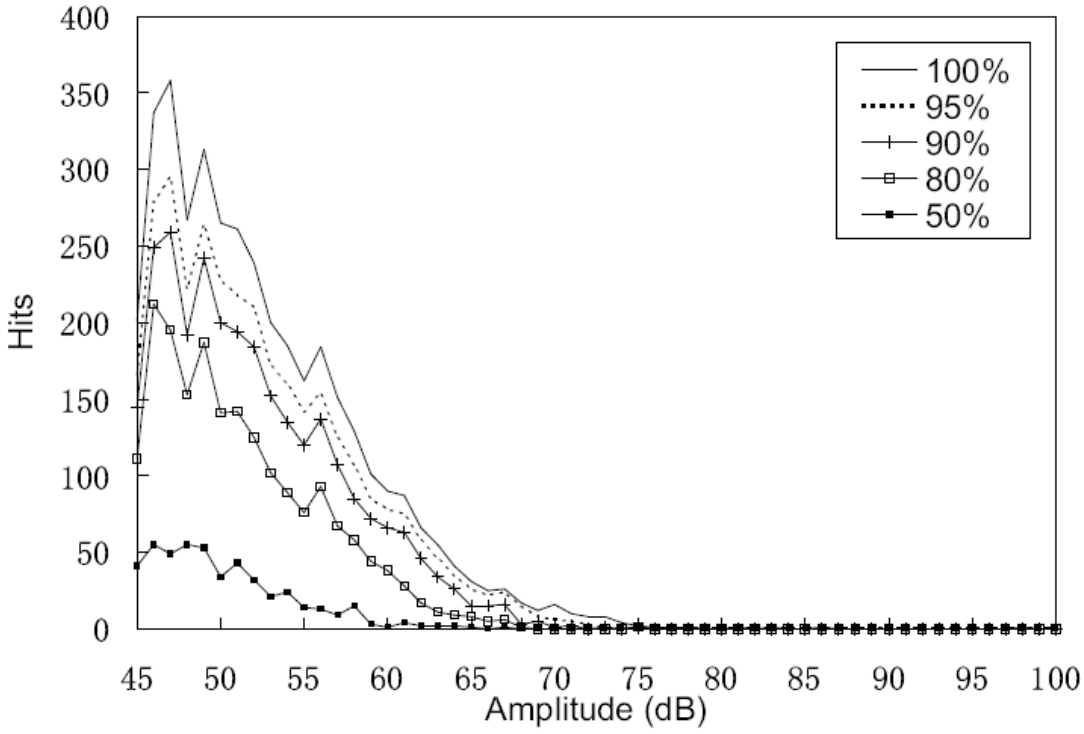

Figure 5-13. Progression of amplitude distribution fatigue test with maximum load 2,000 lbs.

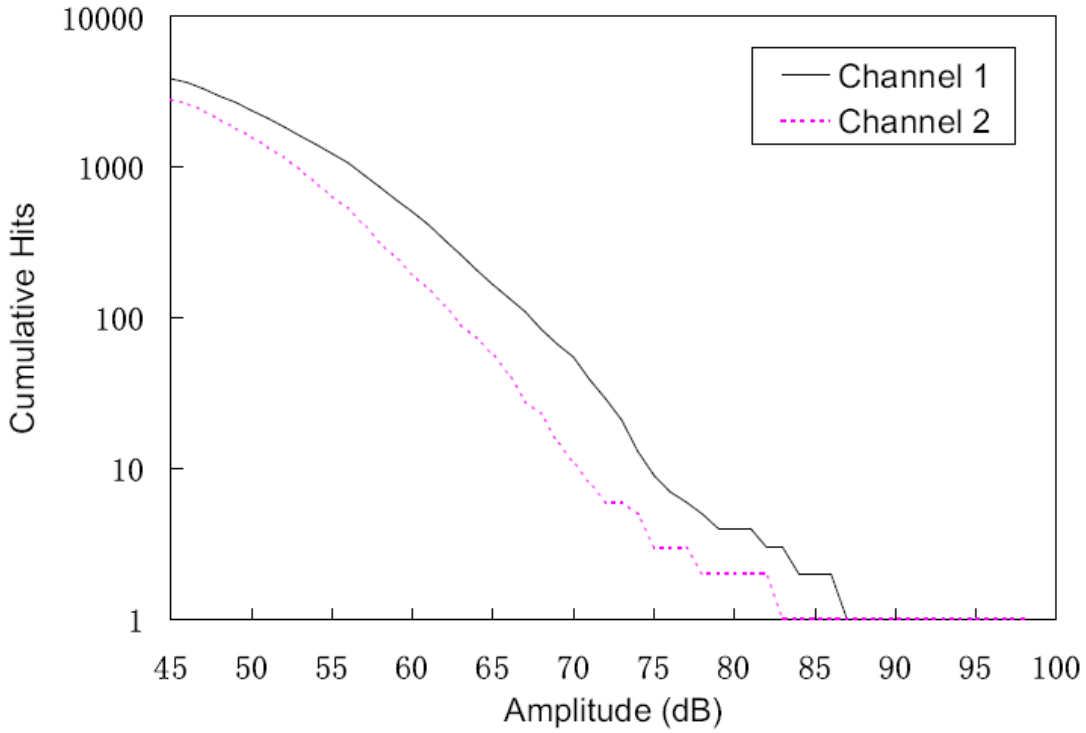

Figure 5-14. Cumulative amplitude distribution fatigue test with maximum load 2,000 lbs.

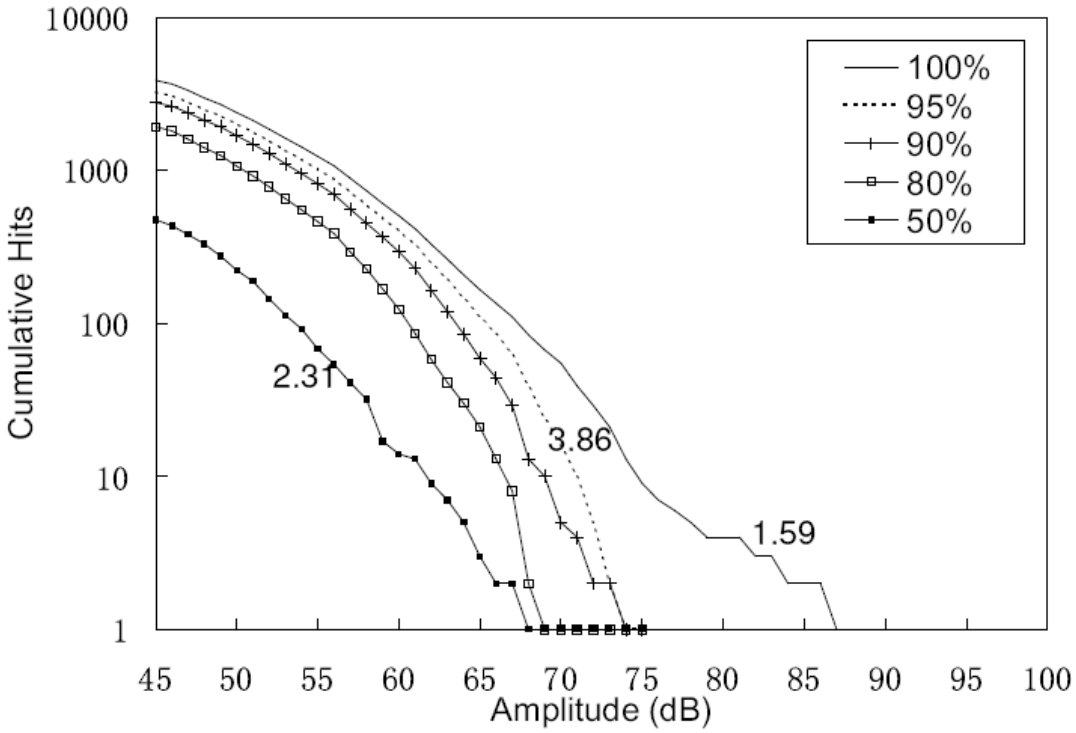

Figure 5-15. Progression of cumulative amplitude distribution fatigue test with maximum load 2,000 lbs.

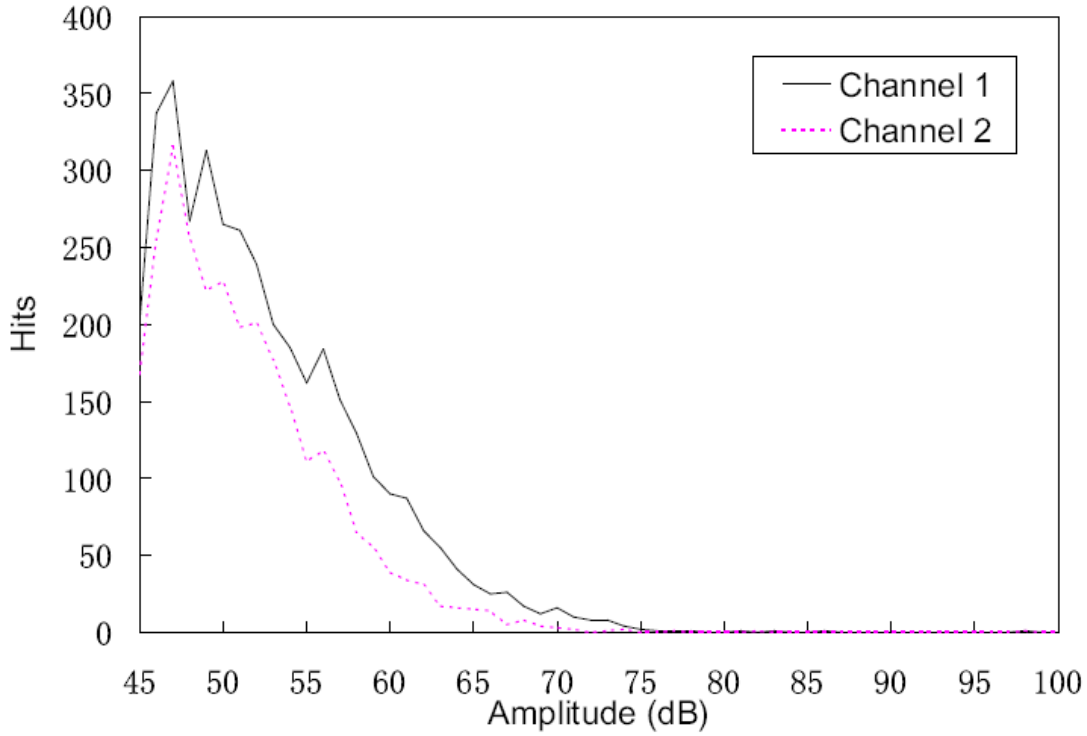

Figure 5-16. Amplitude distribution fatigue test with maximum load 2,000 lbs.

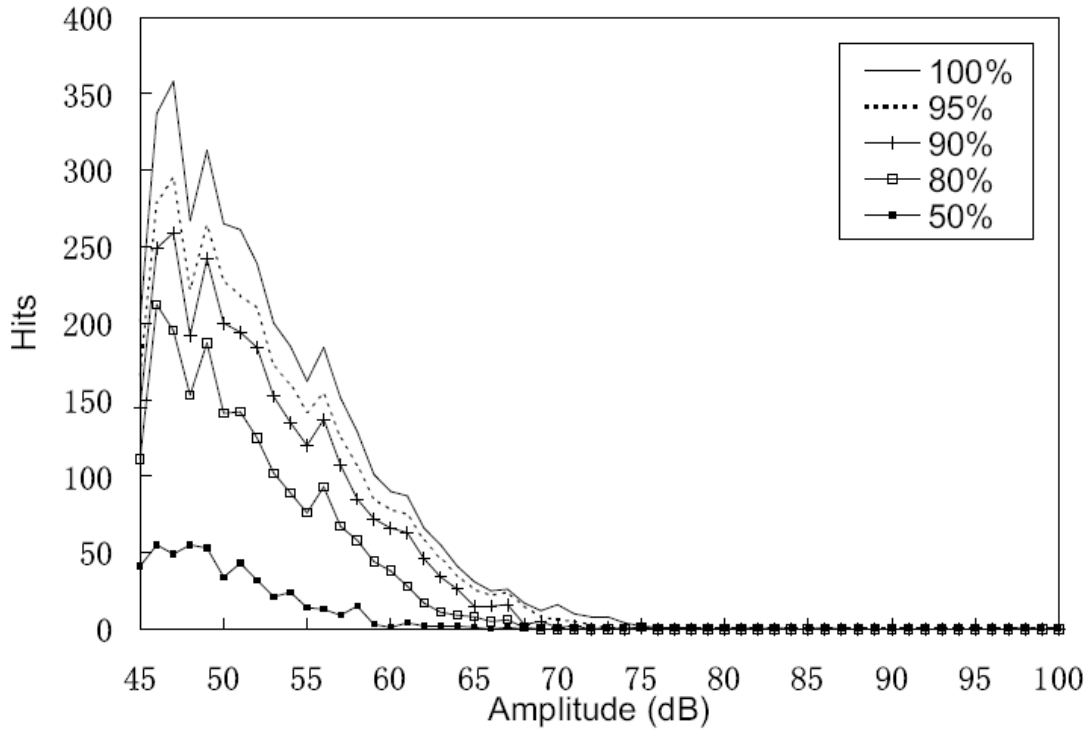

Figure 5-17. Progression of amplitude distribution fatigue test with maximum load 2,000 lbs.

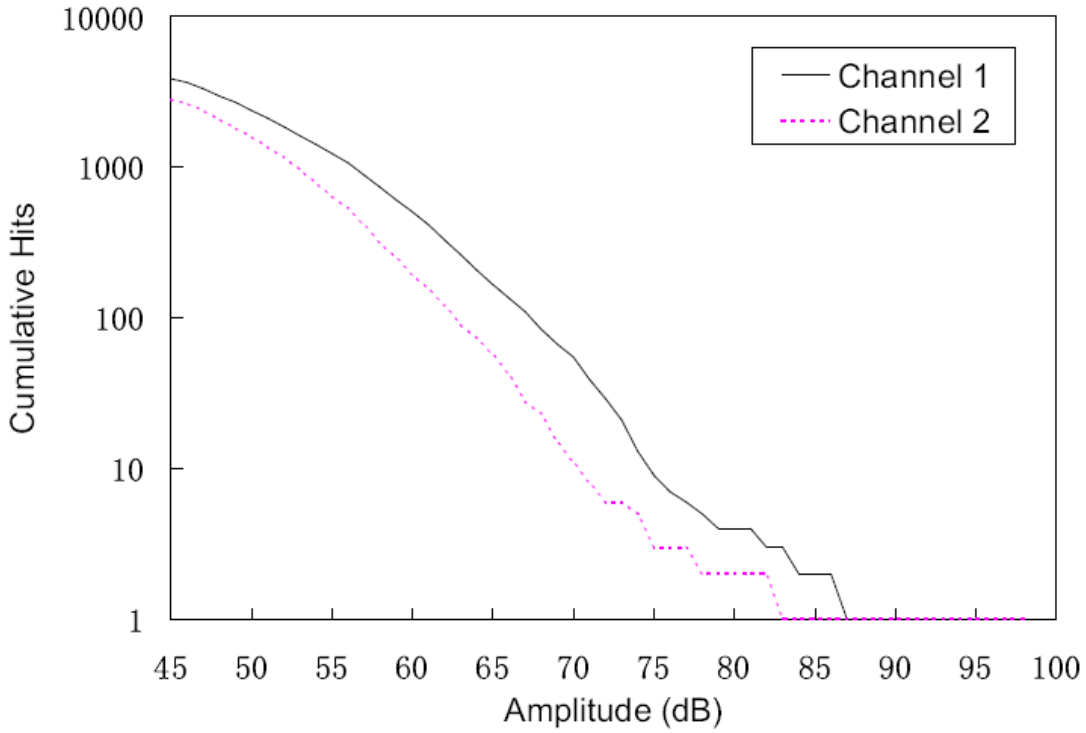

Figure 5-18. Cumulative amplitude distribution fatigue test with maximum load 2,000 lbs.

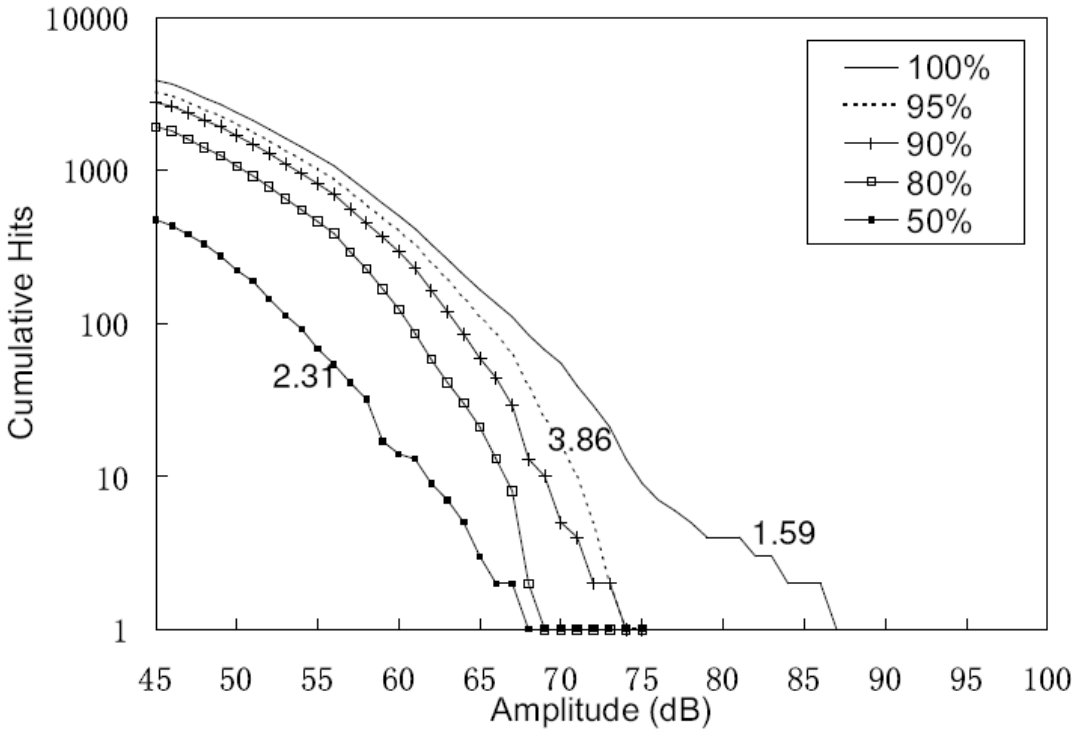

Figure 5-19. Progression of cumulative amplitude distribution fatigue test with maximum load 2,000 lbs.

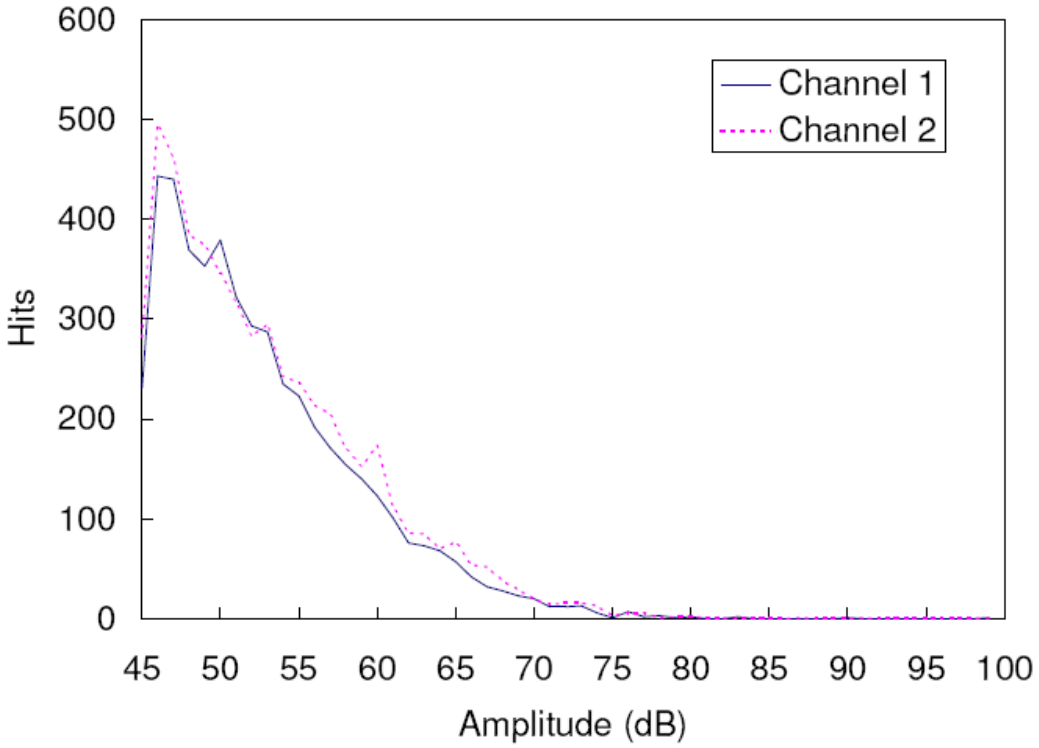

Figure 5-20. Amplitude distribution fatigue test with maximum load 1,800 lbs.

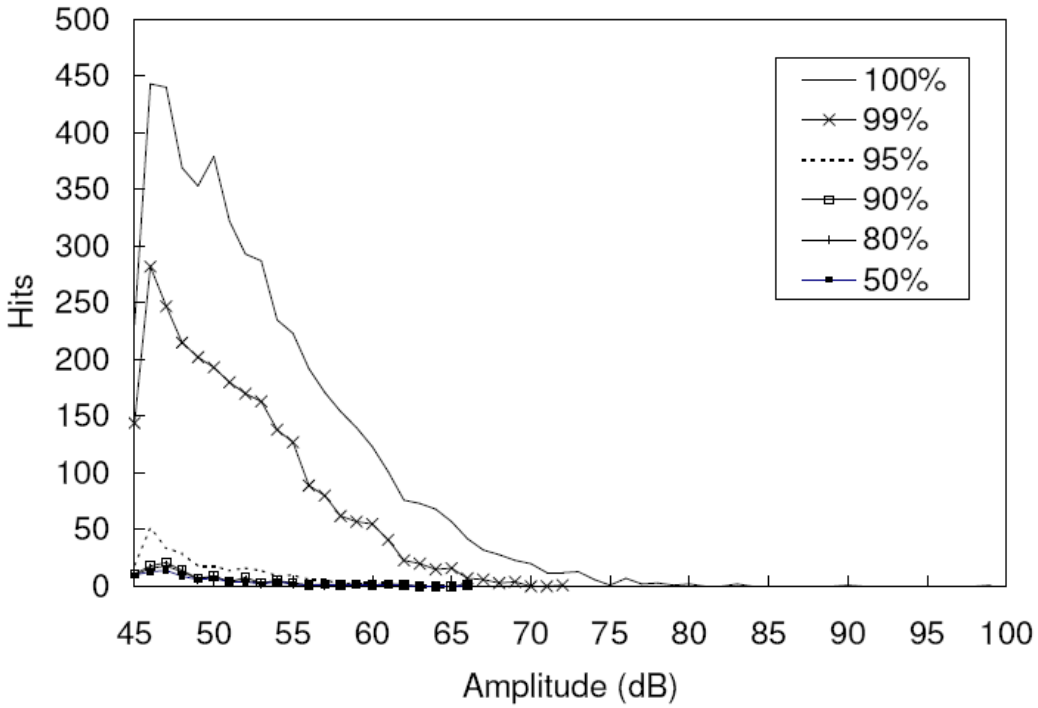

Figure 5-21. Progression of amplitude distribution fatigue test with maximum load 1,800 lbs

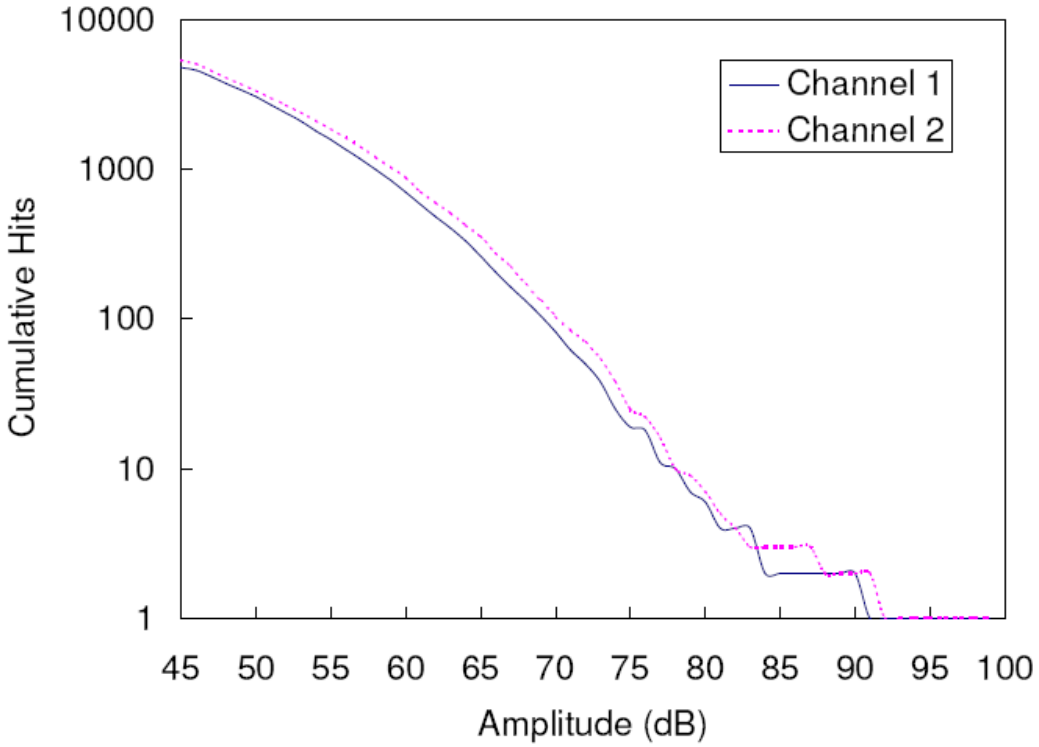

Figure 5-22. Cumulative amplitude distribution fatigue test with maximum load 1,800 lbs.

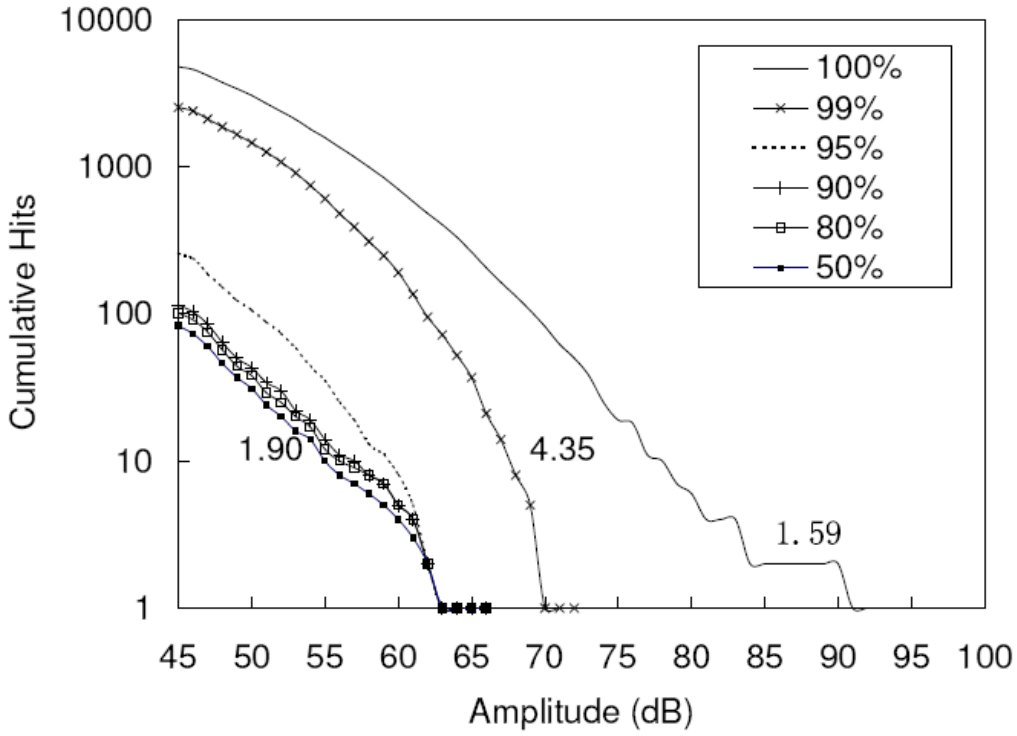

Figure 5-23. Progression of cumulative amplitude distribution fatigue test with maximum load 1,800 lbs.

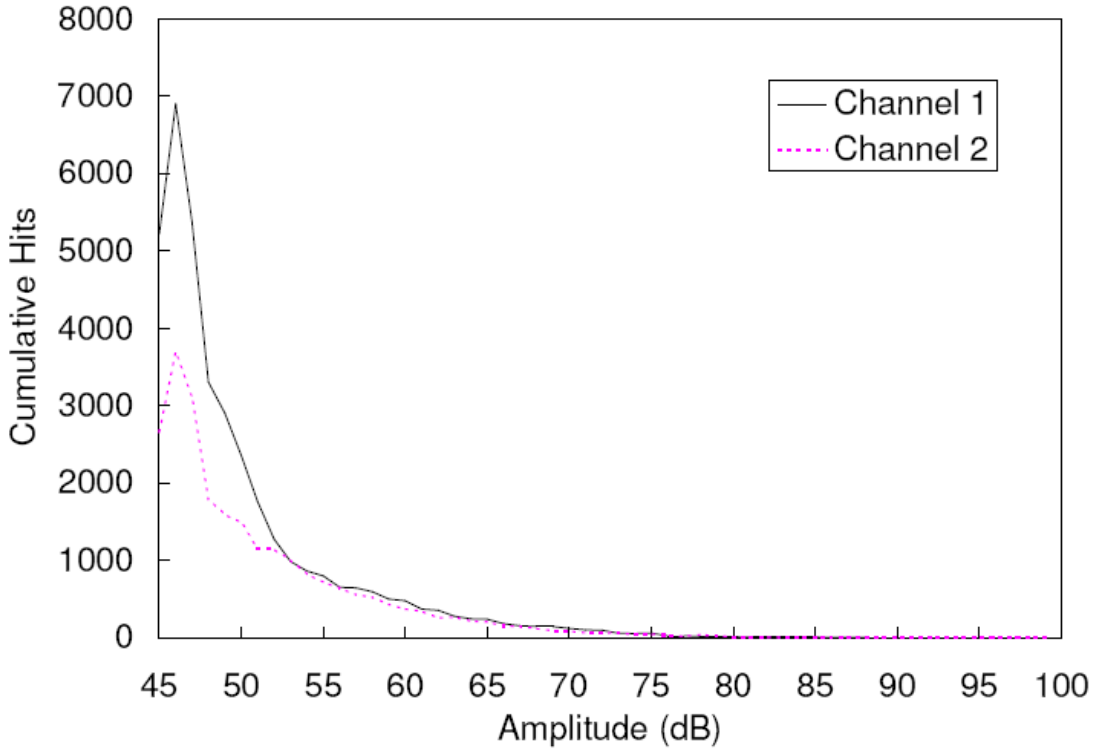

Figure 5-24. Amplitude distribution fatigue test with maximum load 1,600 lbs.

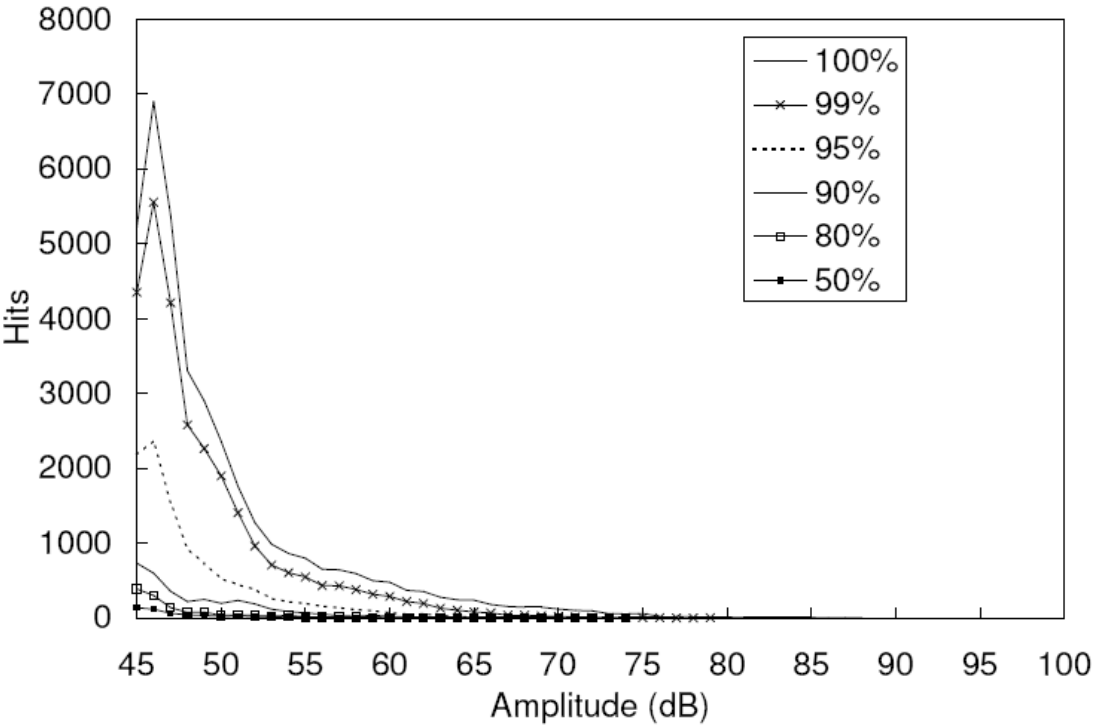

Figure 5-25. Progression of amplitude distribution fatigue test with maximum load 1,600 lbs.

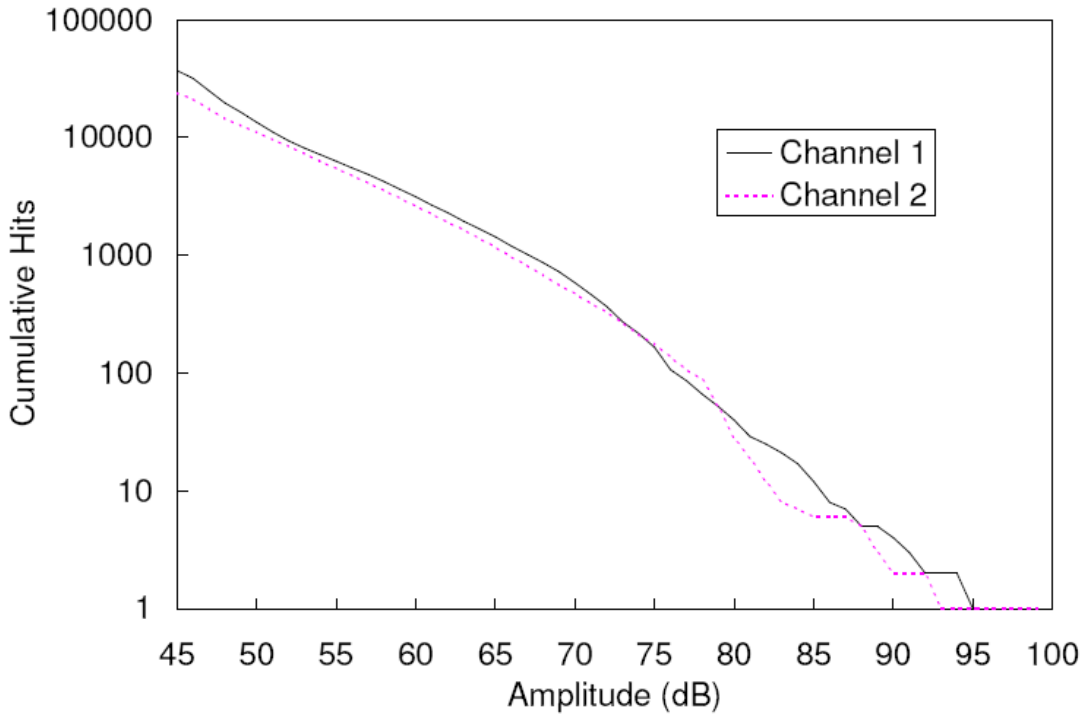

Figure 5-26. Cumulative amplitude distribution fatigue test with maximum load 1,600 lbs.

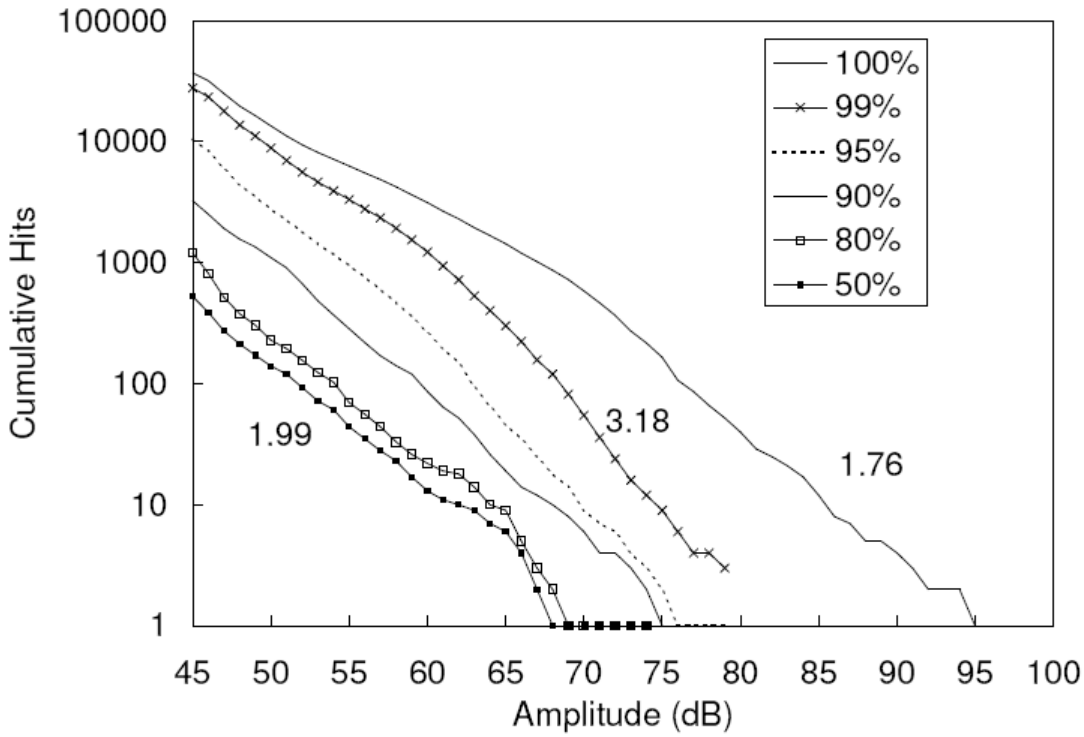

Figure 5-27. Progression of cumulative amplitude distribution fatigue test with maximum load 1,600 lbs.

CHAPTER 6
PIPE SECTION TESTING USING AE

In this chapter, results of ASTM three-edge-bearing tests on full scale pipe sections are discussed. The sections were 18 inches long and 24 inches inside diameter. Three types of tests were conducted. One was a dry pipe, another submerged in water for three months, and the third submerged in water for six months. A monotonic load test was performed on the first, with cyclic load tests also conducted on all three pipe conditions. The AE analysis methods described in the previous chapters, such as cumulative emission data, historic index, cumulative amplitude distribution and b-value, were used in this full scale experiment. The objective is to evaluate each AE analysis method and provide recommendations for conducting in-situ tests on CFRC pipes.

Experimental Program

Specimens Preparation

The dimensions of the pipe sections were: 18 inches long, 24 inches outside diameter, with 2 inches wall thickness. In the three-edge-bearing tests the pipe sections were saturated for three and six months to examine its effect.

The experimental setup, including AE sensors (AE) and strain gage (SG) placement were determined according to ASTM C497 as shown in Figure 6-1. The sensors were mounted close to the expected crack locations in order to obtain strong signals.

Load Procedure

Two types of loading were conducted in this program. One was monotonic, in which the load was applied at a rate of 300 lbs/min. The other was cyclic

loading. During the cyclic test, the pipe sections were subjected to low-frequency load, followed by static hold and unload in cycles until they failed with the maximum loads during each cycle increased gradually. The minimum load during each cycle remained 100 lbs. The static hold time at 100 lbs and maximum loads were 60 seconds. The load rate was set as 1,000 lbs/min and unload rate was set as 3,000 lbs/min. The cyclic loading procedure is shown in Figure 6-2.

Testing Facilities

The three-edge-bearing tests were conducted in the Soil Mechanics Research Lab at the Civil and Coastal Engineering Department, University of Florida. The testing machine used in the program was an MTS 810 Material Test System (Figure 6-3). The frame has 120 kips maximum capacity for compression testing.

Monotonic Loading Test on Dry Specimen

Failure Process Study

The load and amplitude versus top deflection relationships are plotted in Figure 6-4. The load was applied at 100 lbs/min. At first, very little AE was produced until the load reached 6,000 lbs, when massive AE signals started to occur. The load deflection relation remained linear, with the AE amplitude below 65 dB. It is believed that low amplitude AE indicates the occurrence of minor damage, or, matrix cracking. The coincidence of low amplitude AE and linear load deflection relation agrees with the conclusion made in the static third-point bending tests. The deviation of linear relation of load-deflection curve occurred after the first AE signal higher than 65 dB appeared at the load of 7,945 lbs. After that the AE amplitude kept increasing until it reached its peak value, 94 dB at the

load of 8,287 lbs. Middle and high amplitude AE shows that fiber/matrix debonding and fiber breakage occurred during this nonlinear segment. Visual inspection identified the occurrence of the first macro-cracking through the crown and bottom locations. However, the pipe section did not collapse, but continued to pick up extra 450 lbs before a second macro-crack occurred around the springline. It was a 5.7% increase in load; and the deflection increased from 0.224 inches to 0.308 inches, a 29% increase in deflection. During this loading, both middle amplitude and high amplitude AE occurred. A combination of cement matrix cracking, fiber/matrix debonding and fiber breakage was occurring. The second macro-cracking signified the final failure of the pipe section.

It was shown in Figure 6-4 that the deflection kept increasing because the loading machine maintained the load at the ultimate load, which continued to force the pipe section down.

From the above observations, one is able to confirm the conclusions in Chapter 4. Before middle amplitude AE appears, the load deflection relationship remains linear, which indicates a generally sound condition of the pipe with the major damage of cement cracking. The massive occurrence of middle amplitude AE always accompanies a nonlinear load deflection relationship. During this process, fibers are believed to be involved in the matrix-cement interaction, and redistribute stresses within the cement matrix. Therefore cement micro-cracking continues to spread throughout the structure until fiber breakage occurs. The macro-cracking is related to high amplitude AE, which corresponds to fiber breakage.

From the above discussion one concludes that the ability of fiber to distribute stresses within the cement matrix is crucial to CFRC's durability and strength. This ability is believed to closely relate to bonding capability between the fiber and matrix. Although it was not this project's objective to improve CFRC, both in material and structural respects, further research on this particular topic is recommended.

AE Data Analysis

Conventional AE Analysis

The conventional AE plots are shown in Figure 6-5. They are cumulative hits, cumulative counts, cumulative signal strength and cumulative energy versus normalized load. It is apparent that the occurrence of first macro-cracking is happened along with an exponential increase in cumulative hits, counts, signal strength and energy. The trend of the later three is more obvious than the cumulative hits. However, the four plots do not provide the exact moment when the first macro-cracking occurs. The historic index, on the other hand, reaches its peak values at exactly when the first and second macro-cracking occurs.

Amplitude Distribution Analysis

The amplitude distribution is shown in Figure 6-6. The results for different AE channels are plotted together for comparison purposes. Channels 1 and 2 have lower values of hits than channels 3 and 4. Considering the fact that channels 1 and 2 were located on one side of the pipe, while 3 and 4 were mounted on the other side, it is believed that the difference between them results from local attenuation of AE waves. Channel 3 provided the strongest signals.

Progression of Amplitude Distribution

In Figure 6-7 the progression of amplitude distribution is shown for 80%, 90% and 100% of ultimate load. The majority of AE signals were produced during the last 10% of the failure process. The majority of the hits are low amplitude below 55 dB. Therefore, most of the damage is cement cracking. The progression of amplitude distribution follows the same trend at different stages of damage.

Cumulative Amplitude Distribution

The cumulative amplitude distribution is shown in Figure 6-8 for each channel. It is seen that although the results for each channel are influenced by local attenuation, especially around channel 1 and 2, the four channels actually yielded similar b-values. It was concluded that when plotted in log plot, the cumulative amplitude distribution and b-values are less influenced by attenuation.

Progression of Cumulative Amplitude Distribution

The cumulative amplitude distribution of channel 3 is analyzed in Figure 6-9, for different load levels. The b-value is found to increase from the start up to 90% of ultimate load, and then decreases to 2.12 at the final phase. This observation is believed to be useful since the decreasing of b-value can be used as an indication of impending final failure.

Summary on AE Data Analysis

In this section, the AE techniques were applied to analyze the monotonic three-edge-bearing test. The most useful methods were found to be amplitude, historic index and cumulative amplitude distribution. In the following section the

aforementioned techniques will be applied on the cyclic three-edge-bearing test on dry, saturated for 3 and 6 months pipes.

Cyclic Loading Test

AE Data Analysis

The analysis methods found useful in the previous section are applied on cyclic three-edge-bearing tests. Comparison is made between three different pipes, which were dry, saturated for 3 and 6 months. In addition, Kaiser and Felicity effects are observed and discussed as well.

Amplitude and Load versus Time

The amplitude versus time and load versus time are plotted together in Figure 6-10. The number of cycles decreased for the extended soaking time. The dry specimen required 12 cycles and failed at 8,133 lbs. The 3-month saturated specimen took 11 cycles and failed at 7000 lbs. The 6-month took 10 cycles and failed at 7,400 lbs. It is obvious that the durability is reduced after months of soaking.

It is noted that the number of hits for the dry specimen is higher than the other two specimens. At the same time, the middle amplitude hits, that is, hits with amplitude between 65 dB and 75 dB, first appeared at the 5^{th} cycle for the dry pipe, and the 10^{th} cycle for both the 3 and 6 month specimens. The latter two collapsed soon after the middle amplitude AE occurred, showing brittle failure characteristics. This means fibers in the dry specimen were involved in the early stage of damage, and help redistribute stress within matrix. Consequently, there was much more cement matrix cracking in the dry specimen before it failed. The maximum deflections after each cycle are shown in Table 7-1. In this table, one

can see that dry specimen deflection is larger than the other two, which means it is more ductile due to more interaction between fibers and matrix.

Conventional AE Data Analysis

Plots of the cumulative hits, cumulative counts, cumulative signal strength and cumulative energy versus load are provided in Figure 6-11. For comparison purpose, results for the three specimens are included in the same plots. One can see that for the 3 and 6 months specimens, the cumulative signals are more concentrated in the final cycle. The dry specimen damage is more evenly distributed in each cycle. This means that after months of being saturated the specimens became more brittle.

Historic index is shown in Figure 6-12. Results from the most representative AE channels are given. As in the monotonic loading test, the maximum historic index at each cycle corresponds with the maximum load, when the maximum damage occurs. Due to the larger number of hits for the dry specimen, the historic index can indicate the damages produced at each cycle more accurately.

Cumulative Amplitude Distribution

The cumulative amplitude distribution is shown in Figure 6-13 for each specimen. The b-values of all specimens follow the same evolutionary trail. The b-value is relatively small for the early cycles, ranging from 1.93 to 2.20, with amplitudes below 60 dB. With the occurrence of middle amplitude AE, the b-value increased to around 4.22 for the dry specimen, 3.43 for the 3 month and 3.11 for the 6 month specimen. At the final failure phase, the b-value decreased again due to the occurrence of fiber breakage.

It is expected that the cumulative amplitude distribution can be valuable for in-situ inspection. The varying of b-value is an indicator of different failure mechanisms.

Kaiser and Felicity Effects

Kaiser and Felicity effects are observed in the cyclic tests. Figure 6-14 shows the plot of AE energy versus load, which is a conventional way of showing them. It was found that Kaiser effect only occurred for the 3 and 6 month specimens, while the dry specimen showed Felicity effect after the first cycle. Figure 6-15 shows the Felicity ratios after each cycle. For the 3 month and 6 month specimens, a Felicity ratio larger than 1 is reassigned as 1, which is considered to be Kaiser effect. After 4 cycles, the 3 month and 6 month specimens started to show Felicity effect, and with the development of damage, the felicity ratio decreased. The Felicity ratio for the dry specimen showed a dramatic reduction after 7 cycles, decreasing from 0.76 to 0.33.

Summary

In this chapter, results of three-edge-bearing tests for different specimens are discussed. The significant findings from this chapter are as follows.

1. Months of saturation in water reduced the durability of CFRC pipes. The durability was decreased with longer saturation.
2. The bonding ability between fiber and matrix is important to the durability of CFRC. It was found that for the dry specimen, although it eventually failed at a higher cycle and load, the initiation of fiber/matrix debonding occurred earlier than the more brittle specimens. This is because when micro-cracking occurred in the cement matrix, the fibers redistributed local stresses to the cement matrix, thereby prevented the structure from brittle failure.
3. The more ductile dry pipe section produced much larger felicity ratios than the more brittle ones. Therefore the felicity ratio can be used as a quality control parameter.

4. AE techniques were discussed in this chapter. In the monotonic load test, among all the conventional AE techniques, the historic index is found to best detect macro-cracking and final failure.

5. The cumulative amplitude distribution and b-value method is an effective method to detect the overall failure progression. As failure progresses, b-values evolve in accordance with the same trend for different tests and material conditions. It begins low, then increases as the failure progresses, and decreases with the occurrence of fiber breakage.

Table 6-1. Maximum top deflection for cyclic three-edge-bearing tests

Number of cycles	Maximum top deflection (in.)		
	Dry	Saturated, 3 months	Saturated, 6 months
1	0.084	0.072	0.074
2	0.097	0.086	0.087
3	0.110	0.099	0.101
4	0.124	0.112	0.116
5	0.137	0.129	0.133
6	0.153	0.145	0.151
7	0.171	0.161	0.171
8	0.197	0.184	0.195
9	0.234	0.219	0.230
10	0.268	0.376	Final Failure
11	0.301	Final Failure	N/A
12	Final Failure	N/A	N/A

A

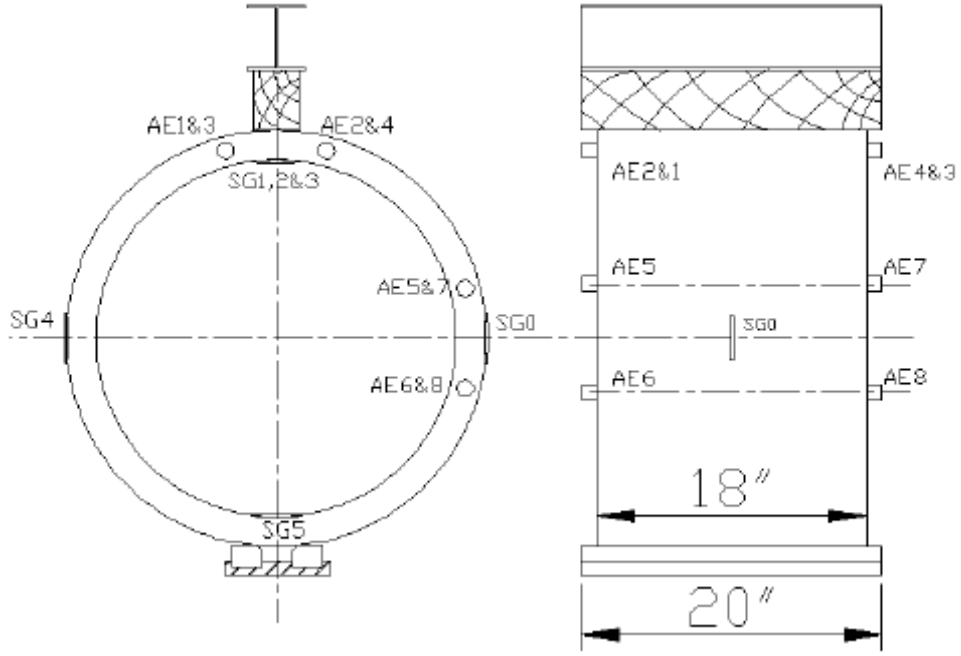

B

Figure 6-1. Three-edge-bearing test setup.

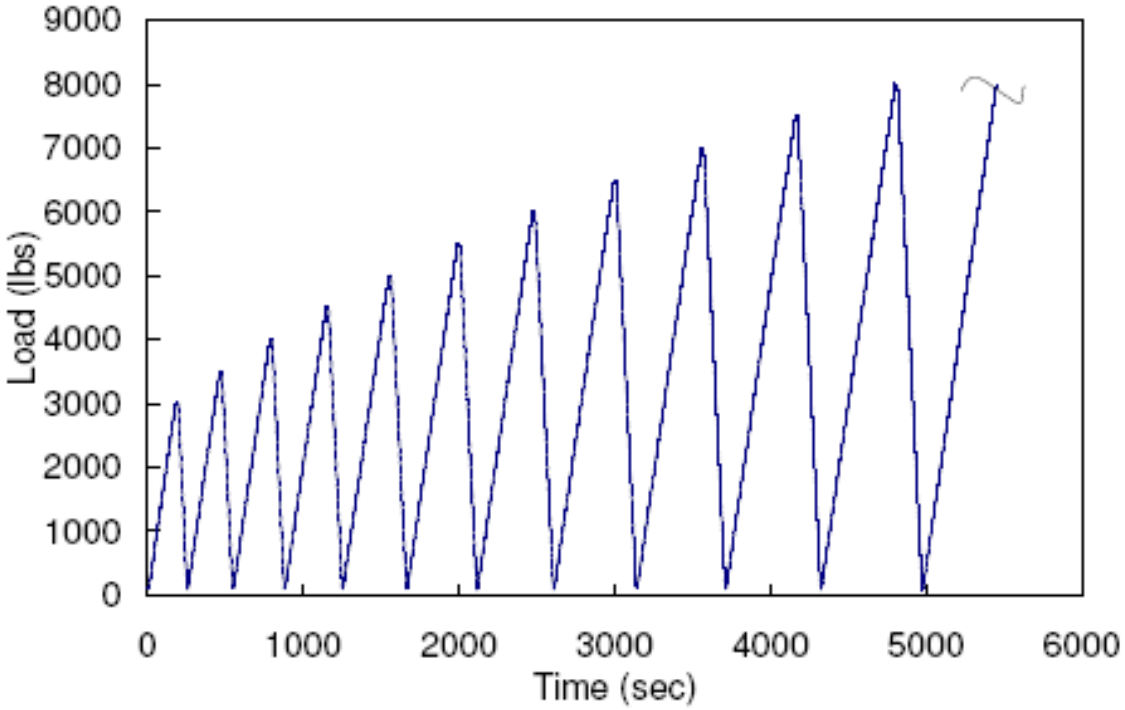

Figure 6-2. Three-edge-bearing cyclic test, load procedure.

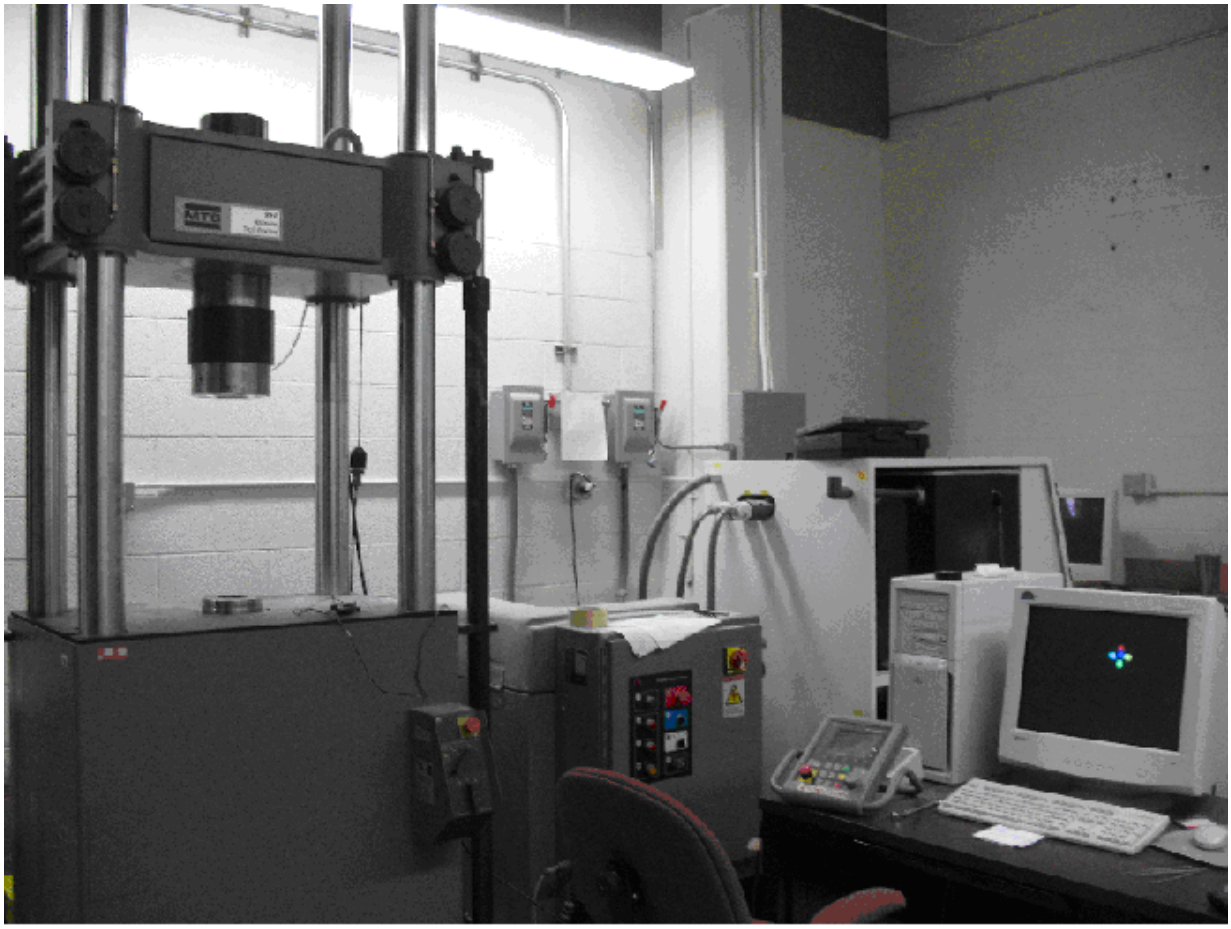

Figure 6-3. Three-edge-bearing test machine, MTS 810 material test system.

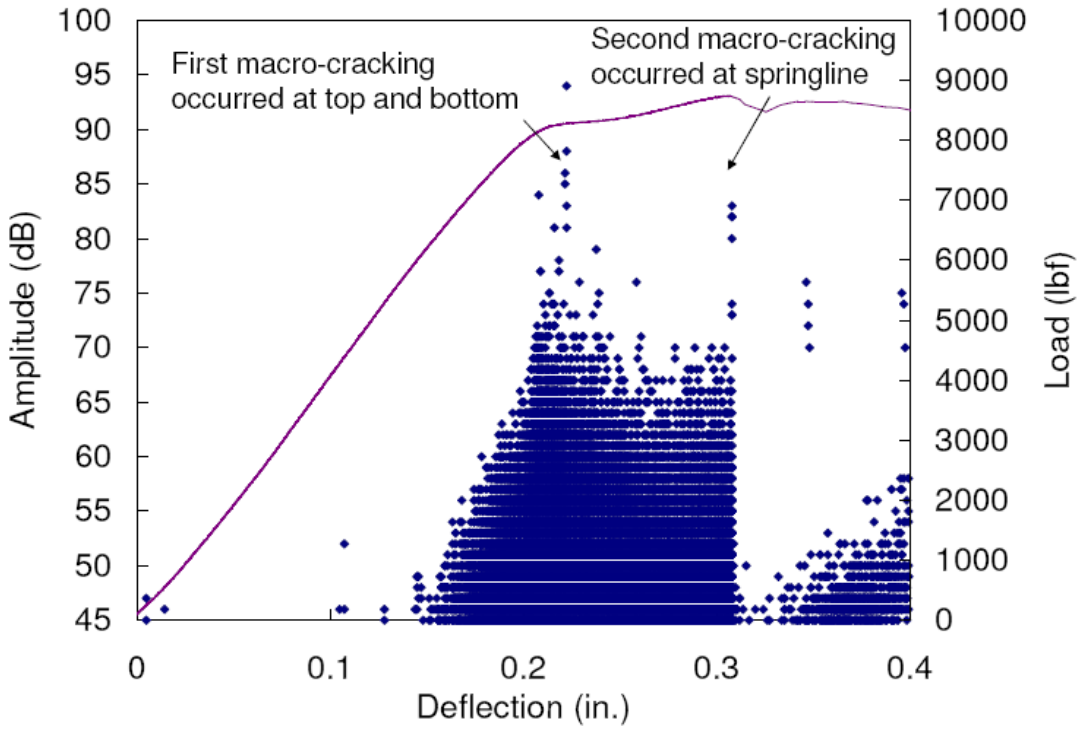

Figure 6-4. Amplitude and load versus deflection for dry specimen, monotonic test

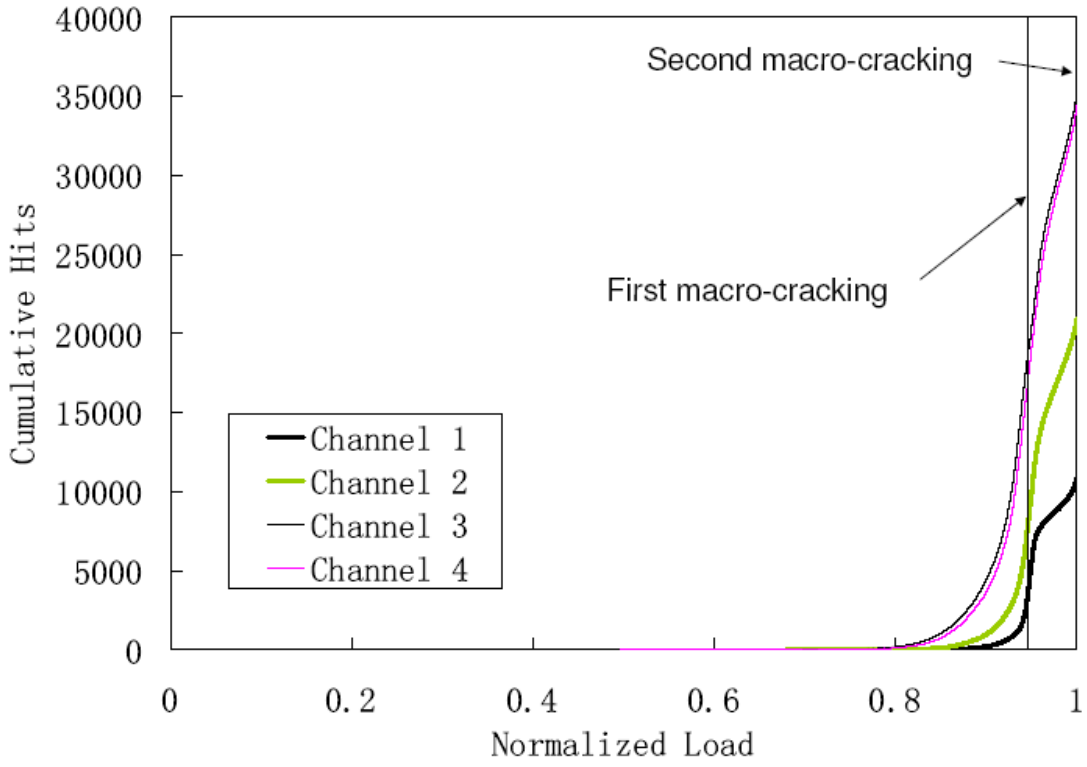

A

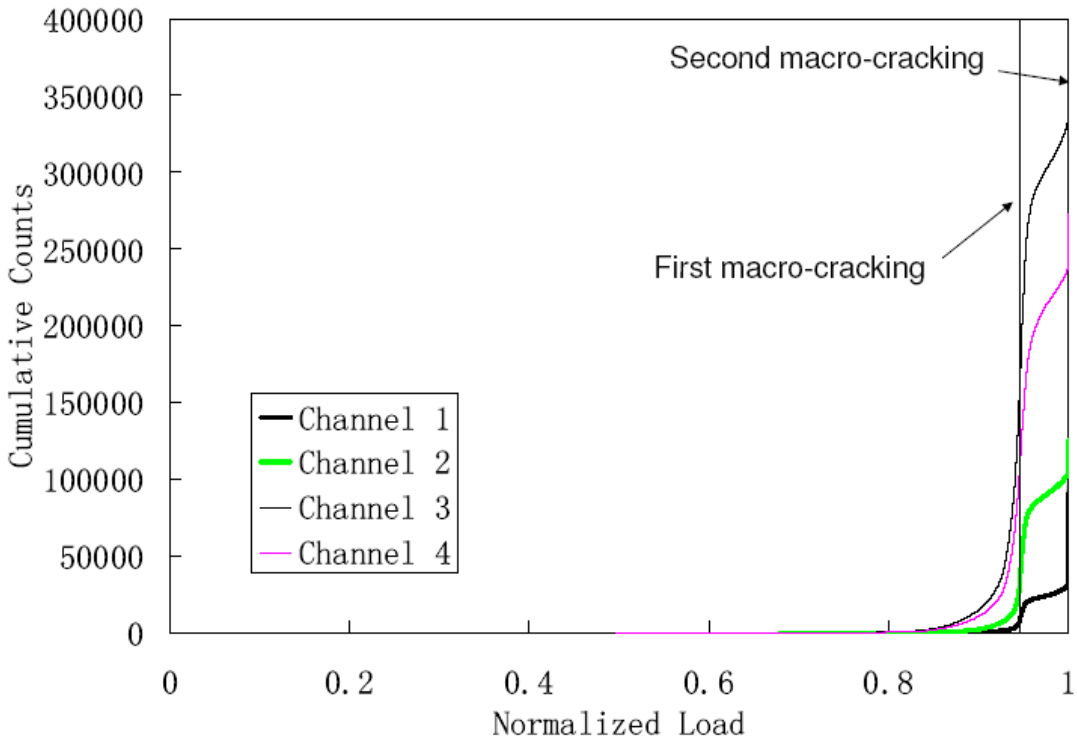
Second macro-cracking
First macro-cracking
Channel 1
Channel 2
Channel 3
Channel 4
Cumulative Counts
Normalized Load
400000
350000
300000
250000
200000
150000
100000
50000
0
0
0.2
0.4
0.6
0.8
1

B

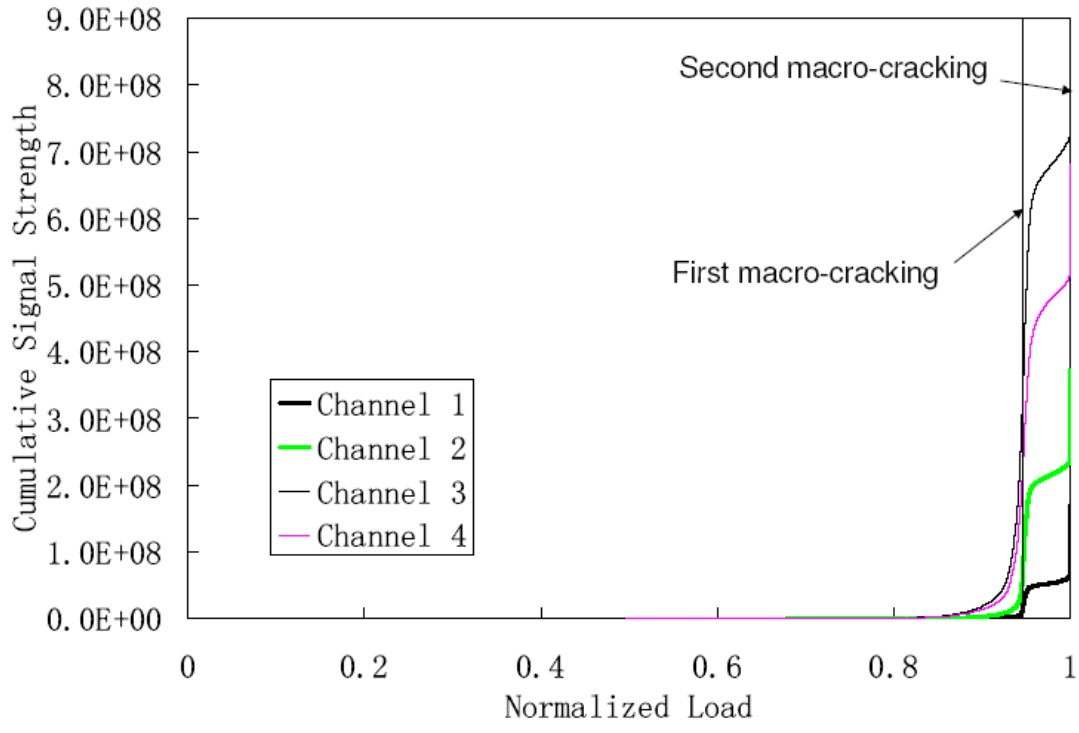
Second macro-cracking
First macro-cracking
Channel 1
Channel 2
Channel 3
Channel 4
Cumulative Signal Strength
Normalized Load
9.0E+08
8.0E+08
7.0E+08
6.0E+08
5.0E+08
4.0E+08
3.0E+08
2.0E+08
1.0E+08
0.0E+00
0
0.2
0.4
0.6
0.8
1

C

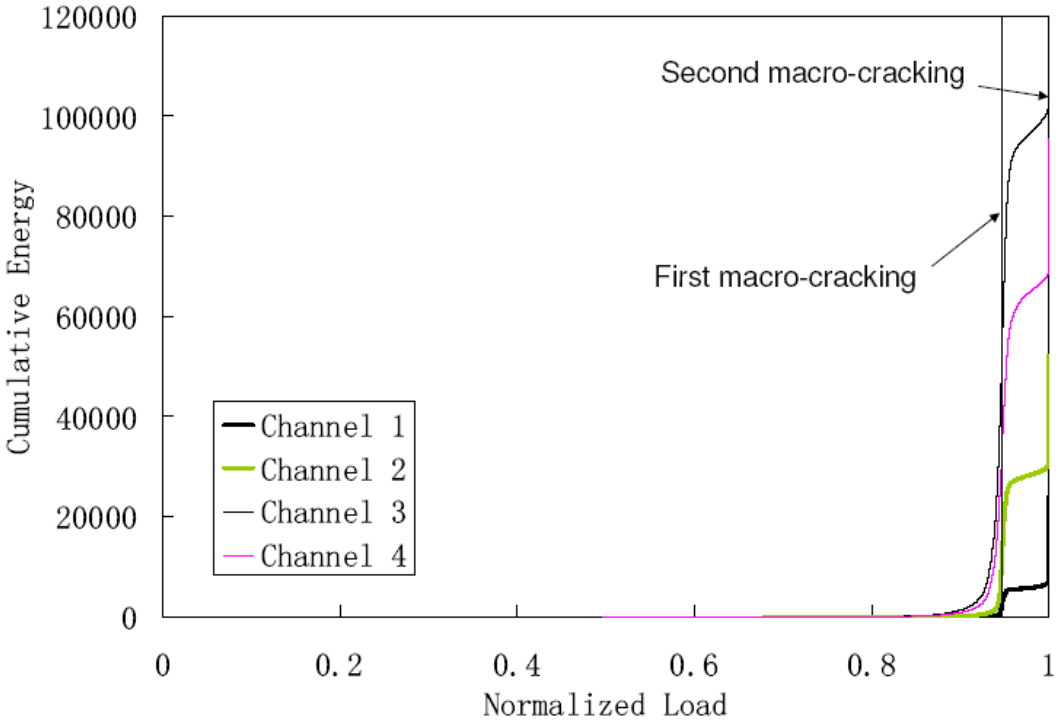

D

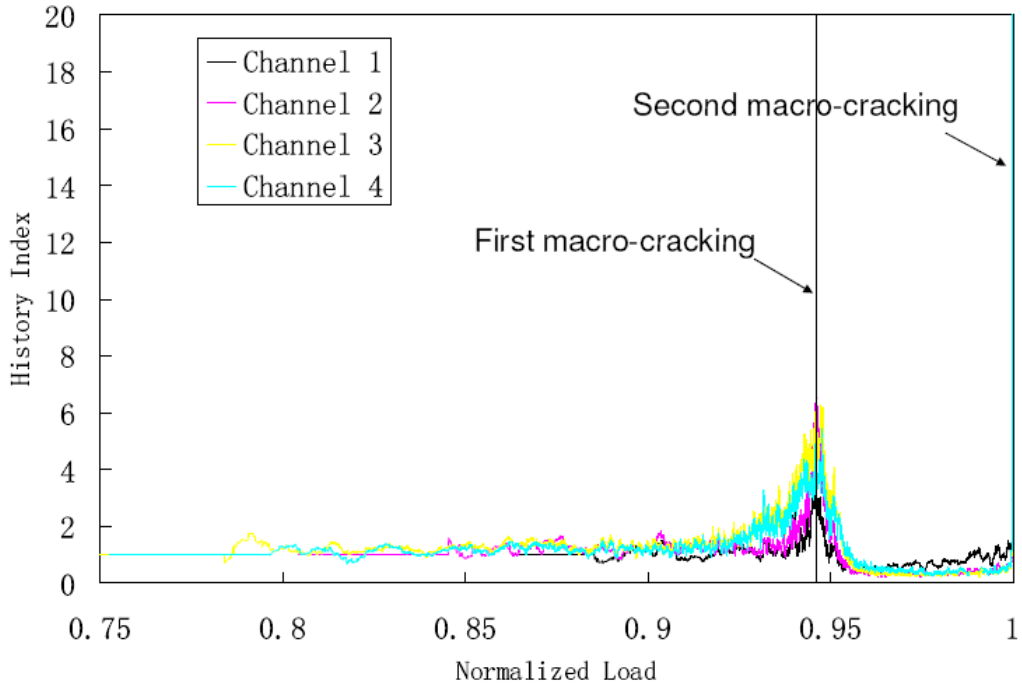

E

Figure 6-5. Conventional AE results for monotonic three-edge-bearing test A. Cumulative hits versus normalized load; B. Cumulative counts versus normalized load; C. Cumulative signal strength versus normalized load; D. Cumulative energy versus normalized load. E. Historic index versus normalized load

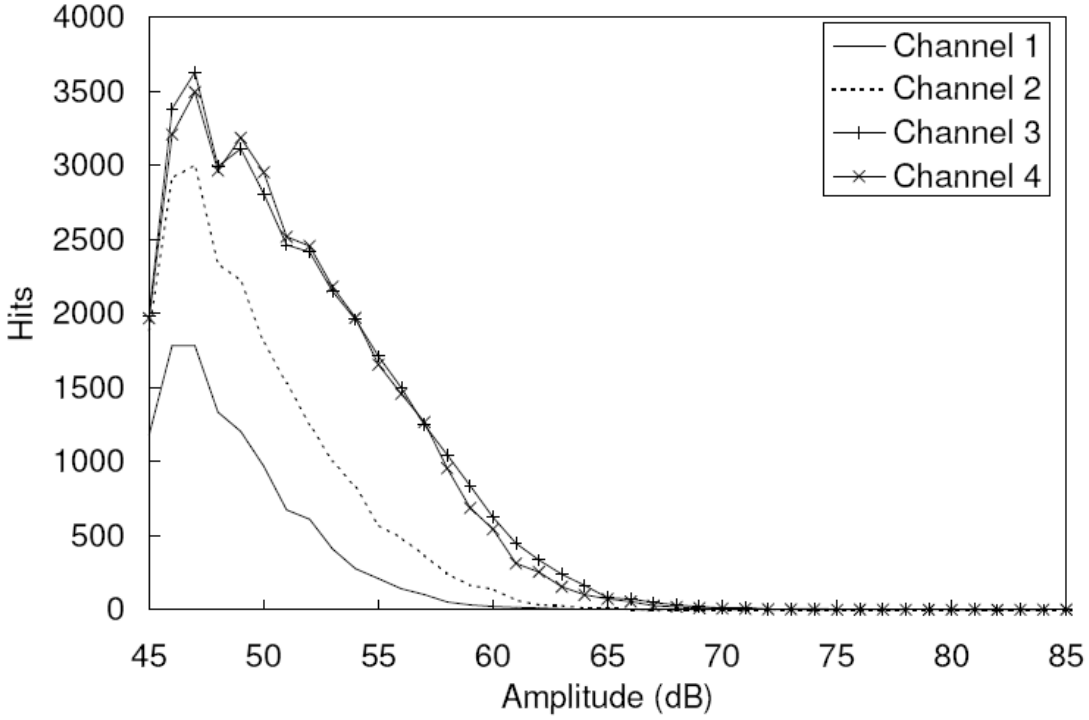

Figure 6-6. Amplitude distribution for monotonic three-edge-bearing test

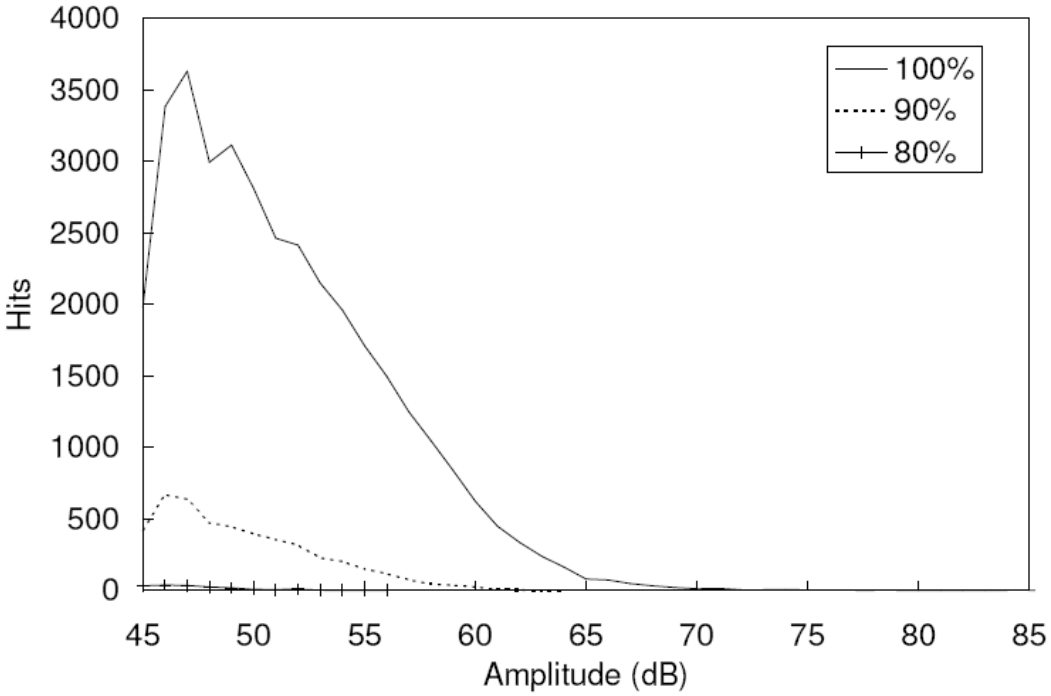

Figure 6-7. Progression of amplitude distribution for monotonic three-edge-bearing test, channel 3.

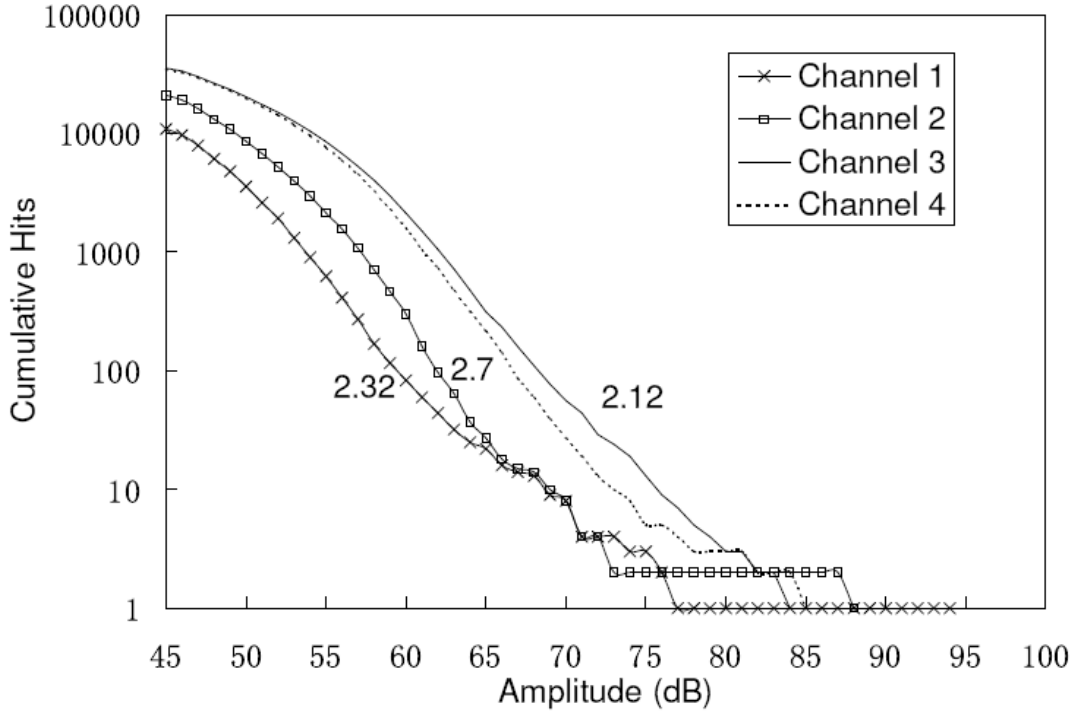

Figure 6-8. Cumulative Amplitude distribution for monotonic three-edge-bearing test

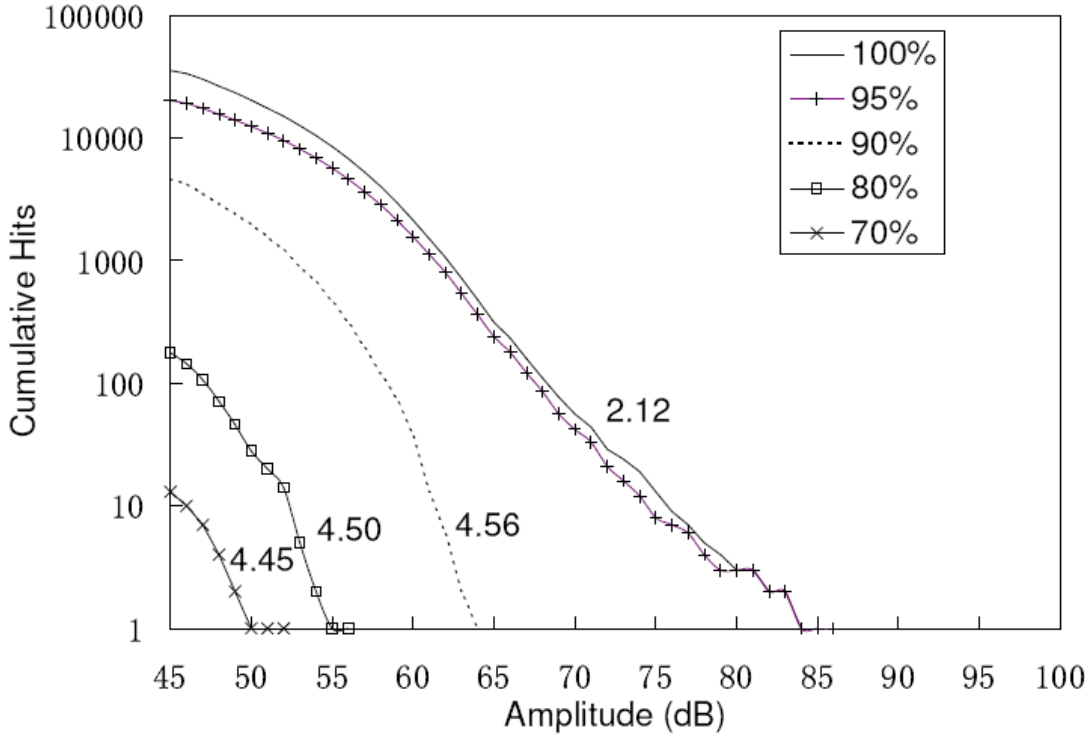

Figure 6-9. Progression of cumulative amplitude distribution for monotonic three-edge-bearing test

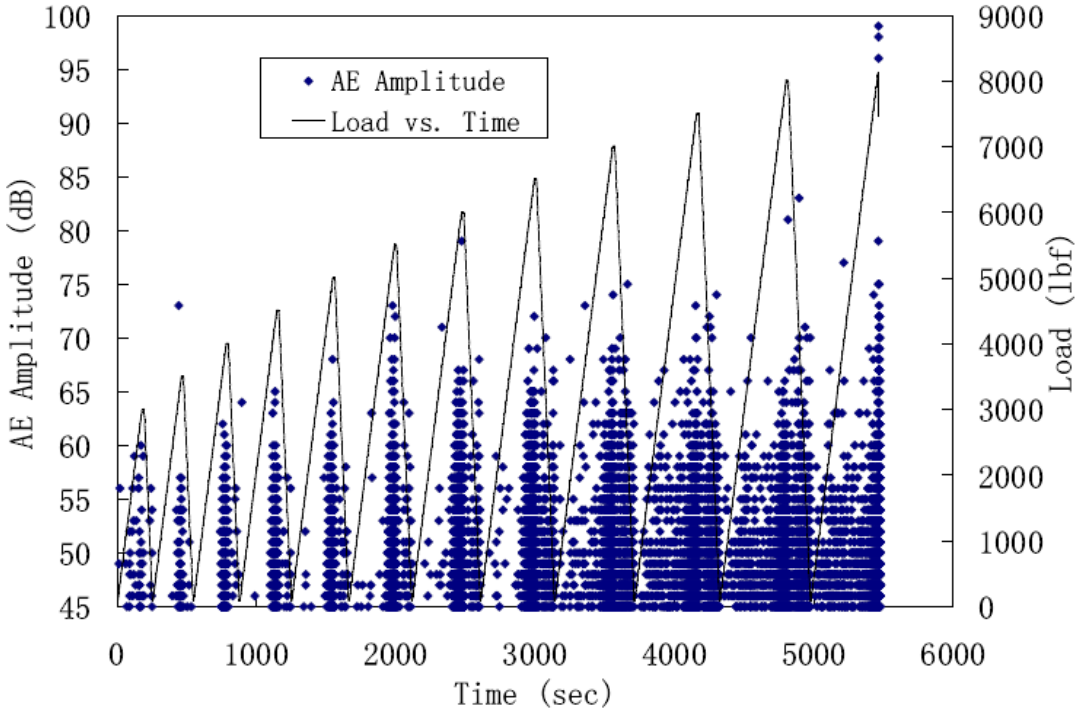
AE Amplitude
Load vs. Time
AE Amplitude (dB)
Load (lbf)
Time (sec)
100
95
90
85
80
75
70
65
60
55
50
45
9000
8000
7000
6000
5000
4000
3000
2000
1000
0
0
1000
2000
3000
4000
5000
6000

A

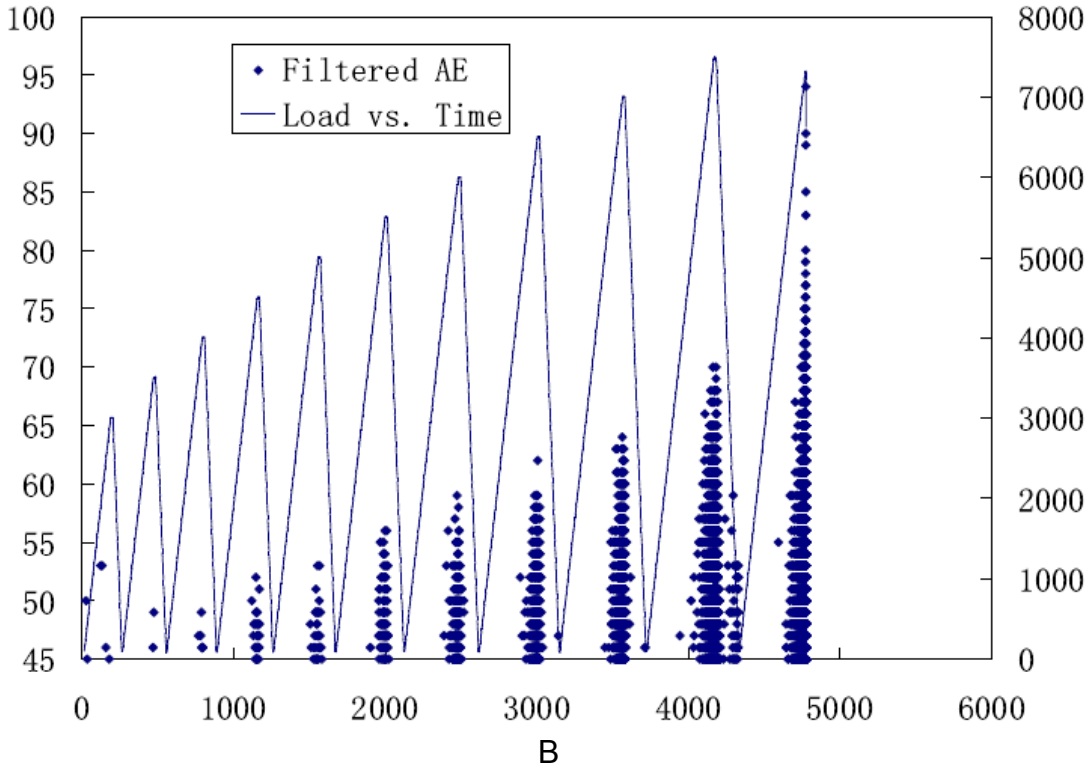
Filtered AE
Load vs. Time
100
95
90
85
80
75
70
65
60
55
50
45
8000
7000
6000
5000
4000
3000
2000
1000
0
0
1000
2000
3000
4000
5000
6000

B

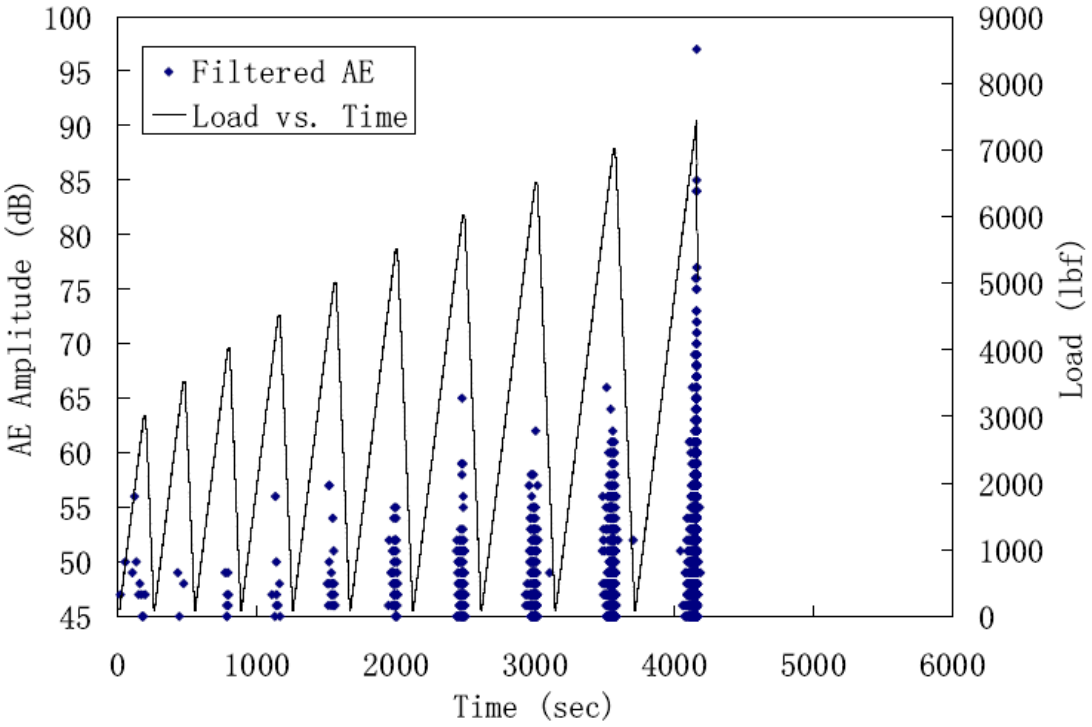

C

Figure 6-10. Amplitude and Load versus Time A. Dry specimen; B. Saturated for 3 months; C. Saturated for 6 months.

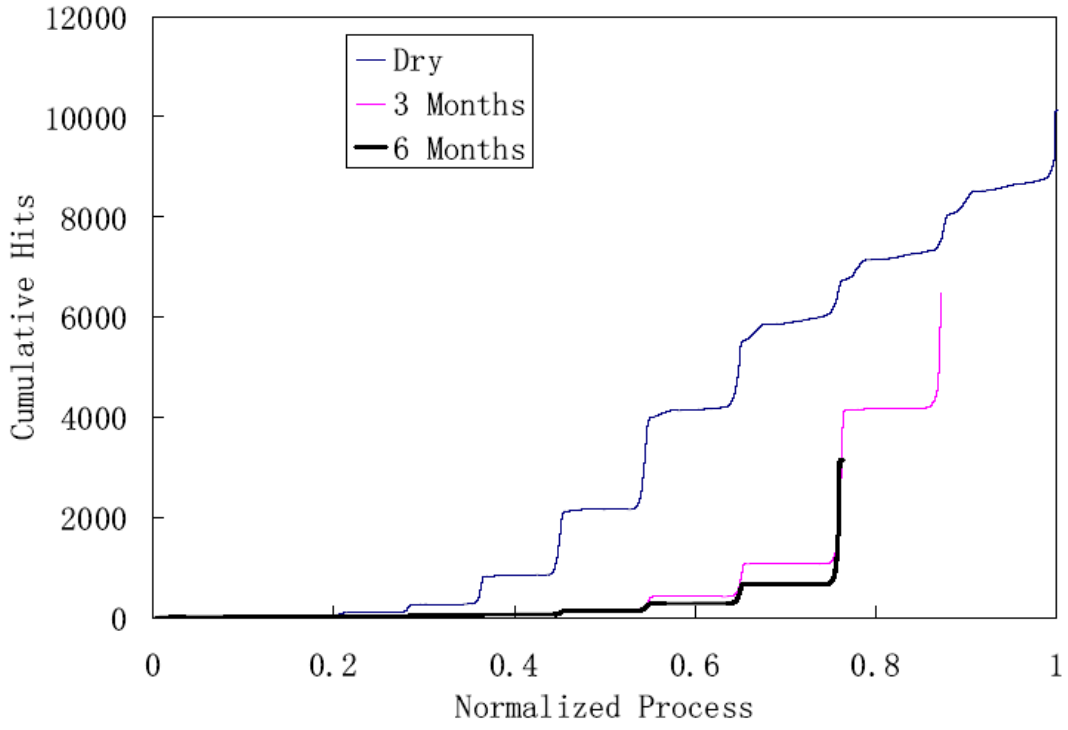

A

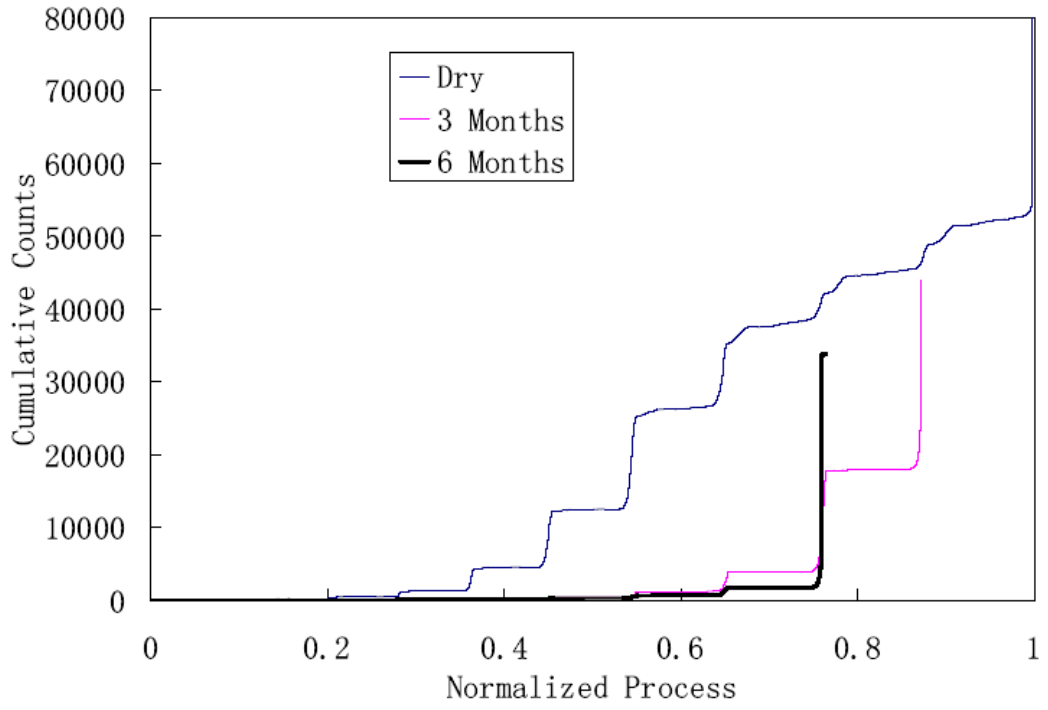
80000
70000
60000
50000
40000
30000
20000
10000
0
Cumulative Counts
Dry
3 Months
6 Months
0
0.2
0.4
0.6
0.8
1
Normalized Process

B

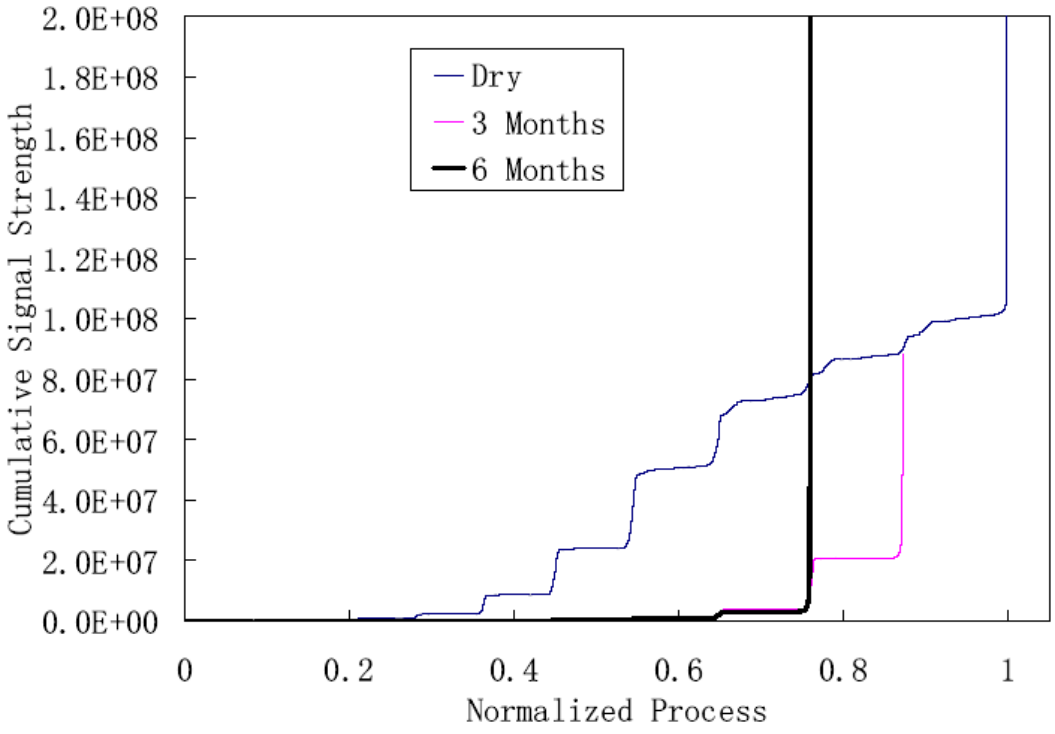
2.0E+08
1.8E+08
1.6E+08
1.4E+08
1.2E+08
1.0E+08
8.0E+07
6.0E+07
4.0E+07
2.0E+07
0.0E+00
Cumulative Signal Strength
Dry
3 Months
6 Months
0
0.2
0.4
0.6
0.8
1
Normalized Process

C

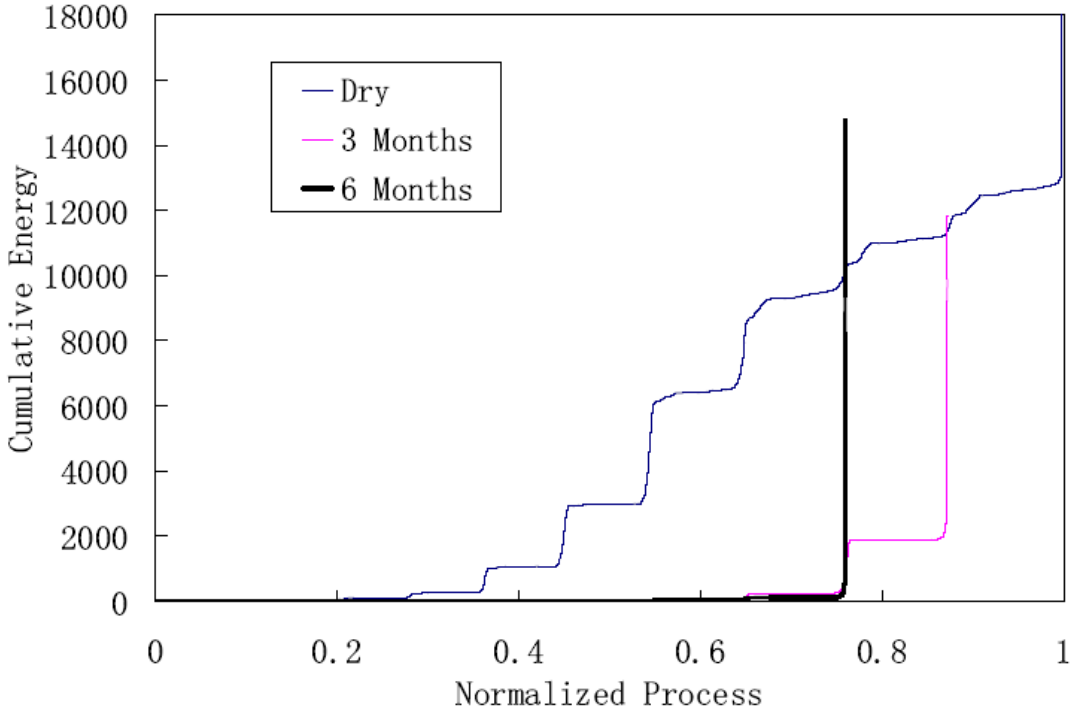

D

Figure 6-11. Conventional AE analysis A. Cumulative hits; B. Cumulative counts; C. Cumulative signal strength; D. Cumulative energy.

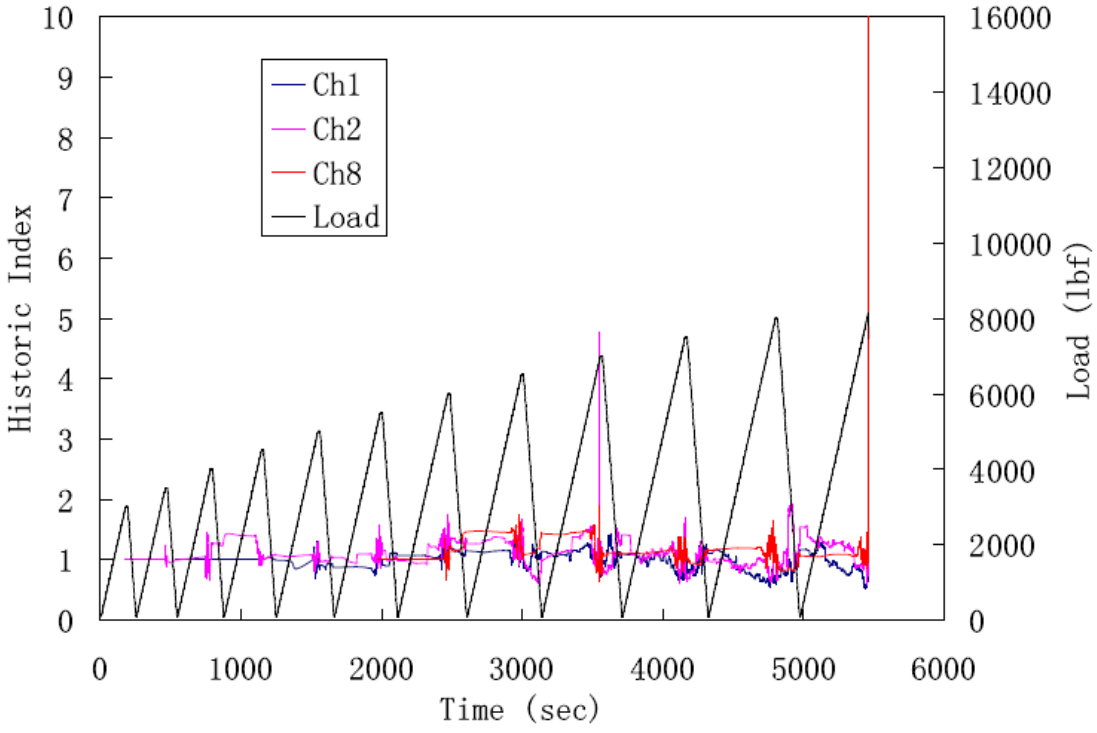

A

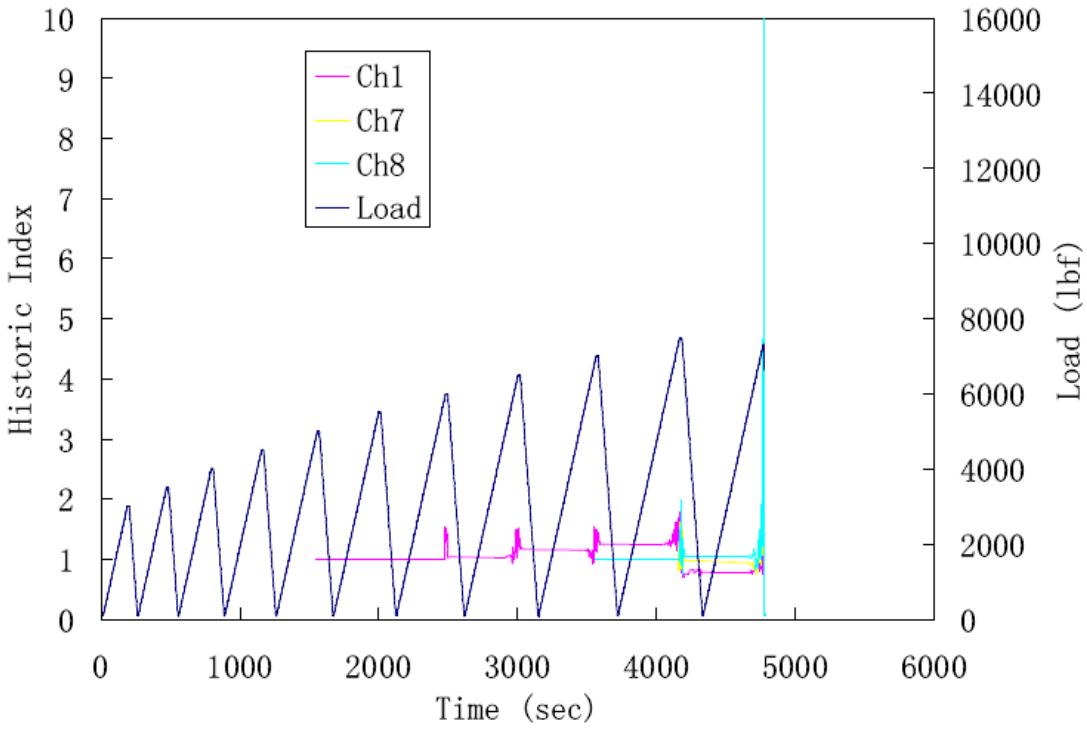

B

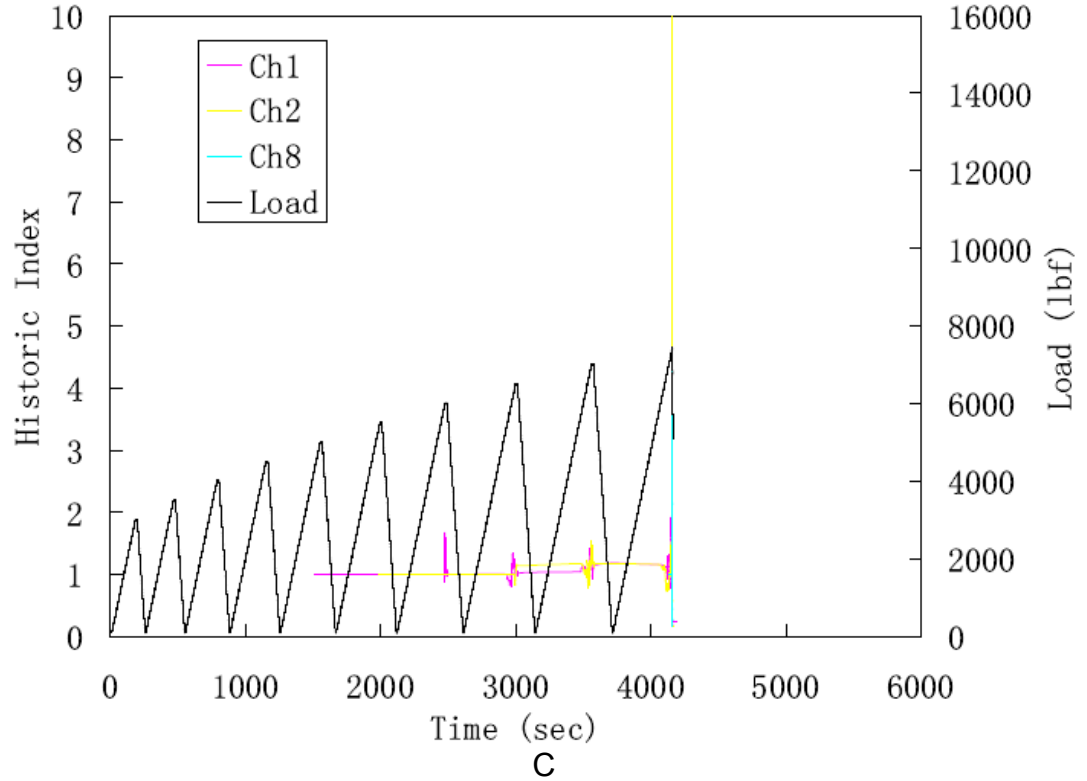

C

Figure 6-12. Historic index versus Time A. Dry specimen; B. Saturated for 3 months; C. Saturated for 6 months.

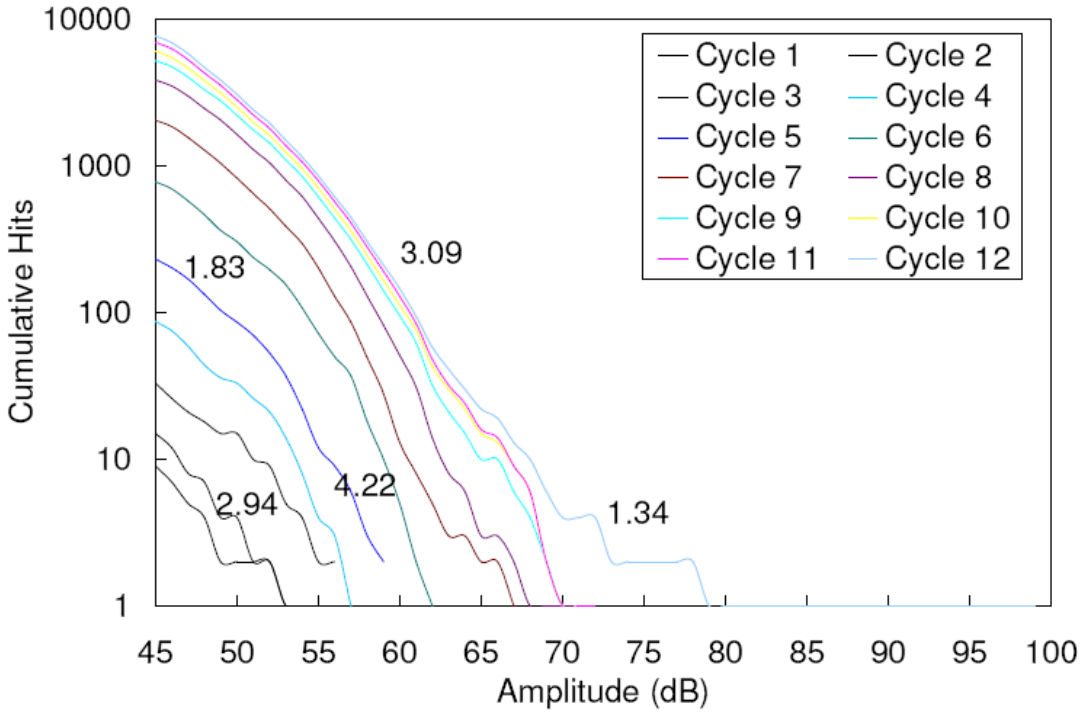
10000
1000
100
10
1
Cumulative Hits
45
50
55
60
65
70
75
80
85
90
95
100
Amplitude (dB)
Cycle 1
Cycle 2
Cycle 3
Cycle 4
Cycle 5
Cycle 6
Cycle 7
Cycle 8
Cycle 9
Cycle 10
Cycle 11
Cycle 12
1.83
3.09
2.94
4.22
1.34

A

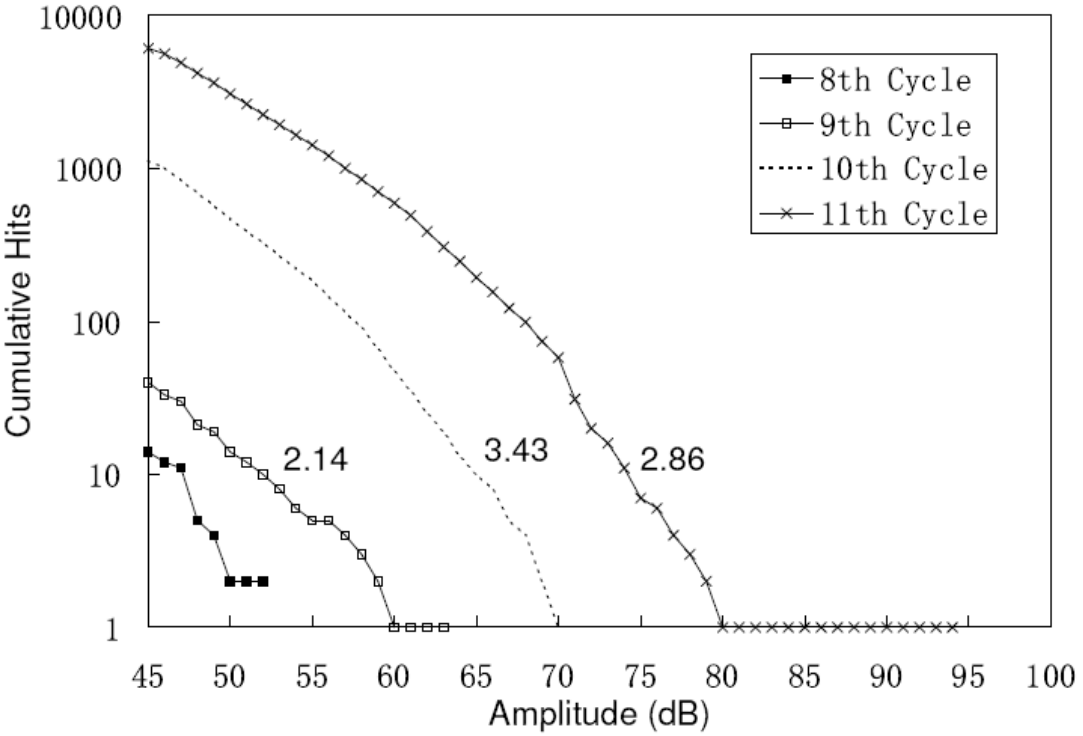
10000
1000
100
10
1
Cumulative Hits
45
50
55
60
65
70
75
80
85
90
95
100
Amplitude (dB)
8th Cycle
9th Cycle
10th Cycle
11th Cycle
2.14
3.43
2.86

B

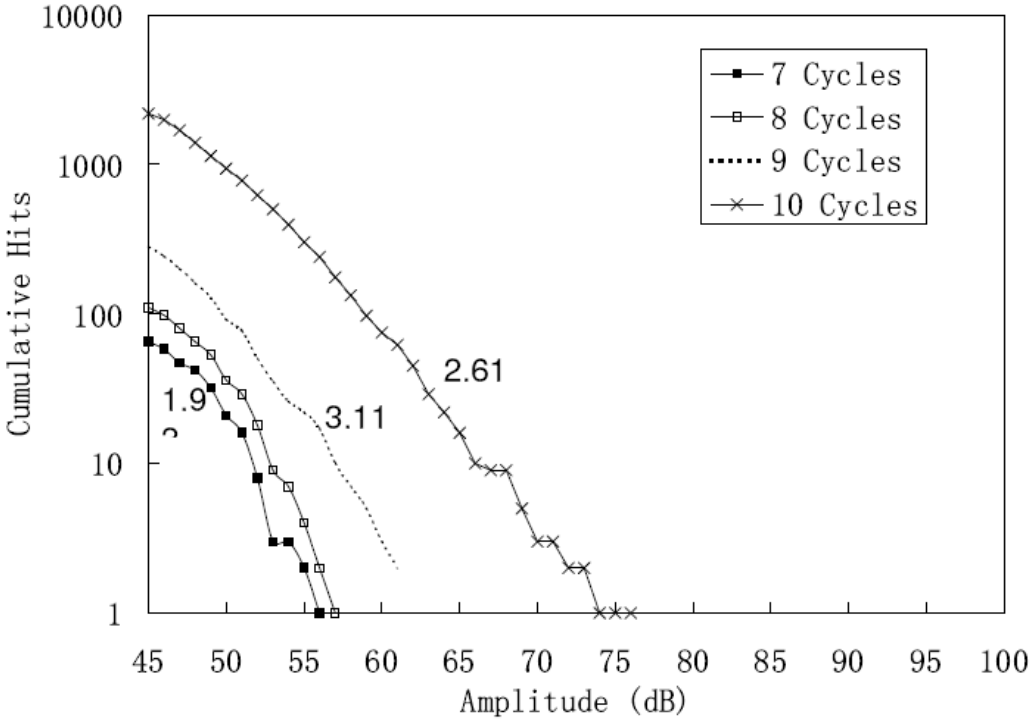

C

Figure 6-13. Cumulative amplitude distribution. A. Dry specimen; B. Saturated for 3 months; C. Saturated for 6 months.

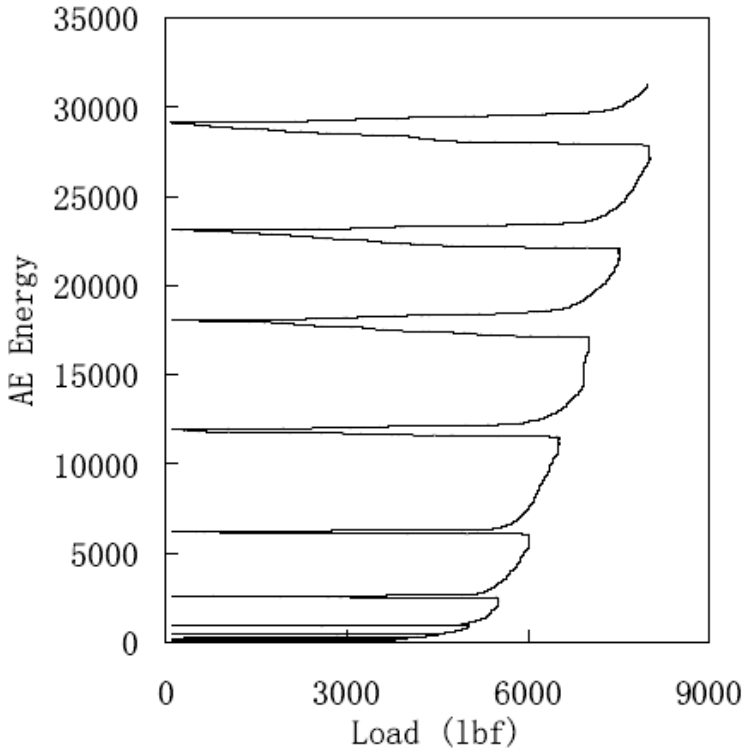

A

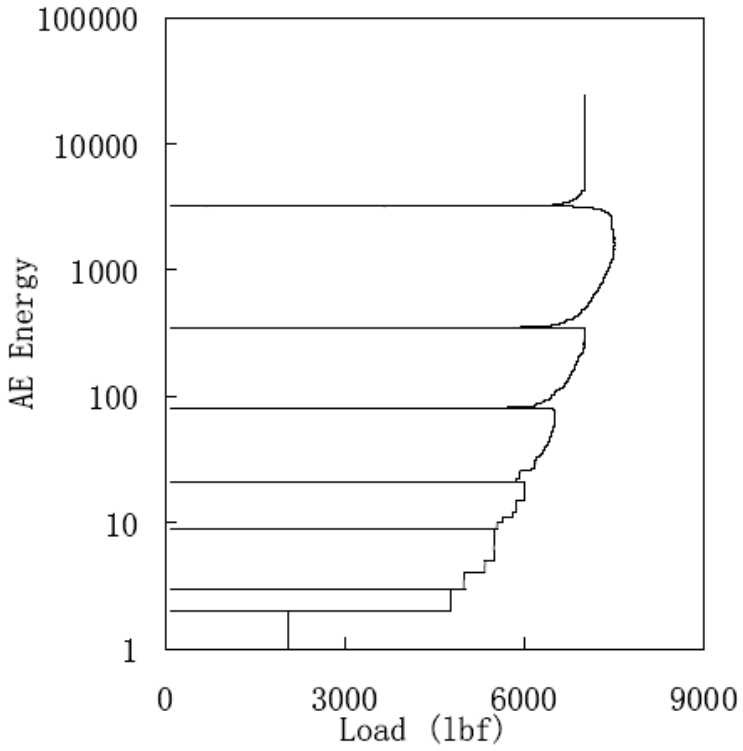

B

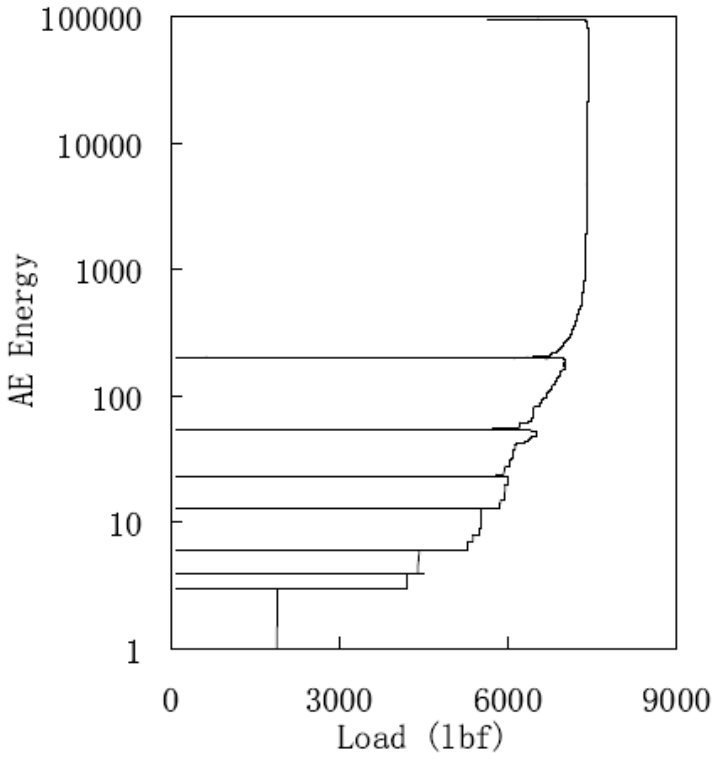

C

Figure 6-14. Kaiser and Felicity effects. A. Dry specimen; B. Saturated for 3 months; C. Saturated for 6 months.

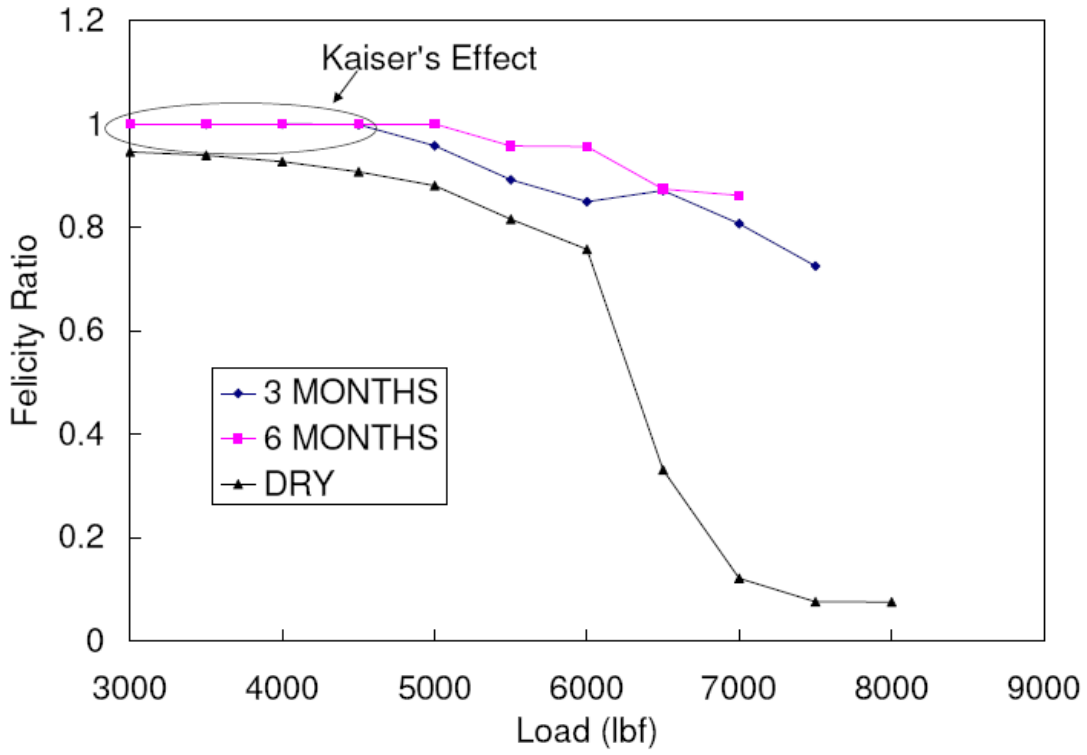

Figure 6-15. Felicity ratio for all specimens.

CHAPTER 7
CONCLUSIONS AND RECOMMENDATIONS

Conclusions

The research focused on two parts. The first is correlating the fracture mechanism with AE data. The second involves three tests including static third-point bending test, fatigue third-point bending test and three-edge-bearing test on pipe sections.

In the first part, the observation of micro damage mechanism was performed with the aid of SEM. Here, fracture mechanisms were identified and correlated to AE data. The fracture mechanisms occurring in CFRC are cement matrix cracking, fiber/matrix debonding and fiber breakage. The three are found to be correlated to low amplitude AE (45 to 65 dB), middle amplitude AE (65 to 75 dB) and high amplitude AE (higher than 75 dB) respectively.

The second focus of the research applied the knowledge obtained, and focused on AE data analyses for pattern recognition.

In the static third-point bending test, the specimens were prepared in several ways: saturating in water for four and eight weeks, and exposing the specimens to one, five and fifteen wet/dry cycles. The AE plots for each of the specimens were compared AE results. Four weeks saturation in water increases the material's ultimate and yield flexural strength. However, the material also becomes more brittle since the fibers don not delay crack propagation within matrix. Eight weeks saturation, on the other hand, decreases the material's ultimate and yield strength. Wet/dry treatment not only reduces the strength but also makes the material more brittle.

In the fatigue third-point bending test, different maximum loads were applied. AE results were analyzed to discuss the damage levels during testing. AE techniques were used to help analyzing the patterns such as the slope of the cumulative amplitude distribution (b-value) and the “knee” of the cumulative AE curves. These analyses were found to yield good correlation with mechanical properties.

In the three-edge-bearing test on pipe sections, three types of sections were tested. One was a dry specimen, one was saturated for three months, and the last was saturated for six months. Monotonic and cyclic tests were conducted on the dry specimen, while cyclic tests were conducted on the saturated specimens. Comparison was made to evaluate the influence of moisture effects. It was found that months of saturation reduced the durability and flexibility of CFRC pipe.

Through the application of AE during the project, it has proved to be an effective tool to analyze failure progress and detect the occurrence of damage and its development. The AE techniques, with their advantages and disadvantages for future inspection practices are outlined below.

Amplitude: Amplitude is the most important AE parameter. Correlation exists between the amplitude and failure mechanism. The occurrence of middle amplitude AE signifies the onset of damage. The occurrence of high amplitude indicates the final failure phase. For brittle specimens, like S4 and WD15 during monotonic bending test, the lack of middle amplitude AE implies little fiber/matrix debonding.

Cumulative AE: Cumulative AE usually includes cumulative hits, counts, signal strength and energy. For sound structures, the “knee” location of these curves correlates well with the yield points. For structures with pre-existing damages, the knee locates earlier than the yield points.

Historic index: This parameter works best for fatigue and large scale three-edge-bearing tests. The monotonic bending test does not provide a valid historic index due to the limited number of hits.

Amplitude distribution: It is often used to discuss fracture mechanism. Sound specimens showed multi-peaks which concentrate within low amplitude range. For brittle specimens, only one peak amplitude was detected.

Cumulative amplitude distribution and b-value: This parameter is an effective method to analyze the evolution of damage levels. The specific fracture mechanism corresponds to different b-value ranges. The influence of attenuation is minimal compared with other methods.

Kaiser and Felicity effects: The two effects were found in cyclic three-edge-bearing tests. Kaiser effect only appeared at the early cycles for brittle specimens, while for the more ductile specimen, only Felicity effect was observed. The ductile CFRC specimen yielded a smaller felicity ratio than brittle ones.

Recommendations

All the tests reported in this research were laboratory based. However, in a field application, testing will experience many conditions nonexistent in the lab, such as attenuation and environmental noise. Further research on the

identification and isolation of noise will have a significant effect on AE inspection success.

A key component of this research was to correlate the failure mechanisms with AE amplitude. SEM observations should be conducted to more accurately identify failure mechanisms after being treated with soaking and wet/dry cycles.

The sensors used in this project were R15I, a common sensor for lab testing on small specimens. However, since the attenuation of CFRC is significant, a more sensitive sensor with lower peak frequency response, R5, is recommended.

The bonding ability between fiber and matrix is crucial to CFRC's strength, ductility and durability. Research on improving the bonding between fiber and matrix will improve CFRC based structures.

LIST OF REFERENCES

A. A. Moslemi, Emerging Technologies in Mineral-Bonded Wood and Fiber Composites, Advanced Performance Materials 1999;6:161-179.

A. A. Pollock, Acoustic Emission Amplitude Distributions, International Advances in Nondestructive Testing 1981;7:215-239.

A. R. Tognon, R. K. Rowe, and R. W. I. Brachman, Evaluation of side wall friction for a buried pipe testing facility, Geotextiles and Geomembrances 1999;17:213-230.

B. B. Tinkey, T.J. Fowler, and R. E. Klingner, Nondestructive Testing of Prestressed Bridge Girders with Distributed Damage, Structural Assessment of In-service Bridges with Premature Concrete Deterioration, 2000; Texas Department of Transportation.

B. J. Mohr, H. Nankoand, K.E. Kurtis, Durability of kraft pulp fiber-cement composites to wet/dry cycling, Cement & Concrete Composites 2005;27: 435-448.

C. K. Shield, Comparison of Acoustic Emission Activity in Reinforced and Prestressed Concrete Beams under Bending, Construction and Building Materials 1997;11(3):189-194.

C. Y. Barlow, J. A. Peacock, and A. H. Winkle Relationships Between Microstructures and Fracture Energies in Carbon Fibre/PEEK Composites 1990;21(5)5:383-388.

D. S. Nyce, Linear Position Sensors, Theory and Application 2004;John Wiley and Sons, Hoboken, NJ.

D. Valentin, A Critical Analysis of Amplitude Histograms Obtained During Acoustic Emission Tests on Unidirectional Composites with an Epoxy and a PSP Matrix, Composites 1985;16(3): 225-230.

E. E. Herceg, Handbook of Measurement and Control 1976; Schaevitz Engineering, Pennsauken, NJ.

J. M. Berthelot, and J. Rhazi, Different Types of Amplitude Distributions in Composite Materials, Second International Symposium on Acoustic Emission from Reinforced Composites 1986; The Society of the Plastics Industry, Inc., Reinforced Plastics/Composites Institute, Montreal, Canada, July 21-25: 96-103.

J. Bohse, Acoustic Emission Characteristics of Micro-failure Processes in Polymer lends and Composites, Composites Science and Technology 2000;60:1213-1226.

J. P. Monchalin, Optical and Laser NDT: A Rising Star, Industrial Materials Institute, NRC, Boucherville, Quebec, Canada

K. Komai, K. Minoshima, and T. Shibutani, (1991). Investigations of the Fracture Mechanism of Carbon/Epoxy Composites by AE Signal Analyses, JSME International Journal 1991;34(I):381-388.

K. Minolta, Non-contact 3D Digitizer Vivid 910/VI-910 Instruction Manual.

M. Ohtsu, AE application to fracture mechanics, JCI Trans 1989;11:673-678.

M. Surgeon, and M. Wevers, Modal Analysis of Acoustic Emissions from CFRP Laminates, NDT & E International 1999;32:311-322.

N. Sato, and T. Kurauchi, Interpretation of Acoustic Emission Signal from Composite Materials and its Application to Design of Automotive Composite Components, Research in Nondestructive Evaluation 1997;9: 119-136.

P. J. De Groot, P.A.M. Wijnen, and R.B.F. Jansen, Real-time Frequency Determination of Acoustic Emission for Different Fracture Mechanisms in Carbon/Epoxy Composites, Composites Science and Technology 1995; 55: 405-412.

P. Rizzo, and Lanza di Scalea, F. Acoustic Emission Monitoring of Carbon-fiber-reinforced-polymer Bridge Stay Cables in Large-scale Testing, Experimental Mechanics 2001; 41(3): 282-290.

R. A. Parmalee, A study of soil structure interaction of buried concrete pipe, Concrete Pipe and the Soil-Structure System, ASTM STP 630, American Society for Testing and Materials1977;99: 66-75.

R. W. I. Brachman, I. D. More and R. K. Rowe, The design of a laboratory facility for evaluating the structural performance of small diameter buried pipes, Canadian Geotechnical Journal 2000;37: 281-295.

R. W. I. Brachman, I. D. More, and R. K. Rowe, The performance of a laboratory facility for evaluating the structural response of small-diameter buried pipes, Canadian Geotechnical Journal 2001;38:260-275.

S. Barre, and M. L. Beneggagh, On the Use of Acoustic Emission to Investigate Damage Mechanism in Glass-fiber-reinforced Polypropylene, Composites Science and Technology 1994;52:369-376.

S. Mindess, J. F. Young, D. Darwin, Concrete 2003;91:372-381.

T. Uomoto, Application of Acoustic Emission to the Field of Concrete Engineering, Journal of Acoustic Emission 1987;6(3):137-144.

Y. K. Ji, and J.W. Ong, A Study on the Acoustic Emission Characteristics of the Carbon Fiber Reinforced Plastics, Nondestructive Characteristics of Materials 1994;6:207-214.

Z. Li, and S.P. Shah, Microcracking in concrete under uniaxial tension, ACI Material Journal 1994;91:372-381.

BIOGRAPHICAL SKETCH

Yu Chen was born in Qingdao, Shandong Province, China. The younger of two children, she grew up in Qingdao, Shandong, graduating from Qingdao No. 2 Middle School in 1996. She earned her B.S. and Master's degree in civil and environmental engineering from Zhejiang University, China, and from National University of Singapore in 2000 and 2003, respectively.

In January 2004, Chen entered the graduate program at the Department of Civil and Coastal Engineering at University of Florida, Gainesville, Florida. Chen is pursuing her Ph.D degree in civil engineering under the supervision of Dr. David Bloomquist.